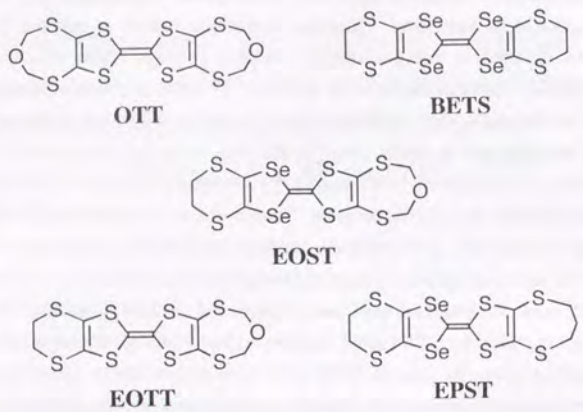

Scheme 4.1.

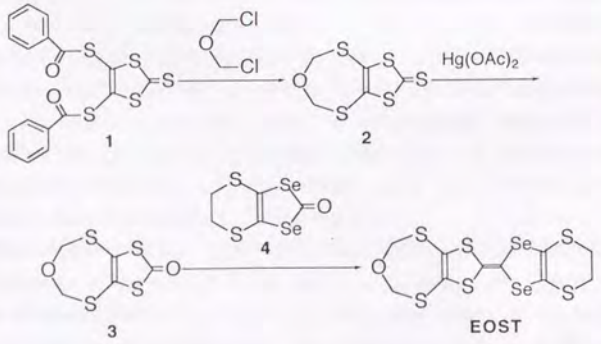

Scheme 4.2.

4-2. Experimental

Materials

All chemicals were reagent grade from Wako Chemical Co. and used as received unless noted otherwise. Triethyl phosphite was vacuum distilled, sealed under nitrogen and stored in the refrigerator until use. All solvents were degassed with high purity dry nitrogen for at least a few minutes before use.

4,5-(2-oxatrimethylenedithio)-1,3-dithiole-2-thione, **2**

There are some reports of synthetic routs of **2** and **3** [4 – 6]. In a 1 l three-necked flask equipped with 200 and 500 mL dropping funnels with pressure-equalizers, 4,5-bis(benzoylthio)-1,3-dithiole-2-thione **1** [7] (20.28 g, 50 mmol) was treated with a solution of sodium (6.90 g, 0.3 mol) in 150 ml of methanol under a nitrogen atmosphere. To this dark-red solution added was 500 ml of methanol containing ammonium acetate (25 g) followed by bis(chloromethyl) ether [8] (11.50 g, 100 mmol) in 125 ml of methanol with stirring. The solution immediately turned crimson-red with a sticky orange precipitate. The mixture then became dark red again within a few minutes and was stirred overnight at room temperature. The precipitates were filtered off, washed with methanol followed by hexane, dried *in vacuo*. The light yellow sponges obtained were redissolved in CH_3Cl (0.1 g 25 ml^{-1}) and evaporated to a fifteenth volume under reduced pressure. The resulting pale yellow needles were collected, washed succesively with acetone, methanol, ethanol, hexane and finally with ether and dried *in vacuo*; yield: 8.52 g (71 %). The crude product could be recrystallized also from $CHCl_3$ or $CHCl_3$–ether (1:5) or CH_2Cl_2, but the appearance of the purified product depended upon the solvent and the temperature used.

4,5-(2-oxatrimethylenedithio)-1,3-dithiole-2-one, **3**

$Hg(OAc)_2$ (3.077g, 9.657 mmol) was added, in one portion with stirring, to a solution of **2** (1.123 g, 5.013 mmol) in 225 ml chloroform and 225 ml glacial acetic acid in a 500 ml Erlenmyer flask. The stirring was continued at room temperature for 30 min. The milky suspension was filtered and the filtrate was washed succesively with water, saturated aquaous sodium hydrogencarbonate and water again. The organic layer was dried with anhydrous sodium sulfate, then decanted off, evaporated to dryness *in vacuo* and the residue was chromatographed on silica gel using the mixed solvent of chloroform and hexane (1:1) as an eluent. The first colorless portion gave a crude product of **3**; yield: 0.779 g (74 %) The off-white needles obtained turned colorless after recrystallization from ethanol; m.p. 163-164°C. Elemental analysis:
$C_5H_4S_4O_2$ = 224.35 calclated (%) H: 1.80 C: 26.77 S: 57.17 O: 14.26, found

H: 1.77 C: 26.82 S: 57.13, m/e = 224 (M^+). ^{1}H-NMR (CS_2) : δ = 4.82 (s, 4H, CH_2)

4,5-bis(ethylenedithio)-1,3-diselenole-2-one, **4**

This compound was synthesized by following the procedure of ref.[1].

4,5-ethylenedithia-4',5'-(2-oxatrimethylenedithia)-diselenadithiafulvalene (EOST):

Method A

Compounds **2** (0.54g, 2.23 mmol) and **4** (0.67g, 2.23 mmol) were suspended in triethyl phosphite (50 mL) under a dry nitrogen atmosphere and slowly warmed to 110-120 °C with stirring and held in that temperature range for 30 min. The resultant orange mixture was allowed to cool to room temperature and reddish-brown precipitates were filtered off, washed succesively with acetone, methanol, ethanol and hexane, dried *in vacuo* . The reaction was highly selective and only a trace amount of self-coupling products formed. Recrystallization from boiling CS_2 (1 l) followed by column-chromatography (silicagel, eluent CS_2 : CH_2Cl_2 = 1 : 1) gave analytically (HPLC) pure red shiny blocks; yield: 550 mg (50 %). Elemental analysis:
$C_{10}H_8S_6Se_2O$ = 494.49 calculated (%) H: 1.63 C: 24.29 S: 38.91 Se: 31.94 O: 3.24
found (%) H: 1.63 C: 24.20 S: 39.15 Se: 30.69. m/e = 496 (M^+)
IR (KBr): 1418 (w), 1303 (w), 1224 (vw), 1055 (m), 920 (m), 719 (vw), 681 (vw), 490 cm^{-1} (vw). For the crystal data, see Table 4.2 (later).

Method B

The similar procedure to method A was followed with **3**, (0.500g, 2.23 mmol) instead of **2**. This allowed more formation of self-coupling products than method A and thus required more tedious work-up for isolation of the desired compound; crude coupling products were filtered off from triethyl phosphite, washed with methanol, dried *in vacuo* and purified by column-chromatography (silicagel / CS_2), then HPLC (Kusano Kagaku-kikai Co., Ltd; Si-10), and finally recrystallized first from o-$C_6H_4Cl_2$, then from CS_2 : CH_2Cl_2 = 4 : 3; yield: 287 mg (26 %)

Charge-transfer Salts of EOST

The single crystals of the charge-transfer salts of EOST was prepared by use of standard elctrocrystallization techniques. All chemicals were purified prior to use [9] and handled inside a drybox. The crystal growth was carried out in a standard H-cell (without glass frit) using platinum electrodes of 1mm in diameter under a nitrogen atmosphere. A typical procedure began with 7-10 mg of EOST and 50-100 mg of the tetrabutylammonium salt of the corresponding anion as the supporting electrolyte in 20 ml

of tetrahydrofuran (THF) or chlorobenzene or sometimes the mixture of the two at a constant current of 1.5-3.4 μA or a constant voltage of 6.5-7.5 V at room temperature (20 °C) for several days. Some of the successful conditions are tabulated in Table 4.1. After many attempts the single crystals of $(EOST)_2I_3$ were obtained using 1,1,2-trichloroethane as the solvent instead of those mentioned above. After one or two days thin fibrous crystals were observed to have grown on the tip of the electrode and the anode was thickly covered with many thin needles after a further two days.

X-ray structural analyses

The X-ray crystal structure analyses were made on EOST and its several charge-transfer salts. Details of the crystal data, intensity measurement and data processing for the structures are summarized in Table 4.2. The intensities were measured by the ω-2θ scan on a Rigaku automated four-circle diffractometer with graphite-monochromated Mo $K\alpha$ (λ = 0.7107 Å) radiation. Three standard reflections were measured every 100 or 150 reflections. Backgrounds were counted for 2.0 seconds at both ends of the scan. The data were corrected for Lorentz and polarization effects. Corrections for absorption were made on ICl_2, IBr_2 salts and the neutral EOST. No significant intensity variation was observed for the other samples and no correction was made for absorption. The unit cell dimensions were determined from 20 reflections with 20 ≤ θ/degrees ≤ 35 { I_3, IBr_2 and $Au(CN)_2$ salts }, from 25 reflections with 30 ≤ θ/degrees ≤ 40 (I_2Br and ICl_2 salts) or from 23 reflections with with 39.3 ≤ θ/degrees ≤ 40 (neutral EOST) by least-squares refinement. The structures were solved by the heavy-atom (Patterson) method (I_3 salt and the neutral EOST) or the direct method (MULTAN [10] for $Au(CN)_2$ salt, SHELXS for ICl_2 salt) and the succeeding Fourier syntheses.

Table 4.1. Electrolytic conditions of preparation of EOST salts

counter ion (X^-)	I_3	$AuBr_2$		I_2Br
crystal habit[a]	plates	(α-) plates, (β-) needles		plates
current / μA[d]	0.8	1.5		1.0
voltage / V[e]			6.9	
$(^nC_4H_9)_4NX$ / mg	66	62	83	58
EOST / mg	10	12	8	10
solvent[f]	TCE	CB	THF	CB
time / days	7	7	1	7

Table 4.1. Electrolytic conditions of preparation of EOST salts (continued)

counter ion (X^-)	ICl_2	$Au(CN)_2$		IBr_2	
crystal habit[a]	plates	blocks[b], needles[c]		(α-) plates, (β-) needles	
current / μA[d]	1.5	0.8	1.5	1.0	1.5
$(^nC_4H_9)_4NX$ / mg	63	80	61	45	63
EOST / mg	19	6	14	16	7
solvent[f]	CB	THF	CB	CB	CB
time / days	9	1	6	7	7

Table 4.1. Electrolytic conditions of preparation of EOST salts (continued)

[a] All crystals are black. Plates are often elongated and appear needles at first sight.

[b] Insulating phase [c] Highly conducting phase ($T_{M\text{-}I} \leq 40$ K)

[d] Galvanostatic condition [e] Potentiostatic condition [f] 20 ml TCE = 1,1,2-trichloroethane, CB = chlorobenzene, THF = tetrahydrofurane.

Table 4.2. Structure determination summary*

	$EOST_2I_3$	α-$EOST_2IBr_2$
Crystal data		
Empirical formula	$Se_4S_{12}C_{20}O_2H_{16}I_3$	$Se_4S_{12}C_{20}O_2H_{16}IBr_2$
Formula weight, M	1369.71	1275.71
Crystal color, habit	black plate	black plate
Crystal size/mm	0.30 × 0.10 × 0.01	0.20 × 0.45 × 0.01
Crystal system	Triclinic	Triclinic
Space group	P $\bar{1}$	P $\bar{1}$
a/Å	11.748(3)	11.634(3)
b/Å	16.441(5)	16.283(4)
c/Å	4.789(1)	4.758(1)
α/°	93.93(2)	93.18(2)
β/°	96.37(2)	95.93(2)
γ/°	72.86(2)	73.55(2)
V/$Å^3$	877.7(4)	859.5(4)
Z	1	1
D_{calc}/Mgm^{-3}	2.591	2.464
μ/cm^{-1}	74.603	81.444
F(000)	639	603
Data collection		
Scan width, A	1.09[a]	1.12[a]
2θ max/°	55.0	55.0
Index ranges	$-15 \leq h \leq 15$ $-21 \leq k \leq 21$ $0 \leq l \leq 6$	$-15 \leq h \leq 15$ $-21 \leq k \leq 21$ $0 \leq l \leq 6$
Reflections collected	4554	4460
Independent reflections	4064	4076
Observed reflections	3604	3661
[$\lvert F_o \rvert > 3\sigma(F_o)$]		
Solution and refinement		
Weighting scheme, w^{-1}	c	c
No of parameters refined	191	191
Final R, R_w	0.051, 0.061	0.052, 0.067
Goodness of fit	0.30	0.23

Table 4.2. Structure determination summary*(continued(1))

	EOST$_2$I$_2$Br	EOST$_2$ICl$_2$
Crystal data		
Empirical formula	$Se_4S_{12}C_{20}O_2H_{16}I_2Br$	$Se_4S_{12}C_{20}O_2H_{16}ICl_2$
Formula weight, M	1322.69	1186.81
Crystal color, habit	black plate	black plate
Crystal size/mm	0.21 × 0.45 × 0.01	0.26 × 0.22 × 0.012
Crystal system	Triclinic	Triclinic
Space group	P $\bar{1}$	P $\bar{1}$
a/Å	11.736(2)	11.604(4)
b/Å	16.429(2)	31.105(7)
c/Å	4.793(3)	4.747(3)
α/°	93.83(1)	89.96(3)
β/°	96.30(1)	95.80(4)
γ/°	72.89(1)	83.47(2)
V/Å^3	877.3(2)	1693(1)
Z	1	2
D_{calc}/Mgm^{-3}	2.504	2.328
μ/cm^{-1}	77.201	62.502
F(000)	621	1134
Data collection		
Scan width, A	0.89[b]	1.05[b]
2θ max/°	55.0	55.0
Index ranges	$0 \le h \le 15$	$0 \le h \le 15$
	$-21 \le k \le 21$	$-40 \le k \le 40$
	$-6 \le l \le 6$	$-6 \le l \le 6$
Reflections collected	4349	8352
Independent reflections	2845	3118
Observed reflections	2721	2791
[$\lvert F_o \rvert > 3\sigma(F_o)$]		
Solution and refinement		
Weighting scheme, w^{-1}	c	c
No of parameters refined	191	280
Final R, R_w	0.055, 0.065	0.070, 0.079
Goodness of fit	0.37	0.49

Table 4.2. Structure determination summary*(continued(2))

	EOSTAu(CN)$_2$	EOST
Crystal data		
Empirical formula	$Se_2S_6C_{12}N_2OH_8Au$	$Se_2S_6C_{10}OH_8$
Formula weight, M	743.54	494.45
Crystal color, habit	black plate	orange plate
Crystal size/mm	0.30 × 0.10 × 0.01	0.15 × 0.30 × 0.10
Crystal system	Monoclinic	Monoclinic
Space group	$P2_1/c$	$P2_1/c$
a/Å	14.116(9)	6.745(1)
b/Å	10.338(5)	14.151(2)
c/Å	14.380(9)	17.109(2)
β/°	116.64(5)	110.02(9)
V/Å^3	1876(2)	1534.2(6)
Z	4	4
D_{calc}/Mgm^{-3}	2.659	2.141
μ/cm^{-1}	123.198	55.43
F(000)	1380	960
Data collection		
Scan width, A	1.93[a]	1.05[b]
2θ max/°	50.0	55.0
Index ranges	$-16 \le h \le 16$	$-8 \le h \le 0$
	$0 \le k \le 12$	$-18 \le k \le 0$
	$0 \le l \le 17$	$-21 \le l \le 21$
Reflections collected	3672	4001
Independent reflections	3525	3700
Observed reflections	2638	2198
[$\lvert F_o \rvert > 3\sigma(F_o)$]		
Solution and refinement		
Weighting scheme, w^{-1}	d	$4\lvert F_o \rvert^2/\sigma^2(F_o)$
No of parameters refined	198	196
Final R, R_w	0.070, 0.093	0.044, 0.053
Goodness of fit	1.07	1.72

* Details in common: Rigaku automated four-circle diffractometer AFC-6 [I_3, IBr_2 and $Au(CN)_2$ salts] or AFC-5R (I_2Br, ICl_2 salts and neutral molecule); Mo K_α radiation (λ = 0.7107 Å); graphite monochromator; 296±1 K; ω–2θ scans; ω scan speed 8° min^{-1} (except for neutral: 4° min^{-1}); three standard reflections every 100 [I_3, IBr_2 and $Au(CN)_2$ salts] or every 150 (I_2Br, ICl_2 salts and neutral molecule); refinement by block-diagonal least-squares (except for neutral: full-matrix least-squares) minimizing $\Sigma w (\lvert F_o \rvert - \lvert F_c \rvert)^2$; [a] $\Delta\omega = A + 0.50 \tan\theta$ [b] $\Delta\omega = A + 0.30 \tan\theta$ [c] $\lvert F_0 \rvert < 30.0$, $w^{-1} = 20.0 + 0.01 \lvert F_0 \rvert^2$; $\lvert F_0 \rvert \ge 30.0$, $w^{-1} = \sigma^2(F_0) + 0.01 \lvert F_0 \rvert^2$ [d] $\lvert F_0 \rvert < 20.0$, $w^{-1} = 15.0 + 0.005 \lvert F_0 \rvert^2$; $\lvert F_0 \rvert \ge 20.0$, $w^{-1} = \sigma^2(F_0) + 0.005 \lvert F_0 \rvert^2$

As for α-EOST$_2$IBr$_2$ and I$_2$Br salt, which were found by X-ray to be isostructural with the I$_3$ salt, the atomic parameters of the I$_3$ salt were used for the refinement. All were refined by the block-diagonal least-squares method using unique reflections of $|F_o| > 3\sigma(F_o)$ except for the neutral EOST, which was refined by the full-matrix least-squares method. Atomic scattering factors were taken from ref. [11]. All non-hydrogen atoms were refined with anisotropic thermal parameters except for the light atoms of the $Au(CN)_2^-$ ion which were refined with isotropic thermal parameters. Some hydrogen atoms were found on D-maps, other hydrogen atoms were located at the calculated positions with $B_{iso} = 4.0$ Å^2. The charge-transfer salts computation was carried out by using the UNICS III program package [12] and HITACHI M-680H computer at The Computer Centre of The University of Tokyo, while all calculation were performed using the TEXSAN [13] on neutral EOST.

Resistivity Measurements

The electrical resistivities were measured by a conventional four-probe method. The electrical contacts on the sample are made with 15 μm gold wires attached to the crystal with gold conducting paste. The typical dimension of the sample was *ca.* 0.4 mm along the needle axis.

4-3. Results and Discussion

Syntheses

The synthesis of EOST, as depicted in Scheme 4.2, was achieved in two ways; the cross-coupling of **2** and **4** or of **3** and **4**. EOST and two self-coupling compounds formed as by-products are quite different from each other in properties such as colour, crystal habit and solubility, which permits easy separation. Yet method A is more convenient for obtaining EOST in high yield. The solubility in the usual polar solvents was improved relative to the original symmetrical donors. After various conditions of electrocrystallization were examined with various counter-anions, very thin needls were obtained in some cases: the voltage between cathode and anode was found to be a more important factor than the current or the solubility. Black thick needles of *ca.* 0.4 mm length of the I$_3$ salt were obtained by the galvanostatic (0.8 μA) electrolysis of EOST (10 mg) with $(C_4H_9)_4NI_3$ (66 mg) in trichloroethane (20 mL) at 20 °C for 1 week. Au(CN)$_2$ salt was collected as curved thin needles by the electrolysis of EOST in THF at 20 °C. When THF–C_6H_5Cl (*ca.* 1:1 – 2:1) or THF–CS_2 (3:1) was used as solvent instead of THF alone a mixture of curved thin needles and thick needles was produced regardless of the potential or the current. Two kinds of AuBr$_2$ salts crystallized depending on the electrolytic conditions. One (α - phase) was obtained by electrolysis in

chlorobenzene with a constant current, 1.5 μA. It consisted of elongated plates with the dimensions *ca.* 1 × 0.1 mm^2. The other (β - phase) was obtained by electrolysis in THF and consisted of thin needles. The voltage between anode and cathode was kept constant at 6.9 V. ICl$_2$ salt was obtained after galvanostatic electrolysis of the donor with a current of 1.5 μA in chlorobenzene for nine days. IBr$_2$ salt was collected in two different phases. One { α - (EOST)$_2$IBr$_2$) ; galvanostatic (1.0 μA) electrolysis in C_6H_5Cl } consisted of shiny square plates, with typical dimension of 4 × 2 mm^2 and the other { β - phase; galvanostatic (1.5 μA) electrolysis in C_6H_5Cl } consisted of elongated plates. The I$_2$Br salt was prepared as black shiny plates by galvanostatic (1.0 μA) electrolysis in C_6H_5Cl .

Electrical Properties of EOST salts

Figure 4.1 shows the temperature dependence of the electrical resistivity of (EOST)$_2$I$_3$. The room-temperature conductivity is *ca.* 40 S·cm^{-1}, which is comparable to the isostructural salt (EOTT)$_2$IBr$_2$ [4]. However, the behaviour of the EOST salt presents an important contrast to the EOTT salt below *ca.* 150 K; the resistivity of the former decreases monotonically down to 4.2 K while the latter has two anomalies. (EOTT)$_2$IBr$_2$ slowly reduces the resistivity (with a small hump around 100 K) down to 15 K where the resistivity saturates and make an upturn. A similar anomaly was found for some other EOTT salts with linear anions [4, 14] but the origin of the anomaly remains to be clarified. Still, the metal instability were actually suppressed in (EOST)$_2$I$_3$.

As shown in Figure 4.2, Au(CN)$_2$ salt exhibited metallic properties down to *ca.*40 K. The room temperature conductivity (σ_{RT}) lies between 15 and 40 S·cm^{-1}. Although the metal–insulator (MI) transitions of the salt was very clear, the transition temperature ($T_{M\text{-}I}$ ≈ 35–40 K) could not be determined clearly for the crystal was especially fragile below 70 – 80 K and had some sample-dependence. The Au(CN)$_2$ salt was found to have another morphology that has a 1:1 ratio of the component. This salt was an insulator.

The α-AuBr$_2$ salt retained metallic conductivity down to 4 K, while the β-AuBr$_2$ salt exhibited sharp MI transition at 28 K (see Figure 4.3). Both σ_{RT} lie around 60 S·cm^{-1}.

The σ_{RT} of the ICl$_2$ salt is *ca.* 60 – 290 S·cm^{-1} and the salt retains its metallic property down to 4 K as shown in Figure 4.4.

α - (EOST)$_2$IBr$_2$ maintained its metallic property down to 4 K, while the β-salt manifested its metallic property down to 27 K, where a clear MI transition occurred (see Figure 4.5). Each σ_{RT} is *ca.* 80 and 100 – 140 S·cm^{-1}, respectively.

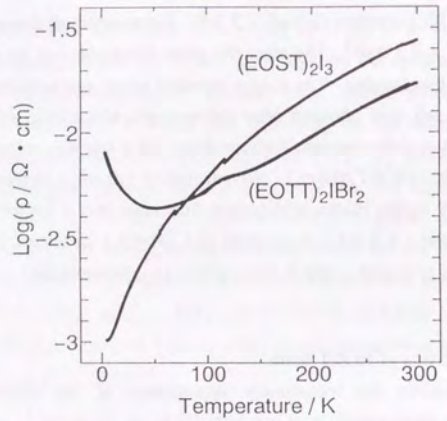

Figure 4.1. Temperature dependence of electrical resistivity (ρ) of $(EOST)_2I_3$ (this work) and $(EOTT)_2IBr_2$ [14]

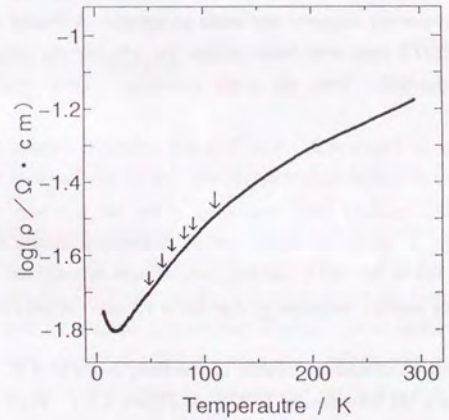

Figure 4.2. Temperature dependence of electrical resistivity (ρ) of the $Au(CN)_2$ salt (metallic phase) of EOST Arrows indicate the insignificant jump in the original data probably due to the micro-cracks in the crystal or some trouble in the contacts, which have been connected by translation.

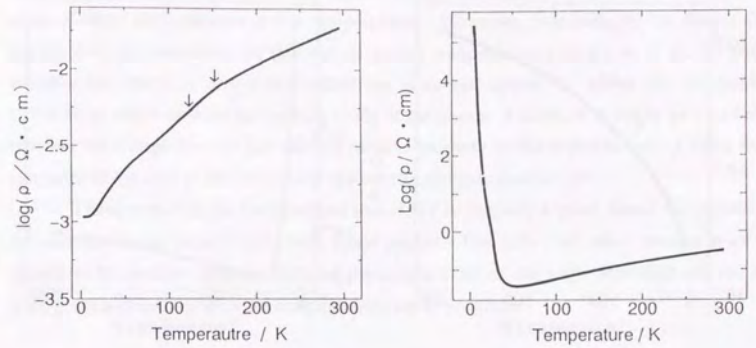

(a) **(b)**

Figure 4.3. Temperature dependence of electrical resistivity (ρ) of the $AuBr_2$ salt of EOST; (a) α−phase; (b) β−phase Arrows indicate the insignificant jump in the original data probably due to the micro-cracks in the crystal or some trouble in the contacts, which have been connected by translation.

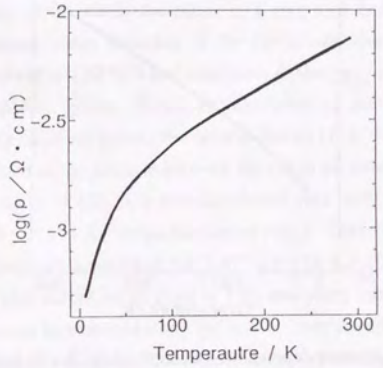

Figure 4.4. Temperature dependence of electrical resistivity (ρ) of $(EOST)_2ICl_2$

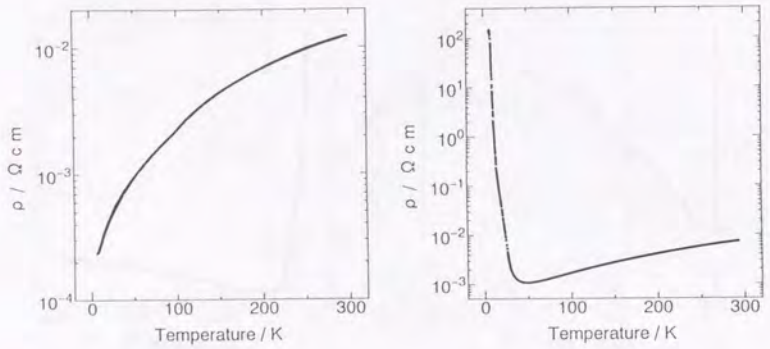

Figure 4.5. Temperature dependence of electrical resistivity (ρ) of the IBr_2 salt of EOST; (a) α–phase; (b) β–phase

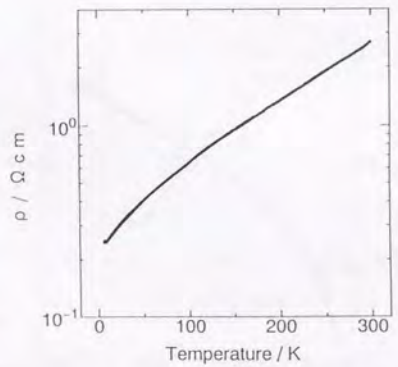

Figure 4.6. Temperature dependence of electrical resistivity (ρ) of $(EOST)_2I_2Br$

I_2Br salt had σ_{RT} of *ca.* 60 $S \cdot cm^{-1}$. In this salt, the unsymmetrical anion ($I\text{-}I\text{-}Br^-$) introduces the disorder at the anion site in the crystal. As for the metallic conductivity, many organic salts including the asymmetric anions have been reported to date [19] and most of them are insulators at low temperatures. However, interestingly, as shown in Figure 4.6, the resistivity of this salt decreased monotonically down to 4 K. Thus, whether the anion is unsymmetrical or not does not appear to affect the electronic structure so much as does the packing mode of the donor. Therefore it might be true that whether the charge-transfer salt exhibits metallic property or not depends mostly upon the character of the donor; the inclination of how to aggregate themselves.

These experimental facts indicate that EOST is certainly a good donor for yielding the metallic charge-transfer salts with linear anions. The salts with other counter anions remain to be studied; measurements of the conductivity of the salts described above, at high pressures and/ or at lower temperatures, are in progress.

Molecular and Crystal Structures of EOST

The molecular and crystal structure of neutral EOST is displayed in Figure 4.7. EOST takes the dimerized structure in the neutral state. The dimers are arranged orthogonal to neighboring dimers and form layers in the *bc* plane. The unit cell contains one crystallographically independent molecule at the general position. This is isostructural to EOTT [4], BETS [1], BEDT-TTF [16] and other similar donors [17]. In the dimer the EOST molecule overlaps the other in a head-to-tail manner with gliding along its long axis. The overlapping mode within the dimer is a ring-over-bond type. The donor molecule is fairly warped; mean deviation of the central diselenadithiaethylene moiety from the least-square plane is 0.0270 Å and maximum deviation is 1.21 Å observed at the carbon atom of the ethylene group. These characteristics of the molecular and crystal structure are commonly observed among the neutral donors [1, 4, 16-18]. The diameters of the heterorings defined as the distance between the sulfur or selenium atoms are 3.477 Å (six-membered ring), 3.175 Å (five-membered ring with Se), 2.977 (five-membered ring with S), 3.395 Å (seven-membered ring). Therefore the ratios between the diameters of the outer and inner rings are 3.477 / 3.175 = 1.10 and 3.395 / 2.977 = 1.14, respectively. These values are so close to 1.00 that many intermolecular chalcogen-chalcogen interactions can be expected along the side-by-side directions [19]. Actually in spite of the short intradimer distance (3.45 Å), the short contacts between chalcogen atoms (S---S ≤ 3.70 Å, S---Se ≤ 3.85 Å, Se---Se ≤ 4.00 Å) are observed more often between dimers than within a dimer. There is no disorder at the ethylene nor oxatrimethylene groups.

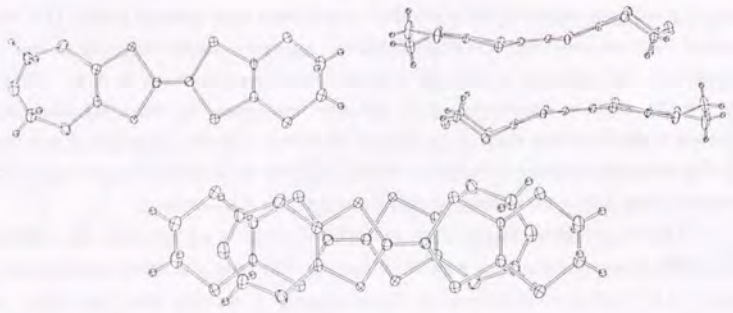

(a)

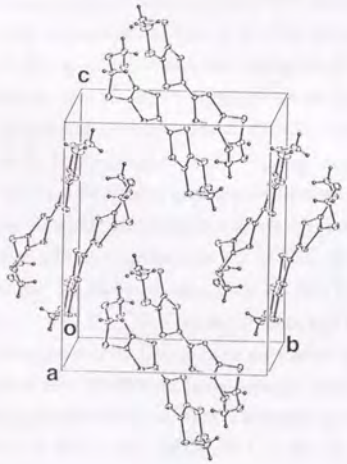

(b)

Figure 4.7. (a) Molecular structure and overlapping mode and (b) crystal structure of EOST

Molecular and Crystal Structures of (EOST)$_2$I$_3$

Figure 4.8(b) shows the crystal structure of (EOST)$_2$I$_3$. The crystal data together with those of other salts are summarized in Table 4.2. The tables of anisotropic thermal parameters, mean square displacement tensor of atoms and final atomic positional parameters with thermal parameters for the salts described herein are deposited.¶ The unit cell contains two EOST molecules at the general positions and the I_3 molecule on the inversion centre. No disorder was observed in the anion. The donor molecules stack along the *c* axis to make a columnar structure, which is isostructural to (EOTT)$_2$IBr$_2$ [4]. The interplanar separation is 3.68 Å, which is almost comparable to those of the isostructural EOTT salts; 3.63 Å for (EOTT)$_2$I$_3$ [14], 3.62 Å for (EOTT)$_2$IBr$_2$ [4], (EOTT)$_2$AuI$_2$ [4] and (EOTT)$_2$AuBr$_2$ [14], 3.61 Å for (EOTT)$_2$ICl$_2$ [14]. The EOST molecule is almost planar except for the ethylene and oxatrimethylene groups. The carbon atoms of the ethylene group have large thermal parameters but no conformational disorder was found. The oxatrimethylene group stands nearly upright on the molecular plane, which increases steric repulsion and hinders the maximal overlap of the π -conjugated system between the neighboring molecules. In fact they stack in such a way that one molecule glides not only along its long axis but also along the short axis above the neighboring molecule. Such an overlapping mode is also found in the series of EOTT salts and contrasts with the neutral EOST. This characteristic molecular structure results in an unusual network of intermolecular interaction where the short chalcogen-chalcogen contacts are observed more often between the neighboring two donors in different columns rather than in the same column. Besides these interactions there was also found the short contact between donor and anion (C-H---I), which some researchers find important in the case of BEDT-TTF salts [20]. Another characteristic of the stacking mode is that the unsymmetrical donors are all oriented in the same direction in the column as shown in Figure 4.8(b). In most of the unsymmetrical donor salts reported to date, the donor molecules stack alternately in a head-to-tail manner within the column [21]. A stacking mode similar to that of (EOST)$_2$I$_3$ was also found in (EOTT)$_2$I$_3$ [14], (EOTT)$_2$IBr$_2$ [4], (EOTT)$_2$ICl$_2$ [14], (EOTT)$_2$AuI$_2$ [4] and (EOTT)$_2$AuBr$_2$ [14]. (EOST)$_2$I$_3$, however, is expected to have smaller anisotropy than these isostructural EOTT salts, judging from the chalcogen-chalcogen contacts (see below) and the fact that the former turned out to be a more stable metal than the latter.

Electronic Structures of (EOST)$_2$X { X = I$_3$, IBr$_2$ (α– type), I$_2$Br and ICl$_2$ }

For estimation of the differences between (EOST)$_2$I$_3$ and the isostructural EOTT salts, the overlap integrals and tight-binding band structure may be convenient tools. The calculated overlap integrals of I_3 salt are summarized together with the arrangement of the

¶ Deposited at the Cambridge Crystallographic Data Centre.

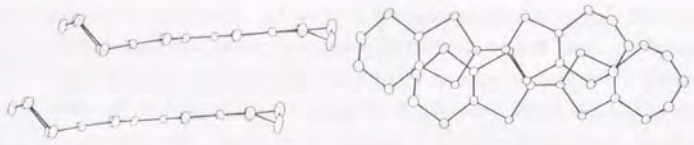

(a)

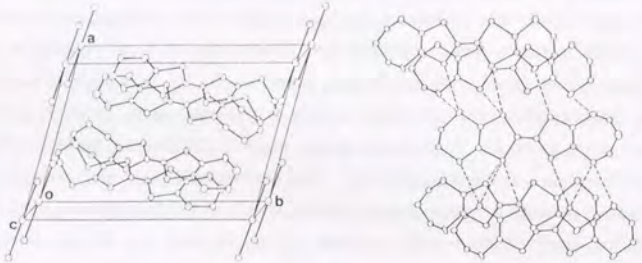

(b)

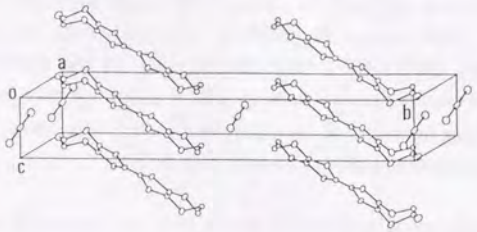

(c)

Figure 4.8. (a) Molecular structure and overlapping mode and (b) crystal structure of $(EOST)_2I_3$ Broken lines indicate the short contacts between chalcogen atoms. (c) Crystal structure of $(EOST)_2ICl_2$

donor molecules with the corresponding suffixes in Figure 4.9(a). Similar calculations on the other salts showed that all these salts have a similar band structure, which is consistent with their similar electrical behavior. As mentioned before, adding to the sulphur atoms, the selenium atoms in EOST take part in the short contacts including those not present in the EOTT salts. With respect to the value of the overlap integrals, the general trend, for example those with suffixes a1 and a2 are dominant, is much the same as for the corresponding EOTT salts. However, the donor molecules have larger overlaps in every direction in EOST salts than in EOTT salts [14]. The previous band calculation on $(EOTT)_2IBr_2$ [4] had revealed that the salt has a quasi-one-dimensional open Fermi surface and that the donors interact strongly nearly perpendicular to the stacking axis, *i.e.* in a side-by-side direction. As for the Fermi surface of $(EOST)_2I_3$ shown in Figure 4.10, the curvature is in substantial agreement with that of $(EOTT)_2IBr_2$ [4, 14]. It was also tried to calculate the band strucutre where the d orbitals of the sulphur and selenium atoms were taken into consideration. The resultant overlap integrals are variable depending on the parameters of the d orbitals. Using the latter overlap integrals, again obtained were similar Fermi surfaces in regard to $(EOTT)_2IBr_2$ [14] and $(EOST)_2I_3$. Therefore the parameters of the d orbitals of chalcogen atoms remain to be settled; however, at this stage it could be safely concluded that all the isostructural salts of EOST in question and $(EOTT)_2IBr_2$ [14] have the similar electronic structure at least qualitatively, and that small additional intracolumnar interactions would effect the electronic structure and thus could lead to such a quantitative difference in the stability of the metallic properties as mentioned above.

Crystal Structures of $(EOST)Au(CN)_2$ and $(EOST)_2X$ { X = IBr_2 (α– type), I_2Br and ICl_2 }

With respect to the crystal structure of the $Au(CN)_2$ salts only the insulating phase has been clarified and is depicted in Figure 4.11. The unit cell contains four EOST and four $Au(CN)_2$ molecules, all of them on the general positions. In this salt a pair of EOST cations are arranged face to face to make the dimeric cation sheet in *bc* plane and the dimer is seperated by a pair of $Au(CN)_2^-$ ions located in the same sheet to reduce the strong Coulombic repulsion between EOST cations. There is no column or sheet which makes the conduction path, so such a structure leads to insulating behavior. In contrast to the case of the I_3 salt, two donors of $Au(CN)_2$ salt directly overlap each other in a head-to-tail manner within the dimer. Another difference from the I_3 salt is that both ethylene and oxatrimethylene groups extend toward the outside so the two molecules appear to bend away from each other.

The ICl_2 salt is isostructural to the I_3 salt as well as α - $(EOST)_2IBr_2$ and $(EOST)_2I_2Br$ (see Table 4.2 and Figures 9 and 10). Accordingly all the features of the

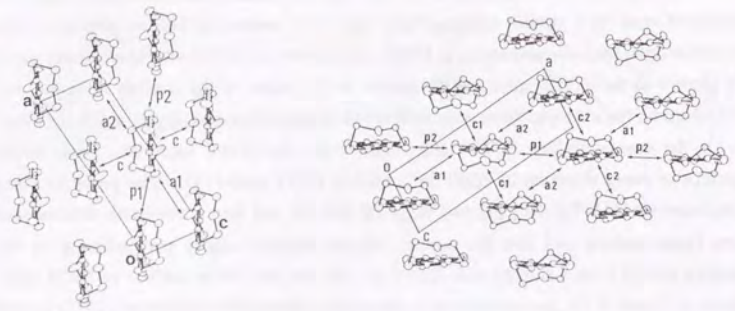

Figure 4.9. Donor arrangement (a) in $(EOST)_2I_3$, α-$(EOST)_2IBr_2$, $(EOST)_2I_2Br$, and (b) in $(EOST)_2ICl_2$ For $(EOST)_2I_3$, c = – 4.21, p_1 = – 4.27, p_2 = – 3.83, a_1 = 15.54 and a_2 = 13.15; for α-$(EOST)_2IBr_2$, c = 4.39, p_1 = – 23.62, p_2 = – 15.41, a_1 = 43.12 and a_2 = 36.60; for $(EOST)_2I_2Br$, c = 3.22, p_1 = – 21.60, p_2 = – 14.89, a_1 = 41.19 and a_2 = 31.83

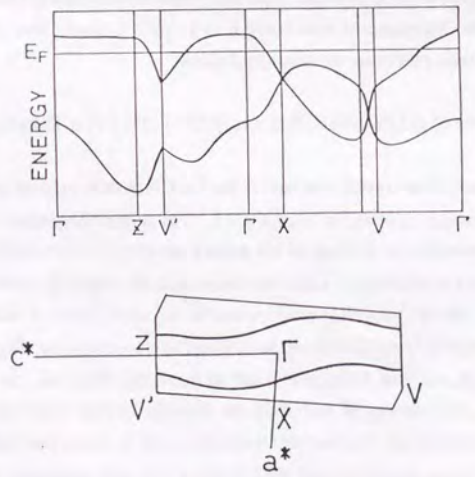

Figure 4.10. Energy band structures of $(EOST)_2I_3$ Present band structure results from the transfer integrals where d orbitals of the sulfur and selenium atoms not accounted for in the calculation. See text.

crystal and molecular structures found for the I_3 salt are also found for the latter two salts. However, the length of the *b* axis of the ICl_2 salt, whose direction is along the long axis of the donor, is double the others. Because there appears to be little interaction between the donor molecules through the anion sheet along this direction, it can be explained why the doubling of the *b* axis does not destroy the metallic electronic structure of the salt. The interplanar distances are 3.690 Å { $(EOST)_2I_2Br$ }, 3.623 Å, 3.531 Å { $(EOST)_2ICl_2$ }, 3.684 Å { α - $(EOST)_2IBr_2$ }. The ICl_2 salt has two crystallographically independent columns of regularly stacking donor molecules and both of these have smaller interplanar distances than those of the other salts. This close stacking, however, again hardly influences the electronic structure of the salt since the band structure depends mainly upon the interactions a1 and a2, as suggested by the calculation mentioned above. The ICl_2, α - IBr_2 and I_2Br salts essentially share the molecular arrangement, intermolecular interactions and thus electronic structures of the I_3 salt.

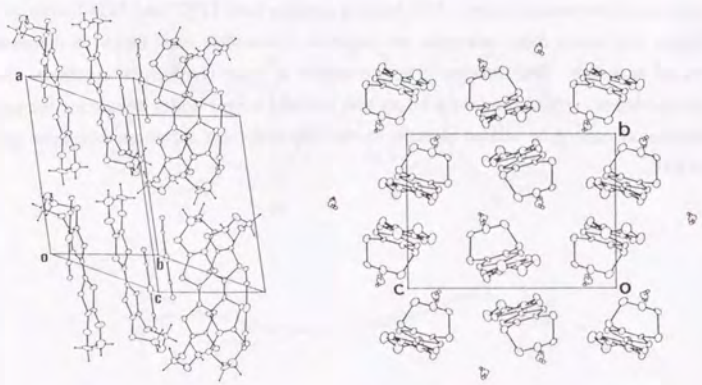

Figure 4.11. Crystal structure of $(EOST)Au(CN)_2$

Comparison of EOST Salts with EPST Salts

The donor EPST {4,5-ethylenedithio-4',5'-(2-propylenedithio)-diselenadithiafulvalene} has been newly synthesized† for comparison of the properties of the cation radical salts with those of the EOST salts. The synthesis of the donor and its radical salts are much the same with those of EOST. The neutral crystal of EPST is identical (vermilion blocks) and isostructural to that of EOST (Figure 4.12). Although the molecular structures resemble each other and electrolytic condition in the preparation of the salts does not differ from each other very much, the crystal structures and eletrical properties of the trihalides of EPST clearly differ from those of EOST (Figure 4.13). All the EPST salts of I_2Br, IBr_2, ICl_2 and I_3 exhibited almost temperature-independent resistivities with identical behavior to each other down to *ca.* 100 K and they rapidly increased the resistivities at lower temperature. From the X-ray photographs they were all found to be isomorphous with α-$BETS_2I_3$ instead of the EOST trihalides. Such a small modfication as the substitution of the methylene group for the oxygen atom resulted in an overall alteration of a donor arrangement and thus the property of the charge-transfer salts. A similar case was reported where relatively small modification of a donor molecule can lead to new structure types rather than simple expansions or contractions of the known structures [22 (d)]. The additional information such as crystal structures of the salts of the all-sulfur analog, EPT [22], and the related symmetrical donor OTT [5] are desired to discuss further details, but unfortunately there are few reports concerning the single crystal data of them. The only one [22 (d)] tells that some EPT salts have dimerized stacking structures where the dimers are linked in a side-by-side fashion to form one-dimensional chains. This trend resembles both EPST and EOST salts to some degree and much more examples are required to elucidate each factor to dominate the crystal structure. The situation is not so simple as some researchers conceived that the bulkier donors would produce a larger unit cell and longer donor distances, for unit cell dimension cannot be related directly to the intermolecular distances nor their packing motiv.

† Elemental analysis: $C_{11}H_{10}S_6Se_2$ calculated (%) H: 2.05, C: 26.81; found (%) H: 2.20, C: 27.68. Crystal data: monoclinic, $P2_1/c$, a = 6.781, b = 14.603, c = 17.167 Å, β = 110.62 °, V = 1591.1 $Å^3$, Z = 4.

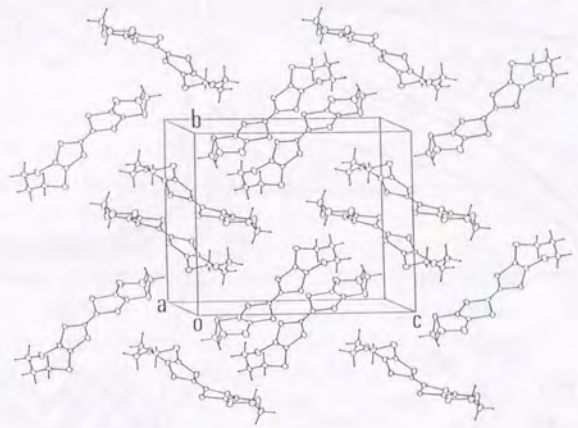

(a)

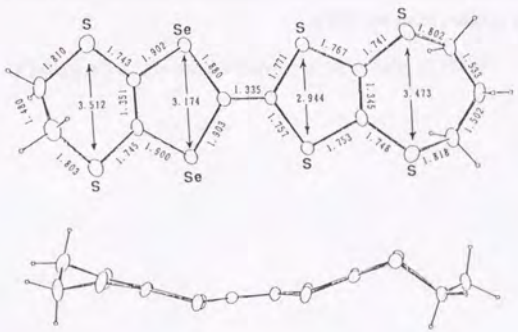

(b)

Figure 4.12. (a) Crystal structure and (b) molecular structure of EPST

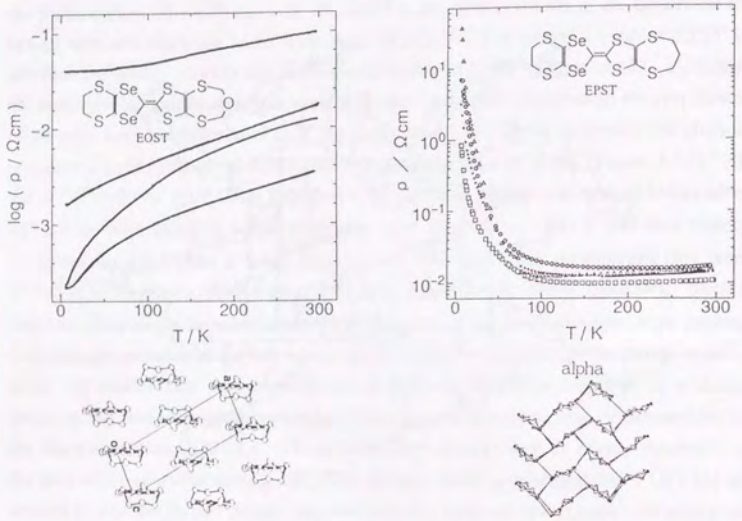

(a) **(b)**

Figure 4.13. (a) Electrical behavior of trihalide salts of EOST and (b) EPST Structural scheme in (b) is taken from ref. [23].

Other EOST salts

Some other anion salts of EOST were also synthesized by a similar electrochemical procedure and the BF_4, ClO_4, ReO_4 and PF_6 salts were obtained, whose electrical behavior is displayed in Figure 4.14. They are all semiconductors; activation energies are 0.04 (ClO_4 salt), 0.03 (BF_4 salt) and 0.01 eV (PF_6 salt), respectively except for the ReO_4 salt (insulator) and did not examined in further detail such as X-ray structural study.

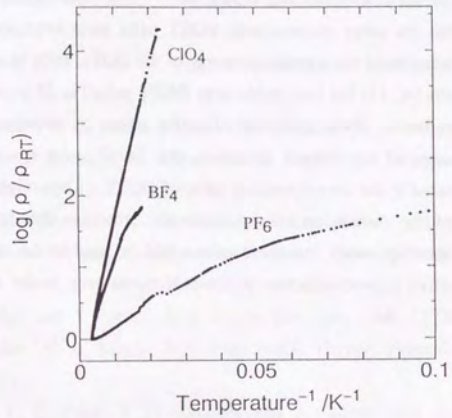

Figure 4.14. Electrical behavior of some salts of EOST

4-4. Summary

As a first step to develop an organic superconductor based on a new donor, EOST and its charge-transfer salts were synthesized. The electrical resistivity of $(EOST)_2I_3$, α-$(EOST)_2IBr_2$, $(EOST)_2ICl_2$, $(EOST)_2I_2Br$ and the α-type $AuBr_2$ salt decrease monotonically down to 4 K. All but the last were found to be isostrucural with $(EOTT)_2I_3$ [14], $(EOTT)_2IBr_2$ [4], $(EOTT)_2ICl_2$ [14], $(EOTT)_2AuI_2$ [4] and $(EOTT)_2AuBr_2$ [14]. Another phase of both the IBr_2 and $AuBr_2$ salts exhibited a clear metal-insulator transition at *ca.* 27 – 28 K. The tight-binding band calculation suggested that $(EOST)_2I_3$ has an open quasi-one-dimentional Fermi surface, *i.e.* has a similar electronic structure to the corresponding EOTT salts. The calculation of their overlap integrals showed that the other isostructural EOST salts also have simillar electronic structures. On the other hand the metallic property of the EOST salts in question is more stable than EOTT salts [4, 14] but less stable than BETS salts [1, 2] as evidenced by the conductivity measurements. By replacement of sulfur atoms by selenium atoms without any unexpected change of the crystal structure, the EOST salts reached more stable metallic states compared to the corresponding salts of EOTT. This might be an example where the control of the dimension of the electronic structure through the molecular structure could be accomplished. All these salts could be said to be sufficiently stable metals to be prospective superconductors at lower temperatures, under some pressure if necessary.

References

[1] R. Kato, H. Kobayashi and A. Kobayashi, *Synth. Metals*, **41-43**, 2093(1991).

[2] (a) T. Naito, A. Miyamoto, H. Kobayashi, R. Kato and A. Kobayashi, *Chem. lett.*, **1991**, 1945;
(b) L. K. Montgomery, T. Burgin, J. C. Huffman, K. D. Carlson, J. D. Dudek, G. A. Yaconi, L. A. Megna, P. R. Mobley, W. K. Kwok, J. M. Williams, J. E. Schirber, D. L. Overmyer, J. Ren, C. Rovira, M. -H. Whangbo, *Synth. Metals*, **55-57**, 2090(1993).

[3] (a) H. Kobayashi, T. Udagawa, H. Tomita, K. Bun, T. Naito, A. Kobayashi, *Chem. Lett.*, **1993**, 1559;
(b) H. Kobayashi, H. Tomita, T. Naito, H. Tanaka, A. Kobayashi and T. Saito, submitted to *J. Chem. Soc., Chem. Commun.*

[4] (a) H. Nakano, K. Yamada, T. Nogami, Y. Shirota, A. Miyamoto and H. Kobayashi, *Chem. Lett.*, **1990**, 2129;
(b) H. Nakano, Ph. D. Thesis (Osaka University, 1991).

[5] H. Nakano, S. Ikenaga, K. Miyawaki, K. Yamada, T. Nogami and Y. Shirota, *Synth. Metals*, **41-43**, 2409(1991).

[6] (a) G. G. Abashev and V. S. Russkikh, *Zh. Org. Khim.*, **23**, 1569(1987);
(b) V. S. Russkikh and G. G. Abashev, *Khim. Geterotsikl. Soedin.*, **1987**, 1438;
(c) H. Müller and Y. Ueba, *Bull. Chem. Soc. Jpn.*, **66**, 1773(1993).

[7] G. Steimecke, H. -J. Sieler, R. Kirmse and E. Hoyer, *Phosphorous and Sulfur*, **7**, 49(1979).

[8] S. R. Buc, C. C. Price, F. D. Brutcher and J. Cohen, *Org. Synth.*, Col. Vol., **IV**, 101(1963).

[9] D. D. Perrin and W. L. F. Armarego, *Purification of Laboratory Chemicals* (Pergamon Press, New York, 3rd edn., 1988.)

[10] (a) G. Germain, M. M. Woolfson, *Acta Crystallogr.*, **B24**, 91(1968);
(b) G. Germain, P. Main and M. M. Woolfson, *Acta Crystallogr.*, **B26**, 274(1970).

[11] *International Tables for X-Ray Crystallography*, Kynoch Press, Bermingham, vol. IV(1974).

[12] T. Sakurai and K. Kobayashi, *Rep. Inst. Phys. Chem. Res.*, **55**, 69(1979).

[13] TEXSAN - TEXRAY Structure Analysis Package, Molecular Structure Corporation (1985).

[14] A. Tateno, T. Udagawa, T. Naito, H. Kobayashi, A. Kobayashi and T. Nogami, *J. Mater. Chem.*, **4**(10), 1559(1994).

[15] (a) H. Kobayashi, R. Kato, A. Kobayashi, G. Saito, M. Tokumoto, H. Anzai

and T. Ishiguro, *Chem. Lett.*, **1985**, 1293;
(b) T. J. Emge, H. H. Wang, M. A. Beno, P. C. Leung, M. A. Firestone, H. C. Jenkins, J. D. Cook, K. D. Carlson, J. M. Williams, E. L. Venturini, L. J. Azevedo and J. E. Schirber, *Inorg. Chem.*, **24**, 1736(1985);
(c) D. Zhu, P. Wang, M. Wan, Z. Yu and N. Zhu, *Solid State Commun.*, **57**, 843(1986);
(d) H. Kobayashi, R. Kato, A. Kobayashi, G. Saito, M. Tokumoto, H. Anzai and T. Ishiguro, *Chem. Lett.*, **1986**, 93;
(e) T. J. Emge, H. H. Wang, P. C. W. Leung, P. R. Rust, J. D. Cook, P. L. Jackson, K. D. Carlson, J. M. Williams, M. -H. Whangbo, E. L. Venturini, J. E. Schirber, L. J. Azevedo and J. R. Ferraro, *J. Am. Chem. Soc.*, **108**, 695(1986);
(f) A. Ugawa, K. Yakushi, H. Kuroda, A. Kawamoto and J. Tanaka, *Chem.. Lett.*, **1986**, 1875;
(g) A. Ugawa, K. Yakushi, H. Kuroda, A. Kawamoto and J. Tanaka, *Synth. Metals*, **22**, 305(1988);
(h) U. Geiser, B. Anderson, A. Murray, C. M. Pipan, C. A. Rohl, B. A. Vogt, H. H. Wang and J. M. Williams, *Mol. Cryst. Liq. Cryst.*, **181**, 105(1990).

[16] H. Kobayashi, A. Kobayashi, Y. Sasaki, G. Saito, H. Inokuchi, *Bull. Chem. Soc. Jpn.*, **59**, 301(1986).

[17] (a) A. M. Kini, M. A. Beno and J. M. Williams, *J. Chem. Soc., Chem. Commun.*, **1987**, 335;
(b) A. M. Kini, T. Mori, U. Geiser, S. M. Budz and J. M. Williams, *J. Chem. Soc., Chem.. Commun.*, **1990**, 647.

[18] (a) C. Katayama, M. Honda, H. Kumagai, J. Tanaka, G. Saito and H. Inokuchi, *Bull. Chem. Soc. Jpn.*, **58**, 2272(1985);
(b) S. Matsumiya, A. Izuoka, T. Sugawara, T. Taruishi and Y. Kawada, *Bull. Chem.. Soc. Jpn.*, **66**, 513(1993).

[19] R. Kato, A. Kobayashi, Y. Sasaki and H. Kobayashi, *Chem. Lett.*, **1984**, 993.

[20] (a) P. C. W. Leung, T. J. Emge, M. A. Beno, H. H. Wang, J. M. Williams, V. Petricek and P. Coppens, *J. Am. Chem. Soc.*, **107**, 6184(1985);
(b) T. J. Emge, H. H. Wang, P. C. W. Leung, P. R. Rust, J. D. Cook, P. L. Jackson, K. D. Carlson, J. M. Wiliiams, M. -H. Whangbo, E. L. Venturini, J. E. Schirber, L. J. Azevedo and J. R. Ferraro, *J. Am. Chem. Soc.*, **108**, 695(1986);
(c) M. -H. Whangbo, J. M. Wiliiams, A. J. Schultz, T. J. Emge and M. A. Beno, *J. Am. Chem. Soc.*, **109**, 90(1987);

(e) D. Jung, M. Evain, J. J. Novoa, M. -H. Whangbo, M. A. Beno, A. M. Kini, A. J. Schultz, J. M. Wiliiams and P. J. Nigrey, *Inorg. Chem.*, **28**, 4516(1989);
(f) U. Geiser, A. J. Schultz, H. H. Wang, D. M. Watkins, D. L. Stupka, J. M. Wiliiams, J. E. Schirber, D. L. Overmyer, D. Jung, J. J. Novoa and M. -H. Whangbo, *Physica C*, **174**, 475(1991).

[21] (a) P. Delhaes, C. Coulon, J. Amiell, S. Flandrois, E. Torreilles, J. M. Fabre and L. Giral, *Mol. Cryst. Liq. Cryst.*, **50**, 43(1979);
(b) K. Kikuchi, M. Kikuchi, T. Namiki, K. Saito, I. Ikemoto, K. Murata, T. Ishiguro and K. Kobayashi, *Chem. Lett.*, **1987**, 931;
(c) G. C.Papavassiliou, G. A. Mousdis, J. S. Zambounis, A. Terzis, A. Hountas, B.Hilti, C. W. Mayer and J. Pfeiffer, *Synth. Metals*, **27**, B379(1988);
(d) A. Terzis, A. Hountas and G. C.Papavassiliou, *Solid State Commun.*, **66**, 1161(1988);
(e) R. Kato, H. Kobayashi and A. Kobayashi, *Chem. Lett.*, **1989**, 781;
(f) L. Ducasse, A. Fritsch, D. Chasseau and J. Gaultier, *Synth. Metals*, **38**, 13(1990);
(g) J. S. Zambounis, C. W. Mayer, K. Hauenstein, B. Hilti, W. Hofherr, J. Pfeiffer, M. Bürkle and G. Rihs, *Adv. Mater.*, **4**, 33(1992);
(h) R. Kato, S. Aonuma, Y. Okano, H. Sawa, M. Tamura, M. Kinoshita, K. Oshima, A. Kobayashi, K. Bun and H. Kobayashi, *Synth. Met.*, **61**, 199(1993).

[22] (a) H. Tatemitsu, E. Nishikawa, Y. Sakata and S. Misumi, *J. Chem. Soc., Chem. Commun.*, **1978**, 18;
(b) A. M. Kini, S. F. Tytko, J. E. Hunt and J. M. Williams, *Tetrahedron Lett.*, **28**(36), 4153(1987);
(c) L. C. Porter, T. J. Allen, K. D. Carlson, M. Y. Chen, U. Geiser, H. -C. I. Kao, A. M. Kini, J. A. Schlueter, H. H. Wang and J. M. Williams, *Acta Crystallogr., Sect. C.: Cryst. Struct. Commun.*, **C44**(10), 1712(1988);
(d) A. J. Schultz, U. Geiser, A. M. Kini, H. H. Wang, J. Schlueter, C. S. Cariss and J. M. Williams, *Synth. Met.*, **27**, A229(1988).

[23] A. M. Kini, M. A. Beno, K. D. Carlson, J. R. Ferraro, U. Geiser, A. J. Schultz, H. H. Wang, J. M. Williams and M. -H. Whangbo, *The Physics and Chemistry of Organic Superconductors*, G. Saito and S. Kagoshima, Eds., Springer Proceedings in Physics, Vol. 51, Springer-Verlag Berlin, Heidelberg, p.334(1990).

Chapter 5.

A Pursuit of Novel Donor Capable of Providing Free Carriers with Localized Moments; Synthesis, Structures and Physical Properties of Charge Transfer Salts of Thiadiazoleethylenedithio-diselenadithiafulvalene (DED)

5-1. Introduction

The pursuit of organic (or more generally, molecular-based) conducting or magnetic materials is an important scientific subject of current interest [1]. In fact an increasing number of chemists, physicists, and theoreticians have entered the field of organic metals or organic ferromagnets over the last two decades. Although the large majority of ferromagnets are metallic compounds in inorganic species, by far the largest proportion of the organic magnets and those of the molecular conductors are chemically disparate. An organic compound with metallic conduction electrons and localized spins, where the two kinds of electrons come from the same molecule has never been reported. The magnetically ordered state and metallic state, of their own, are not necessarily incompatible with each other [2], and in fact a few examples have been reported in metallic organic charge-transfer salts containing transition metal ions [3, 4]. Yet some properties characteristic of organic compounds such as a large on-site Coulomb energy (strong correlation), strong electron-phonon interaction, small intermolecular interaction and large anisotropy (low dimensionality) often stand in the way when researchers design magnetic conducting materials using interactions between localized and delocalized (metallic) states instead of introducing transition metals.

In order to circumvent this problem the author has adopted a novel approach by exploring some molecule which is a combination of two parts corresponding two roles; one plays the role of a good donor which would make a stable metallic π-band in the solid state, and the other has a strong inclination for localizing an unpaired electron in one of its localized orbitals. Asymmetrical donors are very appropriate for such purpose. Yet the latter feature is generally unfavourable for a donor because such an inclination is prone to lower the donor ability and would make it a Louis base rather than an electron donor [5]. If the highest occupied non-bonding (n) orbital, which is a typical example of the localized orbital, in a molecule is HOMO and lies far (a few electron volts or more) above the other occupied orbitals, the cation radical salts of such a molecule may be an insulator because n orbital could not make a wide conduction band enough to stabilize

the metallic property [6]. On the contrary, if the HOMO consists chiefly of π-orbitals and lies far above the highest occupied n orbital, the cation radical salts of such a molecule may be a usual organic conductor without a localized spin; most of the well-known BEDT-TTF salts are the case [1 (a) – (d), 7]. Therefore the most difficult point of this work is how to reconcile the two apparently incompatible conditions in *the same* donor molecule. Direct incorporation, *i.e.* the condensation of the two moieties, whether the chemical species are groups or molecules, results in an unexpected reconstruction of the molecular orbitals as often as not. Another practical problem to overcome concerns the synthesis; many candidates for the spin-carrying moiety could not be expected to survive the usual reaction. So the selection of the candidate molecule is already a problem, though one can make an estimation from molecular orbital calculation to some degree.

By coupling a well-known stable radical and popular donor or acceptor molecules, a number of trials to reinforce an exchange interaction through delocalized π–conjugation in a molecular based system have ever been reported [1 (e) – (h)]. Many of them were expected an alignment of the spins by charge-transfer interaction and/or mediation by conduction electrons. In these systems, of course the interaction between the delocalized and localized electrons are important. Yet all of them have the spin-carrying part which is connected to the π–conjugation moiety by a σ–bond or more distant. Additionally they usually have bulky protecting groups such as tert-butyl group around the spin sources. Such situation often drives them out of coplanar molecular structures with respect to the two parts in question, which helplessly diminishes the intramolecular interaction, much less intermolecular interaction. As a result by far the majority of them have ended up with insulators even if they manage to succeed in ordering of the spins.

In the meantime, the heterocycles including alternate sulfur and nitrogen atoms and their isomers are often reported to be apt to become stable free radicals [8], where their unpaired electrons are believed to largely localize on the nitrogen atoms in some cases [8 (n) – (p)], while some are conceived to delocalize on the π-conjugating systems [8 (q) – (s)], and others are in intermediate situations. Previous studies on them out of various interests have revealed an extensive chemistry such as aromaticities [8 (t) (v)], cycloaddition or ring cleavage reactions [8 (w), (x)], isomerizations or rearrangements [8 (y), (z)], thermal and/or photochemical stabilities [8 (p), (u)] and electrochemical properties [8 (m)], which have proved that the family covers a variety of compounds from potentially good donors [9] to acceptors [10] as well as spin sources [11]. Such fascinating properties seems to be characteristic to them and hardly affected by the substituents [8 (s)], though some of them are rather small π-systems. These facts suggest that there could be a donor whose π-HOMO lies near one of the localized orbitals when an appropriate π-conjugated moiety is combined with one of such heterocycles. Such a donor could be expected to make a π–HOMO band broad enough to cover the

localized level and to interact with its resultant own localized spin in the charge-transfer salt.

In addition to the well-developed chemistry, the sulfur nitrogen heterocycles, as mentioned above, have many suitable characteristics for the "spin-carrying part"; the radicals are planar without bulky substituents as steric protection groups, which feature favors interaction between adjacent molecules and distinguishes them from other stable radicals [2 (c), 12]. In fact a number of short contacts have been observed between sulfur atoms of neighboring molecules or cation and anion [8(a), (f), (h), (l), (p), (q), 11].

On the other hand BETS { BETS = bis(ethylenedithio)tetraselenafulvalene } [3 (b) – (e), 13] has known to produce stable metallic charge-transfer salts very often [3 (b) – (e), 13 (b) – (g)], which characteristic has been utilized to realize organic metals with π–d interactions [3 (b) – (e)] or control of the dimensionality of the electronic and crystal structure of charge-transfer salts [14]. Therefore BETS moiety can be expected to play another important role; providing a metallic wide π–band in the solid state.

In the course of the pursuit of the aforementioned π-donor whose salts may be interesting from *both* viewpoints of the molecular conductors and the molecular magnets *at the same time*, there selected a thiadiazole-condensed BETS derivative: a new asymmetrical donor DED-STF. The chapter here reports the synthesis, structures, electrical and magnetic properties of the charge-transfer salts of a new donor; thiadiazoleethylenedithiodiselenadithiafulavalene, which is abbreviated as DED below.

5-2. Experimental

Calculations

Molecular orbital calculations by the PM3 method were performed with MOPAC Ver. 6.01 [15]. The overlap integrals were calcuated by the extended Hückel method. The electronic band structure were calculated by the tight-binding method.

Materials

All chemicals were reagent grade from Wako Chemical Co. and used as received unless noted otherwise. Triethyl phosphite was vacuum distilled, sealed under nitrogen and stored in the refrigerator until use. All solvents were degassed with high purity dry nitrogen for at least a few minutes before use. The ketone (1) was prepared according to the literature [13 (b)].

Thiadiazoleethylenedithiodiselenadithiafulvalene (DED)

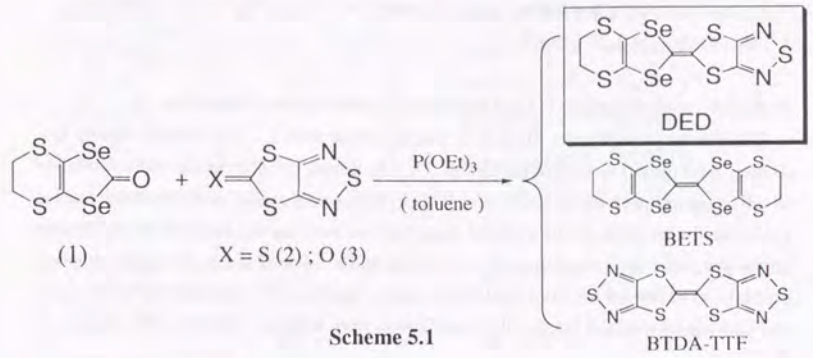

(1) X = S (2) ; O (3)

Scheme 5.1

In the course of attempts to synthesize the unknown intermediate thiadiazole-trithiocarbonate (2) with the aid of some references on close reactions [16], the very compound was reported [17].

A series of coupling conditions were examined and the results are tabulated in Table 5.1.A typical procedure of the coupling reaction is as follows.

Method A:; from the ketone (1) and the thione (2) in the toluene/phosphite.

The ketone (1) (1.45 g; 4.8 mmol) and thione (2) (1.02 g; 5.3 mmol) were dissolved in 128 ml of distilled toluene under nitrogen atmosphere. The yellow solution was slowly heated and the distilled phosphite (32 ml) was added at once *immediately* after starting to reflux. The resultant dark red solution was kept refluxing for another hour, cooled to room temperature and the precipitates (BETS) were filtered. The filtrate was slowly evaporated under reduced pressure to dark reddish brown tarry residue (*ca.* 10 ml) to produce almost analytically pure brilliant red plates, which was thoroughly washed with copious amount of ethanol then 70 ml of toluene, dried *in vacuo*. The yields after further purification (fractional crystallization from toluene / ethanol) is 50 – 65 mg (23 – 30 %). Elemental analysis: $C_8H_4N_2S_5Se_2$ = 446.00 calculated (%) H: 0.90 C: 21.52 N: 6.28 S: 35.92 Se: 35.38, found (%) H: 0.98 C: 21.40 N: 6.35 S: 35.80 Se:

34.05. m/e = 446 (M^+, 100%); IR (KBr): 1410 (w), 1378 (s), 1362 (w), 1284 (vw), 1238 (vs), 1039 (s), 943 (vw),
882 (vw), 771 (vs), 482 (vs), 420 cm^{-1} (vs). Crystal data: reddish orange rhombohedral; crystal dimensions 0.28 × 0.20 × 0.10 mm^3, Monoclinic, space group $P2_1/c$, a = 12.554(5), b = 7.906(1), c = 13.106(5) Å, β = 95.79(3) °, V = 1294.2(7) $Å^3$, Z = 4, D_{calc} = 2.29 $g \cdot cm^{-3}$.

Method B ; from the ketone (1) and the ketone (3) in the toluene/phosphite.

The similar procedure to Method A was followed with 1.2 eqv. of the ketone (3), (0.64g, 3.63 mmol) instead of the thione (2). The ketone (3) allowed far more formation of self-coupling products { BETS and BTDA-TTF, *i.e.* bis(thiadiazole)tetrathiafulvalene } than the thione (2) and thus required more tedious work-up for isolation of the desired compound; after the evaporation of the solvent under reduced pressure, crude coupling products were filtered off from triethyl phosphite, washed with methanol, dried *in vacuo* and purified by repeated fractional crystallization from toluene / ethanol; yield 90 mg (7 %).

The Charge-transfer Salts

The single crystal of the charge-transfer salts were obtained by the galvanostatic (2-3 μA) electrolysis of DED-STF (4 mg : *ca.* 0.4 mM) with an appropriate tetrabutylammonium salt (55 mg : *ca.* 2-6 mM) in THF (20 ml) at room temperature as black rhombic or irregular plates. The actual conditions are tabulated in Table 5.2.

Table 5.1. Synthetic conditions and the results of the cross-coupling

	molar ratio[a]	solv. ratio[b]	condition	yield (%)[c]
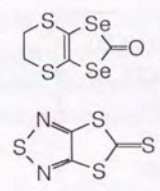	1.0	0	120 °C, 30 min	3 : 9 : 0
	1.1	3	reflux, 1.5 h[e]	0 : 28 : trace (~ 0)
	1.1	3	reflux, 40 min[d]	3 : 7 : 0
	1.1	4	reflux, 1 h[e]	26 : 23 : ≤ 3
	1.1	5	reflux, overnight[e]	0 : 26 : 0
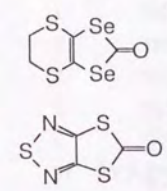	1.2	5	reflux, 7 h[f]	0 : 7 : 74
	1.0	4.6	reflux, 40 min[d]	15 : 8 : 63
	1.0	0	110 °C, 15 min	0 : 0 : 4

a 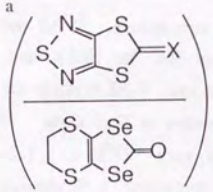

b $\left(\frac{\text{toluene (ml)}}{\text{P(OEt)}_3 \text{ (ml)}} \right)$

c BETS : DED : BTDA-TTF

d $P(OEt)_3$ and $C_6H_5CH_3$ were mixed before refluxing.

e $P(OEt)_3$ was added to the toluene soln immediately after it started to reflux.

f $P(OEt)_3$ was added to the toluene soln 10 – 15 min after it started to reflux.

Table 5.2. Electrolytic condition of the charge-transfer salts of DED[a]

counter ion[b] (X^-)	crystal habit[c]	current[d] /μA	voltage[e] /V	$(C_4H_9)_4NX$ /mg	DED /mg	solvent[f]	time /days
ICl_2	irregular	0.4		41	3.8	CB(3% Et)	9
IBr_2	irregular	0.8		66	4.1	CB(3% Et)	9
$AuCl_2$	rectangular	1.5		97	5.8	THF	3
$AuBr_2$	rectangular	1.5		54	5.6	THF	2
$Au(CN)_2$	rectangular	1.0		90	4.4	THF	4
$AuBr_4$	rectangular	1.5		70	5.5	THF	16
BF_4	rhombic	0.6		35	2.7	THF/CB[g]	4
ClO_4	rhombic	0.8		100	5.9	THF	7
ReO_4	rhombic	0.9		25	5.3	THF	7
PF_6	rhombic	2.5		46	3.0	THF	5
AsF_6	rhombic	2.6		20	4.4	THF	2
SbF_6	square		6.0	17	2.8	THF	7
SbF_6	rhombic	1.3		35	4.1	TCE/CB[h]	10
SbF_6	hexagonal	2.5		82	3.4	THF/CB[g]	4
TaF_6	rhombic	1.1		54	4.5	TCE/CB[h]	8

[a] All syntheses were carried out at (20 ± 1) °C under inert atmosphere. [b] All the supproting electrolytes were tetrabutylammonium salts except for the SbF_6 salt, PPN·SbF_6. PPN = bis(triphenylphosphoranylidene)ammonium ion. [c] All crystals are black plates, which are often elongated and appear to be needles at first sight. [d] Galvanostatic condition [e] Potentiostatic condition [f] 20 ml each TCE = 1,1,2-trichloroethane, CB = chlorobenzene, (3% Et) = the solvent containing 3 % ethanol (vol/vol), THF = tetrahydrofuran [g] 1:1 mixture (vol/vol) [h] 2:1 mixture (vol/vol)

ESR Measurements

Variable-temperature ESR spectra of single crystals were recorded using an ESR spectrometer (X-band) equipped with a JEOL JES-FE3XG electromagnet and a computer, JEOL ES-PRIT 23 ESR DATA SYSTEM. Temperature was controlled with a Scientific Instruments Inc. series 5500 ^{4}He continuous-flow cryostat and temperature controller. Angular dependence of the ESR spectra was measured by use of a goniometer. The freshly prepared single crystals were mounted with silicone grease on a quartz rod immediately after the filtration of the crystals. The crystals used in the measurements were selected to be all well-shaped rectangular thin flat plates with an

average dimension of *ca.* 1 × 2 × 0.05 mm^3. Each edge coinsides with the *a* - and *c* -axies and the developed crystal facet is the *ac* -plane, all of which were confirmed by the X-ray photographs. They were aligned and piled to lay on the developed facets making sure that all their *ac*-planes were parallel to each other, but they were not aligned azimuthally. The quartz rod, the sample tube and the cavity had been checked for magnetic impurities in advance. The atmosphere in the sample tube was purged with a helium gas to avoid the background signal from oxygen. Data were recorded both on an analog chart recorder and in digitized form for further analyses.

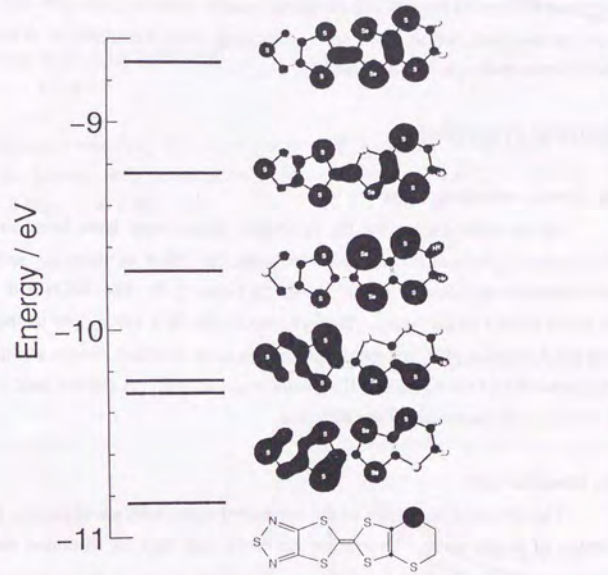

(a)

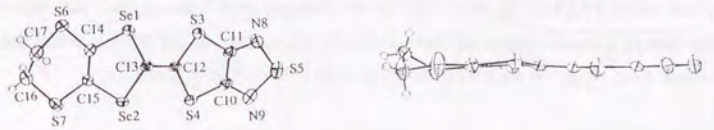

(b)

Figure 5.1. Energy diagram of (a) the highest five molecular orbitals (PM3) and (b) the actual molecular structure (X-ray) of neutral DED

5-3. Results

Molecular Orbitals

The highest five molecular orbitals are schematically shown in Figure 5.1. The optimized molecular structure well agreed with that determined by X-ray structural analysis. The calculation suggested that the HOMO of DED, which consists mainly of pπ-orbitals, lies above the highest occupied *n* orbital by *ca.* 2.1 eV , *i.e.* about three to four times the typical band width of charge-transfer salts of chalcogen donors. In regard to the mono-caion radical, both spin and charge were calculated to delocalize over the whole donor molecule in the π−orbital.

Electrical Properties

The Semiconducting Salts

All the salts except for the octahedral anion ones have been found to exhibit semiconducting behavior from room temperature. Most of them are well described as activation-type semiconductors as shown in Figure 5.2. The ReO_4 salt is an insulator and is not shown in the figure. The behavior of the BF_4 salt at low temperature deviates from the Arrhenius plot, but the details remain to be clarified. Some anomalies are found in the behavior of the ClO_4 and IBr_2 salts at *ca.* 220 K. A similar knot is discernible at *ca.* 180 K in the behavior of the BF_4 salt.

The Metallic Salts

The electrical resistivity of the octahedral anion salts are shown in Figure 5.3 as a function of temperature. Except for the SbF_6 salt they all exhibited metallic behavior down to *ca.* 20 K and their resistivies made a slight upturn at lower temperatures. These crystals are somewhat unstable in the air and lost the luster of their surfaces within a few hours to a few days; the rate varies from salts to salts and the smaller the anion is, the quickly the luster decays. The X-ray photographs, however, proved that the single crystals of the PF_6 salt are robust and do not collapse even a month after the filtration. Even though a certain degree of deterioration of the surface of the crystals could not be avoided, there observed high reproducibility with little sample dependence.

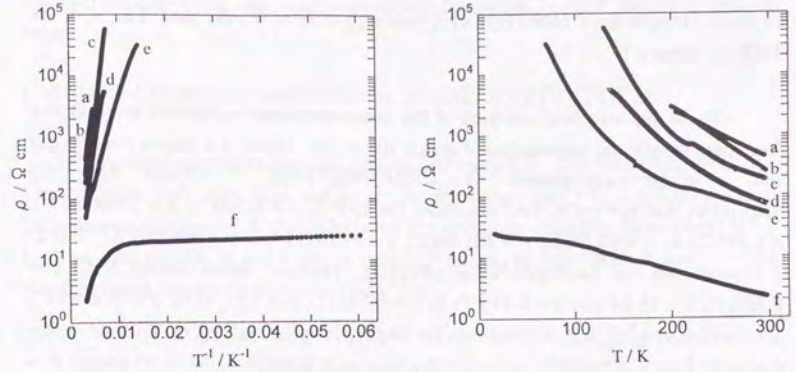

Figure 5.2. Electrical resistivity of semiconducting DED salts vs. temperature (right-hand side) and vs. inverse of the temperature (left-hand side); a: $AuBr_2$, b: $AuBr_4$, c: ClO_4, d: ICl_2, e: IBr_2 and f: BF_4 salts

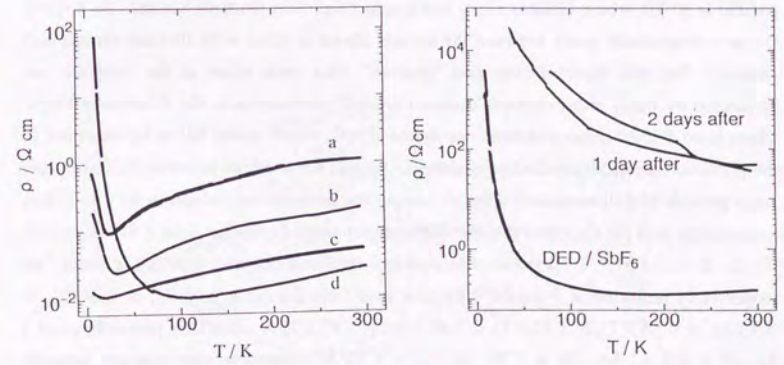

(a) **(b)**

Figure 5.3. Electrical resistivity of metallic DED salts as a function of temperature (a) (left-hand side) a: AsF_6, b: TaF_6, c: PF_6 and d: SbF_6 salts (b) (right-hand side) The crystal got deteriorated with time.

Crystal Structure of $(DED)_2(XF_6)(solv.)_2$ (X = P, As and Ta; solv. = THF or others)

The X-ray structural analyses of the above-mentioned substances revealed that they share unique and unprecedented crystal structures. Figure 5.4 shows the unit cell and molecular arrangement of $(DED)_2PF_6(THF)_2$. Crystal data for $Se_4S_{10}PF_6N_4C_{24}H_{12}O_2$, Triclinic, Space Group P $\bar{1}$, a = 8.760(1), b = 25.006(3), c = 8.395(2) Å, α = 97.56(2), β = 101.96(2), γ = 91.61(1) °, V = 1780.5(6) Å^3, Z = 2. { Crystal data for $Se_4S_{10}AsF_6N_4C_{24}H_{12}O_2$, Triclinic, Space Group P $\bar{1}$, a = 8.822(1), b = 25.249(3), c = 8.419(1) Å, α = 97.43(1), β = 101.76(1), γ = 91.64(9) °, V = 1817.6(4) Å^3, Z = 2. Crystal data for $Se_4S_{10}TaF_6N_4C_{24}H_{12}O_2$, Triclinic, Space Group P $\bar{1}$, a = 8.9487(5), b = 25.657(3), c = 8.4695(9) Å, α = 97.84(1), β = 101.336(7), γ = 93.094(9) °, V = 1882.2(3) Å^3, Z = 2. } There are two crystallographically independent DED molecules (I, II in the figure), an anion and two solvent molecules. Two donors make a dimer with a direct overlap and same orientation; the dihedral angle is 3.37 ° and the distance between the least-square molecular planes is 3.58 Å. The donor dimers and the anions are arranged alternately to form a donor-anion-intermingled layer in the *ac*-plane. Within a layer four dimers surround an anion, holding it approximately in the center. This cavity for the anion leaves room also for the fifth dimer in the neighboring layer to interpose their thiadiazole rings toward the anion. Interstitial solvent occupies void space; one is beside the anion and another is on the inversion center. The later is badly disordered. They make an insulating sheet running parallel to (010), which isolates every two conducting layers from each other. As a result the two dimensional space between the solvent sheets is filled with alternate dimers and anions. The two layers facing and "gearing" with each other at the interface are connected by many short contacts centered around heteroatoms in the thiadiazole rings. There is no distinct donor columns nor donor sheets, which never fail to be observed in the previous molecular conducting materials. Instead the overlaps between the thiadiazole rings provide two dimensional network among the heteroatoms, which in its turn offers an electrical path for the observed metallic conductivity. Particular close (S---N < 3.35 Å, S---S < 3.65 Å) intermolecular contacts mediated by the thiadiazole rings are respectively indicated in Figure 5.4 by thin lines from a to g; a: 2.95(2), b: 3.30(2), c: 3.33(1), d: 3.553(7), e: 3.553(7), f: 3.607(8), g: 3.615(7) Å. Similarly particular close (Se---F < 3.3 Å, Se---Se < 3.70, Se---S < 3.70 Å) intermolecular contacts between donor and anion (90 – 98% of the van der Waals distance), or between chalcogen atoms (90 – 96% of the van der Waals distance) are respectively shown by thin lines with suffixes from A to E (Se---F) and a to e { Se---S(e) }; A: 3.12(1), B: 3.11(1), C: 3.28(1), D: 3.01(2), E: 3.21(2), a: 3.655(3), b: 3.531(7), c: 3.684(3), d: 3.582(7), e: 3.650(3) Å. There may also exsist a significant interaction between the donor and the anion.

Calculated Electronic Band Structure of $(DED)_2(PF_6)(THF)_2$

Calculated overlap integrals are depicted in Figure 5.5. The intradimer overlaps (a in the figure) are very large and so are the interdimer ones (b, c). They are all interactions within layers. It should be noted that among the interlayer interactions (d – g), those with suffixes d and e are as comparably large as those with b and c. The calculated band structure is shown in Figure 5.6.

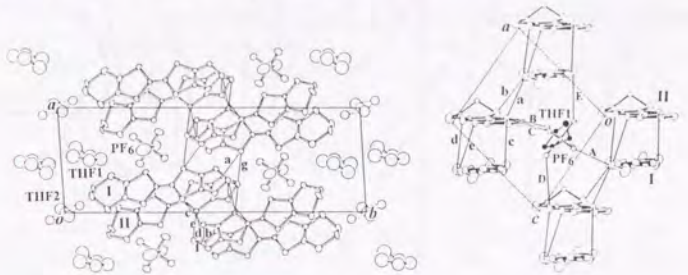

Figure 5.4. Crystal structure of $(DED)_2PF_6(THF)_2$ The thin lines indicate particular short contacts; see text.

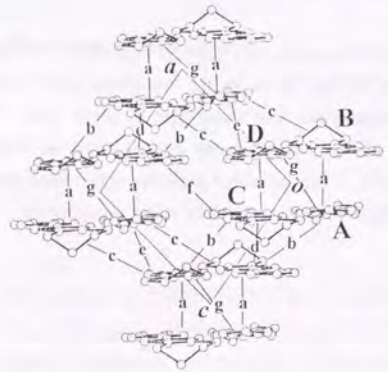

	S (×10^{-3})
a	-50.5
b	-32.8
c	-13.6
d	23.4
e	10.4
f	5.2
g	4.0

Figure 5.5. Calculated overlap integrals (S) in $(DED)_2PF_6(THF)_2$

Due to the small interdimer interactions along the *a*-axis (c, e – g), the resultant Fermi surface indicate that the anisotropy in the *ac*-plane is large and that the system is pseudo-one-dimensional along the *c*-axis.

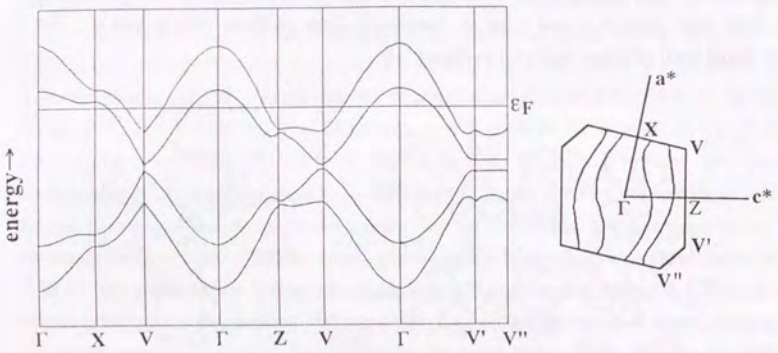

Figure 5.6. Calculated band structure and Fermi surface of $(DED)_2PF_6(THF)_2$

Magnetic Properties of $(DED)_2(PF_6)(THF)_2$

At low temperature, the ESR spectra of $(DED)_2(PF_6)(THF)_2$ are characterized by two Lorenzian signals; Figure 5.7 (d) illustrates the line shape observed at 9 K. The smaller sharp signal has a characteristic line shape of a localized spin. They strongly overlap at high temperatures but gradually become discrete from *ca.* 100 K and well-defined at lower than *ca.* 40 K. The measured total intensities shown in Figure 5.7 showed a pronounced Curie-Weiss-like susceptibility at low temperature.

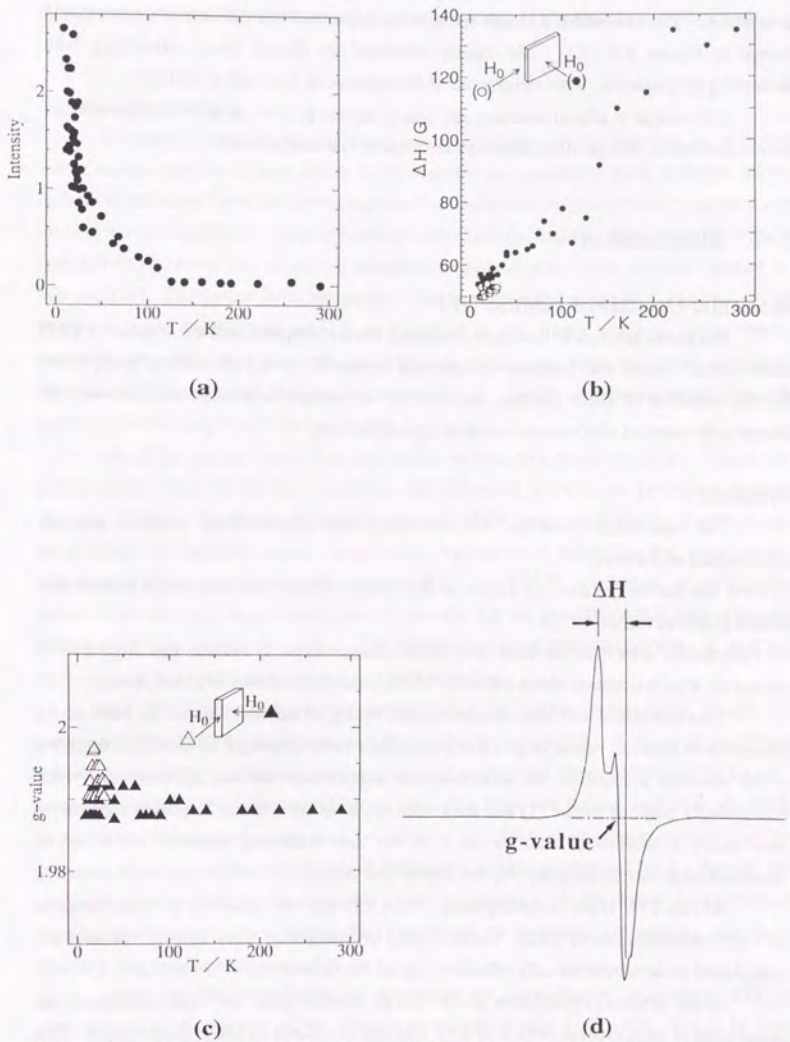

Figure 5.7. ESR results of $(DED)_2PF_6(THF)_2$; temperature dependence of (a) the total intensity of the ESR signal, (b) the linewidth and (c) the g-value The g-value and linewidth are tentatively defined as shown in (d). The empty circles (or triangles) and filled ones correspond to the condition where the magnetic field is in-plane and normal to the developed crystal face, *i.e.* conduction sheets, respectively.

On the other hand the intensities are nearly independent of temperature from 290 K to 120 K. The line width ΔH and the g-value are tentatively defined as schematically shown in Figure 5.7 (d). ΔH clearly exhibited an almost linear narrowing with decreasing temperature. This trend remains irrespective of how ΔH is defined.

The g-value is almost constant and nearly equals to 1.99 at all the temperature of the measurement, though the scatterings are large at low temperature.

5-4. Discussion

Molecular Orbitals of Neutral DED

The result appears to be disadvantageous for the purpose, and the results on DED mono-cation radical was qualitatively identical except for ~ -1.3 eV shift of every level. Yet the situation of these orbitals near HOMO are subject to change with net electric charge and chemical environment such as crystal packing.

Synthesis

The optimized condition for obtaining the asymmetrical product can be summarized as follows.

—First, the ketone (1) and 1.1 equiv. of the thione (2) are dissolved in the toluene and heated gently to reflux.

—Immediately after (or no later than) the toluene starts to reflux, the large excess phosphite which amounts about a third to a fifth volume of toluene is added at once.

This procedure was very sensitive to the timing of the addition and the ratio of the phosphite to toluene, whilst large variations in the time of heating (30 min to overnight) or the absolute amount of the solvent or the temperature did not influence the yield. Interestingly both the thione (2) and the ketone (3) have been found to couple themselves very easily (within 10 min or so) in the neat refluxing toluene, which is an unprecedented case in the coupling reaction of this class.

BTDA-TTF often co-precipitates with DED and the solubility to usual organic solvents resembles that of DED. The fractional crystallization from toluene / ethanol has been found to be almost an only effective way of the isolation.

In the electrocrystallization of the charge-transfer salts, the exact amount of the donor used is most critical, which is very unusual compared to other donor cases. This might have something to do with the fact that DED is extremely soluble to most organic solvents. In fact it was found, for example, that the solubility in 20 ml of chloroform at 23 °C of DED is (61 ± 1) mg, whilst those of BTDA-TTF, BEDT-TTF { = bis(ethylenedithio)tetrathiafulvalene } and BETS are all < 1 mg in the same solvent.

Therefore all the amount of DED added in the solution dissolves and directly dominates the donor concentration, which in turn dominates the rate of the electrocrystallization.

Physical Properties

The general trend of the calculated overlap integrals can be described by a model where independent two donor sheets in the *ac*-plane are connected to be a double layer. In fact the calculated band structure supports this model and suggests that this species can involve a metal instability. However several stable metallic systems have been previously reported to possess a pair of double elongated S-shaped open Fermi surfaces similar to this one [18]. The upturn in the resistivity at low temperature (≤ *ca.* 20 K) is thought to be due to some localization rather than a nesting of the Fermi surface, *i.e.* a metal-insulator (MI) transition since the rise in the resistivity is so blunt and small, while an MI transition ocurring at this temperature range in pseudo-one-dimensional systems usually involve sharp rise in the resistivity.

The ESR spectra shows that there exsist at least two kinds of spins. Since the plural signals have not yet been separated, the following discussions preliminarily treat them as a whole. The Curie-Weiss-like behavior of the spin susceptibility demonstrates an existence of localized spins. Considering the electrical behavior, the experiments showed that they coexist in this salt at least at 20 K – ~ 120 K. However, at present the author does not have experimental data which rule out the possibility that they originate from defects or magnetic impurities. The absolute value of the susceptibility χ, and the spin concentration per formula unit are to be determined.

The temperature-independent susceptibility at higher temperature might be attributed to the Pauli paramagnetism of the conduction electrons. If the desired system where localized and conduction electrons coexsist is obtained, the contribution to the spin susceptibility from the latter would merge into that from the former and thus the ESR intensity would apparently obey the Curie-Weiss law. From the figure it appears that the paramagnetism gives place to the Curie-Weiss-like behavior around 120 K, though the electrical behavior indicates no transition at this temperature. It remains to be confirmed whether the susceptibility is indeed Pauli paramagnetic at higher temperature and there occurs a magnetic transition at ~ 120 K.

When the line broadening is dominated by spin-phonon scattering, ΔH is proportional to the inverse of the transverse relaxation rate T_2^{-1} [19], which in turn related to $t_\perp^2$ and $\tau_{//}^{-1}$ ($t_\perp$ and $\tau_{//}$ are respectively the largest transfer integral perpendicular to the primary conduction path, the single particle scattering rate parallel to the primary conduction path). The experimental facts that the linewidth is nearly isotropic and this system is a quasi-one-dimensional metal are consistent with the narrowing behavior.

The g-values are usually slightly larger than that of a free electron (2.002319), and the stronger the interaction with other spin systems including nuclear spins, the larger the g-values' deviations are. The PM3 calculation indicated that the spin density of the mono-cation radical of DED is distributed almost over the whole π–conjugation system. If this is true the expected g-value, at least that of the conduction electrons, would be large. But in fact, the observed spectra indicated that the respective g-values after the separation of the strongly overlapped signals would be smaller than expected. Since the g-value in question now is not the actual g-value of a specified spin, the quantitative discussion such as why it is smaller than 2 may be not required at present.

For further discussion the detailed analysis of each signal by deconvolution is evidently required and will surely answer the questions above.

5-5. Summary

The radicals containing conjugated thiazyl linkage are known to often exhibit unusual persistence and unique network of sulfur and nitrogen atoms in the solid state. The present author thought that when such thiazyl linkage moiety is incorporated in π–conjugated moiety of strong enough donor with an ability of making wide metallic band in the radical salts, the resultant electronic system might have both free carriers and localized moments with an interaction between them. Based on this idea a new asymmetrical donor thiadiazoleethylenedithiadiselenadithiafulvalene (DED) and its charge-transfer salts have been synthesized and investigated. Among them certain octahedral salts have been found to be unique in the following ways;

—they are the first examples that behave metallic down to low temperatures among the reported many charge-transfer salts based on molecules having conjugated thiazyl linkages,

—they have an unprecedented crystal structure in that it does not possess segregated donor sheets or columns in spite of the usual 2:1 stoichiometry and stable metallic property.

The ESR measurement of the PF_6 salt detected two kinds of electrons, *i.e.* conduction electrons dominant at higher temperature and localized electrons dominant at lower temperature. Details remain yet to be elucidated including whether the localized spins come from the impurities or not.

References

[1] For recent reviews, see

(a) J. M. Williams, J. R. Ferraro, R. J. Thorn, K. D. Carlson, U. Geiser, H. H. Wang, A. M. Kini and M. -H. Whangbo, *The Physics and Chemistry of Organic Superconductors (Including Fullerenes)*, Prentice Hall, New Jersey, 1992;

(b) M. R. Bryce, *Chem. Soc. Rev.*, **20**, 355(1991);

(c) *The Physics and Chemistry of Organic Superconductors*, G. Saito and S. Kagoshima, Eds., Springer Proceedings in Physics, Springer, Berlin, 1990, Vol. 51;

(d) T. Ishiguro and K. Yamaji, *Organic Superconductors*, Springer-Verlag, Berlin, 1989;

(e) J. S. Miller, A. J. Epstein and W. M. Reiff, *Chem. Rev.*, **88**, 201(1988);

(f) *Proc. Symp. Ferromagnetic and High Spin Molecular Based Materials*, J. S. Miller and D. A. Dougherty, Eds., *Mol. Cryst. Liq. Cryst.* **1989**, 176;

(g) *Magnetic Molecular Materials*; D. Gatteschi, O. Kahn, J. S. Miller and F. Palacio, Eds., NATO ASI Series E; Kluwer Academic Publishers: Dordrecht, 1991;

(h) *Chemistry and Physics of Molecular Based Magnetic Materials*, H. Iwamura and J. S. Miller, Eds., *Mol. Cryst. Liq. Cryst.*, **232**, 233(1993).

[2] (a) C. Zener, *Phys. Rev.*, **81**, 440(1951);

(b) P. Day, *Acc. Chem. Res.*, **12**, 237(1979);

(c) J. S. Miller and A. J. Epstein, *Angew. Chem. Int. Ed. Engl.*, **33**, 385(1994);

(d) A. V. Gudenko, V. B. Ginodman, V. E. Korotkov, A. V. Koshelap, N. D. Kushch, V. N. Laukhin, L. P. Rozenberg, A. G. Khomenko, R. P. Shibaeva and E. B. Yagubskii, *The Physics and Chemistry of Organic Superconductors*, G. Saito and S. Kagoshima, Eds., Springer Proceedings in Physics, Springer, Berlin, 1990, Vol. 51, p. 365;

(e) R. P. Shibaeva, V. E. Korotkov and L. P. Rozenberg, *Sov. Phys.–Crystallogr. (Engl. Transl.)*, **36**, 820(1991);

(f) M. Kurmoo, T. Mallah, P. Day, I. Marsden, M. Allan, R. H. Friend, F. L. Pratt, W. Hayes, D. Chasseau, J. Gaultier, and G. Bravic, *The Physics and Chemistry of Organic Superconductors*, G. Saito and S. Kagoshima, Eds., Springer Proceedings in Physics, Springer, Berlin, 1990, Vol. 51, p. 290;

(g) T. Mallah, C. Hollis, S. Bott, P. Day and M. Kurmoo, *Synth. Met.*, **27**, A381(1988);

(h) T. Mallah, C. Hollis, S. Bott, M. Kurmoo and P. Day, *J. Chem. Soc., Dalton Trans.*, **1990**, 859.

[3] (a) P. Day, M. Kurmoo, T. Mallah, I. R. Marsden, R. H. Friend, F. L. Pratt, W. Hayes, D. Chasseau, J. Gaultier, G. Bravic and L. Ducasse, *J. Am. Chem. Soc.*, **114**, 10722(1992);
(b) A. Kobayashi, T. Udagawa, H. Tomita, T. Naito and H. Kobayashi, *Chem. Lett.*, **1993**, 2179;
(c) H. Kobayashi, H. Tomita, T. Udagawa, T. Naito and A. Kobayashi, *Synth. Met.*, in press;
(d) F. Goze, V. N. Laukhin, L. Brossard, A. Audouard, J. P. Ulmet, S. Askenazy, T. Naito, H. Kobayashi, A. Kobayashi, M. Tokumoto and P. Cassoux, *Europhys. Lett.*, **28**(6), 427-431(1994);
(e) F. Goze, V. N. Laukhin, L. Brossard, A. Audouard, J. P. Ulmet, S. Askenazy, T. Naito, H. Kobayashi, A. Kobayashi, M. Tokumoto, C. Faulmann and P. Cassoux, *Synth. Met.*, in press.
[4] (a) S. Hünig and P. Erk, *Adv. Mater.*, **3**, 225, 311(1991);
(b) A. Kobayashi, R. Kato, H. Kobayashi, T. Mori and H. Inokuchi, *Solid State Commun.*, **64**, 45(1987);
(c) H. Kobayashi, R. Kato, A. Kobayashi, T. Mori, H. Inokuchi, Y. Nishio, K. Kajita and W. Sasaki, *Synth. Met.*, **27**, A289(1987);
(d) R. Kato, H. Kobayashi, A. Kobayashi, T. Mori and H. Inokuchi, *Synth. Met.*, **27**, B268(1988);
(e) R. Kato, H. Kobayashi and A. Kobayashi, *J. Am. Chem. Soc.*, **111**, 5224(1989);
(f) H. Kobayashi, A. Miyamoto, R. Kato, A. Kobayashi, Y. Nishio, K. Kajita and W. Sasaki, *Solid State Commun.*, **72**, 1(1989);
(g) H. Kobayashi, A. Miyamoto, H. Moriyama, R. Kato and A. Kobayashi, *Chem. Lett.*, **1991**, 863;
(h) I. H. Inoue, A. Kakizaki, H. Namatame, A. Fujimori, A. Kobayashi, R. Kato and H. Kobayashi, *Phys. Rev. B*, **45**, 5828(1992);
(i) M. Y. Ogawa, B. M. Hoffman, S. Lee, M. Yudkowsky and W. P. Halperin, *Phys. Rev. Lett.*, **58**, 1177(1986);
(j) M. Y. Ogawa, J. Martisen, S. M. Palmer, J. L. Stanton, J. Tanaka, R. L. Greene, B. M. Hoffman and J. A. Ibers, *J. Am. Chem. Soc.*, **109**, 1115(1987);
(k) M. Y. Ogawa, S. M. Palmer, K. Liou, G. Quirion, J. A. Thompson, M. Poirier and B. M. Hoffman, *Phys. Rev. B*, **39**, 10682(1989);
(l) A. L. Tchougreeff and I. A. Misurkin, *Chem. Phys.*, **153**, 371(1991);
(m) A. L. Tchougreeff and I. A. Misurkin, *Phys. Rev. B*, **46**, 5357(1992).
[5] This is apparent when we consider, for example the contrast of the donor abilities between anthracene and phenanthroline.

[6] W. -J. Wang and I. -W. Chuang, *Synth. Met.*, **55-57**, 1956(1993).
[7] (a) J. M. Williams, M. A. Beno, H. H. Wang, P. C. W. Leung, T. J. Emge, U. Geiser and K. D. Carlson, *Acc. Chem. Res.*, **18**, 261(1985).
(b) J. M. Williams, H. H. Wang, T. J. Emge, U. Geiser, M. A. Beno, P. C. W. Leung, K. D. Carlson, R. J. Thorn and A. J. Schultz, *Prog. Inorg. Chem.*, **35**, 51(1987).
(c) J. M. Williams, A. J. Schultz, U. Geiser, K. D. Carlson, A. M. Kini, H. H. Wang, W. -K. Kwok, M. -H. Whangbo and J. E. Schirber, *Science*, **252**, 1501(1991) and references cited therein.
[8] For example, see
(a) G. Wolmershäuser, C. Krüger and Y. -H. Tsay, *Chem. Ber.*, **115**, 1126(1982).
(b) J. Giordan, H. Bock, M. Eiser and H. W. Roesky, *Phosphorus Sulfur*, **13**, 19(1982).
(c) T. Chivers, *Chem. Rev.*, **85**(5), 341(1985).
(d) P. J. Hayes, R. T. Oakley, A. W. Cordes and W. T. Pennington, *J. Am. Chem. Soc.*, **107**, 1346(1985).
(e) R. T. Boeré, C. L. French, R. T. Oakley, A. W. Cordes, J. A. J. Privett, S. L. Craig and J. B. Graham, *J. Am. Chem. Soc.*, **107**, 7710(1985).
(f) R. T. Boeré, A. W. Cordes, P. J. Hayes, R. T. Oakley and R. W. Reed, *Inorg. Chem.*, **25**, 2445(1986.)
(g) G. Wolmershäuser and G. Kraft, *Chem. Ber.*, **123**, 881(1990).
(h) A. W. Cordes, R. C. Haddon, R. T. Oakley, L. F. Schneemeyer, J. V. Waszczak, K. M. Young and N. M. Zimmerman, *J. Am. Chem. Soc.*, **113**, 582(1991).
(i) M. P. Andrews, A. W. Cordes, D. C. Douglass, R. M. Fleming, S. H. Glarum, R. C. Haddon, P. Marsh, R. T. Oakley, T. T. M. Palstra, L. F. Schneemeyer, G. W. Trucks, R. Tycko, J. V. Waszczak, K. M. Young and N. M. Zimmerman, *J. Am. Chem. Soc.*, **113**, 3559(1991).
(j) A. J. Banister, I. Lavender, J. M. Rawson, W. Clegg, B. K. Tanner and R. J. Whitehead, *J. Chem. Soc., Dalton Trans.*, **1993**, 1421.
(k) S. Parsons, J. Passmore and P. S. White, *J. Chem. Soc., Dalton Trans.*, **1993**, 1499.
(l) A. W. Cordes, R. C. Haddon, R. G. Hicks, D. K. Kennepohl, R. T. Oakley, L. F. Schneemeyer and J. V. Waszczak, *Inorg. Chem.*, **32**, 1554(1993);
(m) C. M. Aherne, A. J. Banister, I. B. Gorrell, M. I. Hansford, Z. V. Hauptman, A. W. Luke and J. M. Rawson, *J. Chem. Soc., Dalton Trans.*, **1993**, 967;

(n) E. Dorman, M. J. Nowak, K. A. Williams, R. O. Angus, Jr. and F. Wudl, *J. Am. Chem. Soc.*, **109**, 2594(1987);
(o) G. Wolmershäuser, G. Wortmann and M. Schnauber, *J. Chem. Res. Symp.*, **1988**, 358;
(p) E. G. Awere, N. Burford, C. Mailer, J. Passmore, M. J. Schriver, P. S. White, A. J. Banister, H. Oberhammer and L. H. Sutcliffe, *J. Chem. Soc., Chem. Commun.*, **1987**, 66;
(q) G. K. MacLean, J. Passmore, M. N. S. Rao, M. J. Schriver, P. S. White, D. Bethell, R. S. Pilkington and L. H. Sutcliffe, *J. Chem. Soc., Dalton Trans*, **1985**, 1405;
(r) Y. Matsubara, K. Kitano, Y. Sasaki, M. Yoshihara and T. Maeshima, *Bull. Chem. Soc. Jpn.*, **66**, 3525(1993);
(s-1) S. A. Fairhurst, R. S. Pilkington and L. H. Sutcliffe, *J. Chem. Soc., Faraday Trans.* 1, **1983**, 79, 925;
(s-2) K. F. Preston, J. P. B. Sandall and L. H. Sutcliffe, *Magn. Reson. Chem.*, **26**(9), 755(1988);
(t) A. W. Cordes, M. Hojo, H. Koenig, M. C. Noble, R. T. Oakley and W. T. Pennington, *Inorg. Chem.*, **25**, 1137(1986);
(u) J. L. Morris and C. W. Rees, *J. Chem. Soc., Perkin Trans.* I, **1987**, 217;
(v) S. T. A. K. Daley and C. W. Rees, *J. Chem. Soc., Perkin Trans.* I, **1987**, 203;
(w) S. T. A. K. Daley and C. W. Rees, *J. Chem. Soc., Perkin Trans.* I, **1987**, 207;
(x) J. L. Morris and C. W. Rees, *J. Chem. Soc., Perkin Trans.* I, **1987**, 211;
(y) N. Burford, J. Passmore and J. M. Schriver, *J. Chem. Soc., Chem. Commun.*, **1986**, 140.
(z) W. V. F. Brooks, N. Burford, J. Passmore, M. J. Schriver and L. H. Sutcliffe, *J. Chem. Soc., Chem. Commun.*, **1987**, 69.
[9] (a) G. Wolmershäuser, M. Schnauber and T. Wilhelm, *J. Chem. Soc., Chem. Commun.*, **1984**, 573;
(b) G. Wolmershäuser, M. Schnauber and T. Wilhelm, *Mol. Cryst. Liq. Cryst.*, **120**, 323(1985);
(c) G. Wolmershäuser, M. Schnauber, T. Wilhelm and L. H. Sutcliffe, *Synth. Met.*, **14**, 239(1986);
(d) G. Wolmershäuser and R. Johann, *Angew. Chem. Int. Ed. Engl.*, **28**, 920(1989).
[10] J. Bojes and T. Chivers, *Inorg. Chem..*, **17**, 318(1978).
[11] A. J. Banister, I. Lavender, J. M. Rawson and W. Clegg, *J. Chem. Soc., Dalton Trans.*, **1992**, 859.

[12] (a) A. R. Forrester, J. M. Hay and R. H. Thomson, *"Organic Chemistry of Stable Free Radicals"*; Academic Press: London and New York, 1968;
(b) E. G. Rozantsev, *"Free Nitroxyl Radicals"*; Plenum Press: New York, 1970;
(c) J. F. Keana, *Chem. Rev.*, **78**, 37(1978);
(d) Y. Miura, A. Yamamoto, Y. Katsura, M. Kinoshita, S. Sato and C. Tamura, *J. Org. Chem.*, **47**, 2618(1982);
(e) J. S. Miller, A. J. Epstein and W. M. Reiff, *Chem. Rev.*, **88**, 201(1988);
(f) K. Awaga and Y. Maruyama, *Chem. Phys. Lett.*, **158**, 556(1989);
(g) A. Caneschi, D. Gatteschi, R. Sessoli and P. Rey, *Acc. Chem. Res.*, **22**, 392(1989);
(h) L. Dulog and J. S. Kim, *Angew. Chem., Int. Ed. Engl.*, **29**, 415(1990);
(i) M. Kinoshita, P. Turek, M. Tamura, K. Nozawa, D. Shiomi, Y. Nakazawa, M. Ishikawa, M. Takahashi, K. Awaga, T. Inabe and Y. Maruyama, *Chem. Lett..*, **1991**, 1225;
(j) A. Caneschi, D. Gatteschi and P. Rey, *Prog. Inorg. Chem.*, **39**, 331(1991);
(k) Y. Miura, A. Tanaka and K. Hirotsu, *J. Org. Chem.*, **56**, 6638(1991);
(l) D. A. Dougherty, *Acc. Chem. Res.*, **24**, 88(1991);
(m) Y. Miura, E. Yamano, A. Tanaka and Y. Ogo, *Chem. Lett.*, **1992**, 1831;
(n) H. Iwamura and N. Koga, *Acc. Chem. Res.*, **26**, 346(1993);
(o) Y. Miura, M. Matsumoto and Y. Ushitani, *Macromolecules*, **26**, 2628(1993);
(p) Y. Miura, Y. Ushitani, K. Inui, Y. Teki, T. Takui and K. Itoh, *Macromolecules*, **26**, 3698(1993);
(q) Y. Miura, M. Matsumoto, Y. Ushitani, Y. Teki, T. Takui and K. Itoh, *Macromolecules*, **26**, 6673(1993);
(r) Y. Miura and Y. Ushitani, *Macromolecules*, **26**, 7079(1993);
(s) Y. Teki, Y. Miura, A. Tanaka, T. Takui and K. Itoh, *Mol. Cryst. Liq. Cryst.*, **233**, 119(1993);
(t) Y. Miura, E. Yamano, A. Miyazawa and M. Tashiro, *Chem. Lett.*, **1994**, 867.
[13] (a) R. R. Schumaker, V. Y. Lee and E. M. Engler, *IBM Research Report* (1983).
(b) R. Kato, H. Kobayashi and A. Kobayashi, *Synth. Met.*, **41-43**, 2093(1991);
(c) T. Naito, A. Miyamoto, H. Kobayashi, R. Kato and A. Kobayashi, *Chem. Lett.*, **1991**, 1945;
(d) H. Kobayashi, T. Udagawa, H. Tomita, K. Bun, T. Naito and A. Kobayashi, *Chem. Lett.*, **1993**, 1559;
(e) A. Kobayashi, R. Kato, T. Naito and H. Kobayashi, *Synth. Met.*, **56**, 2078(1993);

(f) L. K. Montgomery, T. Burgin, C. Husting, L. Tilley, J. C. Huffman, K. D. Carlson, J. D. Dudek, G. A. Yaconi, U. Geiser and J. M. Williams, *Mol. Cryst. Liq. Cryst.*, **211**, 283(1992);

(g) L. K. Montgomery, T. Burgin, J. C. Huffman, K. D. Carlson, J. D. Dudek, G. A. Yaconi, L. A. Megna, P. R. Mobley, W. K. Kwok, J. M. Williams, J. E. Schirber, D. L. Overmyer, J. Ren, C. Rovira and M. -H. Whangbo, *Synth. Met.*, **55-57**, 2090(1993).

[14] T. Naito, A. Tateno, T. Udagawa, H. Kobayashi, R. Kato, A. Kobayashi and T. Nogami, *J. Chem. Soc., Faraday Trans.*, **90**, 763(1994).

[15] (a) J. J. P. Stewart, *J. Comput. Chem.*, **10**, 209, 221(1989);

(b) MOPAC Ver. 6, J. J. P. Stewart, *QCPE Bull.*, **9**, 10(1989); revised as Ver. 6.01 by Tsuneo Hirano at The University of Tokyo for HITAC and UNIX machines, JCPE Newsletter, **1**, 10(1989).

[16] (a) J. L. Morris and C. W. Rees, *J. Chem. Soc., Perkin Trans. 1*, **1987**, 217;

(b) G. Wolmershäuser and R. Johann, *Angew. Chem., Int. Ed. Engl.*, **28**, 920(1989);

(c) Ian Hawkins and A. E. Underhill, *J. Chem. Soc., Chem. Commun.*, **1990**, 1593;

(d) O. A. Dyachenko, S. V. Konovalikhin, A. I. Kotov, G. V. Shilov, E. B. Yagubskii, C. Faulmann and P. Cassoux, *J. Chem. Soc., Chem. Commun.*, **1993**, 508;

(e) S. Schenk, I. Hawkins, S. B. Wilkes, A. E. Underhill, A. Kobayashi and H. Kobayashi, *J. Chem. Soc., Chem. Commun.*, **1993**, 1648.

[17] A. E. Underhill, I. Hawkins, S. Edge, S. B. Wilkes, K. S. Varma, A. Kobayashi and H. Kobayashi, *Synth. Met.*, **55-57**, 1914(1993).

[18] See Chapter 4 in this thesis and references cited therein.

[19] (a) Y. Yafet, *Solid State Physics*, H. Ehrenreich, F. Seitz and D. Turnbull, Eds., Academic, New York, 1963, Vol. 14, p.1;

(b) A. N. Bloch, *Organic Conductors and Semiconductors (Lecture Notes in Physics)*, L. Pal, G. Gruner, A. Janossy and J. Solyom, Springer-Verlag, Berlin, Vol. 65, 1977, p.317.

Chapter 6.

The New Synthetic Metals of M(dmise)2: [(CH3)3HN][Ni(dmise)2]2 and (EDT-TTF)[Ni(dmise)2]*

6-1. Introduction

There had been emerging interest in some kinds of metal-complexes with sulfur-contaning ligands, when the dmit ligand (dmit = 4,5-dimercapto-1,3-dithiole-2-thione; 4,5-disulfanyl-1,3-dithiole-2-thione) and its metal-complexes were first reported by Steimecke *et al.* in 1979 [1]. Many of the related work then concentrated on their unusual oxidation states, electrochemical behavior and the ESR study [2]. The dmit ligand at first attracted attention in the field of synthetic metals since it had turned out to be a versatile starting material in the synthesis of various donor molecules related to BEDT-TTF { bis(ethylenedithio)tetrathiafulvalene } [3]. But the ligand has indeed come to the fore after the report of the first molecular superconductor based on its Ni complex, TTF[Ni(dmit)2] [4 (a) – (c)]. This charge-transfer salt consists of segregated stacks of the donor and acceptor molecules and they are connected by S---S short contacts between the sulfur atoms in the thione of the dmit ligands and those in the TTF molecules. This is why Bousseau *et al.* argued that the salt has a quaisi three-dimensional crystal structure [4 (b)], though the tight-binding calculation suggested that the electronic structure can be rather one-dimensional [4 (n), (o), 5 (b)].

The next superconductor of this class was reported in 1987 by Kobayashi *et al.*, which is based on the Ni complex again but that with a closed-shell cation, $(CH_3)_4N[Ni(dmit)_2]_2$ [4 (d) – (o)]. This salt is significant in that it has proved that the dmit-complex for itself, *i.e.* without a donor, can produce the conduction path as a molecular superconductor; in other words $(CH_3)_4N[Ni(dmit)_2]_2$ is the first example of a purely-acceptor-based superconductor. The additional two examples, β–$(CH_3)_4N[Pd(dmit)_2]_2$ and $(C_2H_5)_2(CH_3)_2N[Pd(dmit)_2]_2$, established a consensus about such ability of $M(dmit)_2$ salts within several years [4 (s) – (u)] and an extensive onium salts have been studied [6].

The most striking difference in the electrical properties of the dmit compounds lies in the metal instability despite its molecular structural similarity to BEDT-TTF. Such difference originates from the difference in the symmetry of the frontier orbitals, namely,

* The major part of this work is published; Toshio Naito, Akane Sato, Kouichi Kawano, Akiko Tateno, Hayao Kobayashi and Akiko Kobayashi, *J. Chem. Soc., Chem. Commun.*, **1995**, 351.

the lowest unoccupied molecular orbitals (LUMOs) of M(dmit)$_2$ [5], which dominates the intermolecular interaction concerning the conduction band. Consequently the dmit salts often suffer from low-dimensionality and narrow bands, both of which are apt to lead to a ground state with a band gap. Thus most of [cation]$_x$[M(dmit)$_2$] (M = Ni, Pd, Pt; $0 < x < 1$) are semiconductors, and metallic salts, especially at low temperature, are exceptional at ambient pressure [5 (c), (d), 7].

The conduction path in these salts is generally formed through overlapping orbitals of the sulfur atoms in the ligands. The idea to improve this conduction path by replacing one or more of the sulfur by the larger selenium atoms has already yielded several partially oxidised corresponding compounds, [cation]$_x$[M(C$_3$S$_{5-x}$Se$_x$)$_2$] (M = Ni, Pd; $0 < x < 1$) [8 (a) – (h)]. However it was found that the structural and/or electronic properties of these compounds can be quite different from what had been expected, and many of them have turned out to be no better semiconductors than those of the corresponding dmit salts. A possible cause might be found in the b_{2g} symmetry of the LUMO [5], for the asymmetry often makes the transverse intermolecular overlaps in the M(dmit)$_2$ solids almost cancell out each other, when the size of the chalcogen atoms on the periphery makes little difference.

Another approach to enhance the intermolecular interaction in the M(dmit)$_2$ salts is to use a smaller cation such as alkaline metals and tetramethylammonium ion. The aforementioned superconductors are all successful examples of the latter case, though they still require high pressure to stabilize their metallic states to achieve superconductivity. (C$_2$H$_5$)$_4$N[Ni(dmit)$_2$]$_2$ was reported to be a precursor of the three-dimensional molecular metal [9], where the two-dimensional S---S networks of Ni(dmit)$_2$ layer are weakly connected by the thione-thione contacts. Although this salt actually exhibited semiconducting behavior from room temperature, the possibility that the salt suggested is intriguing. The chemical modification at the thione and/or the cation appears most effective in the stabilization of the metallic state thus far, since it makes the M(dmit)$_2$ molecules in the stack shift to each other along their long axis and leads to the change in relative arrangement in addition to the approach of the two thiones in the neighbouring M(dmit)$_2$ molecules in the different stacks, which sometimes results in gain of both intercolumnar and intersheet overlaps to some degree.

Among the dmit derivatives including both sulfur and selenium atoms [8], dmise (dmise = 4,5-dimercapto-1,3-dithiole-2-selone; 4,5-disulfanyl-1,3-dithiole-2-selone) is therefore a potentially useful ligand which extends an intermolecular interaction towards the third direction through its outstretched part of its π-conjugation system, *i.e.* the selone group [8 (c), (e)]. However, the solid state properties of metal-dmise system have been reported only for two (CH$_3$)$_4$N$^+$ salts [8 (c), (e)]. Of particular interest among the unexplored metal-dmise systems are salts with small cations and charge transfer complexes with chalcogen donors, because not only both of such combinations have

yielded superconductors in Ni(dmit)$_2$ compounds [4 (a) – (o), (v) – (y)] but also they could be expected to exert the structural advantage of the dmise ligand mentioned above. In particular the metal-dmit salts with (CH$_3$)$_4$N$^+$ and (C$_2$H$_5$)$_2$(CH$_3$)$_2$N$^+$ often produce stable metals and superconductors under high pressure [4 (d) – (o), (r) – (u), 5 (c), (d)]. Additionally some cases are known to be rare examples of this class that remain metallic down to the liquid helium temperature [5 (c), (d), 7]. On the other hand the donor-acceptor type compound like (EDT-TTF)[Ni(dmise)$_2$] (EDT-TTF = ethylenedithiotetrathiafulvalene) is as intriguing, for the related compound (EDT-TTF)[Ni(dmit)$_2$] has recently been found to exhibit superconductivity at 1.3 K at ambient pressure [4 (v) – (y)]. All but this important exception the dmit compounds exhibit superconductivity under high pressure. Therefore the results about closely related compounds such as (EDT-TTF)[Ni(dmise)$_2$] and [(CH$_3$)$_4$N][Ni(dmise)$_2$]$_2$ are of particular interest. This chapter presents the synthesis and electrical properties of the two titled salts and some other related salts. A brief account of the crystal and electronic structures of [(CH$_3$)$_3$HN][Ni(dmise)$_2$]$_2$ is also given.

6-2. Experimental

Materials

All chemicals are reagent grade from Wako Chemicals Co. and used as received unless noted otherwise. Chloroform, diethyl ether and methanol were distilled according to the ref. [10 (a)] under a stream of nitrogen, sealed under nitrogen and stored in the refrigerator until use. Acetonitrile was purified following the reported procedure [10 (b)]. All solvents were degassed with high-purity dry nitrogen for at least a few minutes before use. All the materials were confirmed by elemental analyses or spectroscopic methods or some combination of them. The tetraalkylammonium iodide were prepared by usual nucleophilic quarternization between alkyl iodides and an equivalent amount of proper amines in methanol, benzene or dichloromethane at room temperature unless they were commercially available. Their perchlorates were easily obtained by treatment with AgClO$_4$ and used in electrolysis after several recrystallizations from CH$_2$Cl$_2$ / ether. The exact amount of solvents, scales were not critical in the syntheses of these ammonium salts.

4,5-bis(benzoylthio)-2-ethylthio-1,3-dithiolium tetrafluoroborate (**2**)

In 500 ml three-necked flask fitted with a 200 ml pressure-equalizing dropping funnel and a reflux condenser, the bis(thiobenzoyl)-protected dmit (**1**) (6.57 g; 1.6 mmol) [1] dissolved in CHCl$_3$ (67 ml) was treated with (EtO)$_3$CH$^+$BF$_4^-$ prepared *in situ* from HC(OEt)$_3$ (95 %, 3.6 ml; 3.22g; 26 mmol) in CHCl$_3$ (10 ml) and BF$_3$·Et$_2$O

(BF_3 = 46.0 ~ 49.0 %; 10.5 ml; 30 mmol) in $CHCl_3$ (7 ml) and refluxed for 3.5 h with vigorous stirring under a nitrogen atmosphere. The reacting mixture turned from reddish orange to dark red with some blackish precipitates. After it cooled to room temperature ether (280 ml) was added and the mixture was cooled to – 40 °C overnight. Fine brownish yellow precipitates were filtered, washed with ether and dried in *vacuo*. 7.69 g (91 %). All attempts to recrystallize them from usual organic solvents resulted in serious decomposition. The crude product was used in the next step without delay nor further purification. m/e (70 eV): 406 (M – Et), 362 (M – EtSC), 330 (M – EtSCS), 105 ($COPh^+$). IR (Nujol / cm^{-1}): 1680 (s), 1210 (s; C=S), 1050 (vs; BF_4), 1040 (sh; C=S), 1020 (sh; BF_4), 890 (vs).

4,5-bis(benzoylthio)-1,3-dithiole-2-selone {dmise(COPh)2} **(3)**

In 500 ml three-necked flask equipped with a 200 ml dropping funnel and a reflux condenser, the methanol solution of NaHSe prepared *in situ* by careful addition of methanol (62 ml) to Se powder (Soekawa Chemical Co., 99.9 %, 200 mesh; 2.23 g; 28 mmol) and $NaBH_4$ (Kanto Chemical Co., 92 %; 4.25 g; 103 mmol) under a nitrogen atmosphere with cooling in an ice bath [11]. After all solids were consumed to yield a colorless solution, acetic acid (2.8 ml) and then the finely powdered dithiolium salt **(2)** (5.14 g; 9.8 mmol) in several portions were added successively at – 10 °C under inert atmosphere with vigorous stirring. The reacting mixture turned from dull yellow to dark reddish orange soon. The rate of addition was adjusted to allow the colored ylide to be consumed between successive additions or to maintain the small amount of yellow unreacted suspension of the dithiolium salt. The addition required typically 30 – 45 min. The stirring was continued for 3.5 h at – 10 °C, then 30 min at room temperature and excess benzoyl chloride (19.6 ml) was added dropwise to the dark red-purple solution. Immediately exothermic reaction occurred and bright orange fine powder precipitated. After stirring for another 2 h with cooling again in an ice bath, the fine needles were filtered, washed with methanol, recrystallized from cold CH_2Cl_2 / methanol and dried in *vacuo*. Further purification could be carried out by silica gel column chlomatography (CH_2Cl_2 / hexane 1 : 1) if necessary. Reddish orange needles, 3.35 g (75 %). Elemental analysis: $C_{17}H_{10}S_4SeO_2$ = 453.49 calculated (%) H: 2.22 C: 45.03 S: 28.28 Se: 17.41, found (%) H: 2.35 C: 44.77 S: 27.92 Se: 16.91, m/e (70 eV): 454 (M^+), 160, 105 ($COPh^+$), 77 (Ph^+), 28. IR (KBr / cm^{-1}): 1689 (s; C=O), 1673 (s; C=O), 1452 (s; –Ph), 1180 (s; –Ph), 1064 (s; C=S), 1037 (w; C=S), 1006 (m; C=S), 958 (m; C=Se), 921 (sh; C=S), 901 (sh; C=S), 888 (s; C–S), 690 (sh; C–S), 683 (s; –Ph), 642 (s; –Ph), 620 (w; –Ph), 521 (w; –Ph).

Synthesis of (cation)$_n$[M(dmise)2] (M = Ni, Pd, Pt; n = 1, 2)

The metal complexes were prepared in analogy to the synthesis of the corresponding dmit complexes as described by Steimecke *et al.* [1].

Preparation of Single Crystals of M(dmise)2 Compounds

The single crystals of the charge-transfer salts were obtained by electrocrystallization of [$(C_4H_9)_4N$][Ni(dmise)2] or [$(C_4H_9)_4N$]2[Pd(dmise)2] (7–10 mg) in acetonitrile or acetone / acetonitrile (1:1 vol/vol) (20 ml) with a perchlorate salt of the desired ammonium cation as supporting electrolyte under a nitrogen atmosphere at room temperature (20 °C) for one or two weeks unless noted otherwise. A cell with fine porosity glass frit (G2 or G3) and platinum electrodes (each 1 mmϕ wire) were used. The current was kept constant. The detailed conditions of each case are tabulated in Table 6.1.

Table 6.1. The Condition of Electrochemical Synthesis of M(dmise)2 Compounds

Species[a]	[M(dmise)2]$^{n-}$ [b] / mg	$R_4N{\cdot}ClO_4$[c] / mg	solvent[d] / ml	current / μA	time / days
[Me_4N][Ni]2	15.0	35.6	A / 13.0	2.0	5
α–phase (needle)					
β–phase (plate)					
[Me_3EtN][Ni]2	6.8	33.1	A / 15.0	0.5	10
[Me_3HN][Ni]2	4.4	83.2	A / 13.0	0.2	7
[Me_2Et_2N][Ni]2	4.5	21.2	B / 14.0	0.2	14
	6.0	10.6	B / 15.0	0.2	9
[$MeEt_3N$][Ni]2	5.0	29.0	A / 15.0	0.5	5
[Et_4N][Ni]2	5.1	50.4	A / 15.0	0.8	3
[Me_4N][Pd]2	5.2	61.8	A / 15.0	0.4	12
(EDT-TTF)[Ni]	6.3	1.9[e]	A / 15.0	0.4	11

[a] [Ni], [Pd] imply [Ni(dmise)2] and [Pd(dmise)2], respectively. Me = CH_3, Et = C_2H_5. [b] M = Ni, n = 1; M = Pd, n = 2; the counter cation is tetrabutylammonium ion for both. [c] R_4N indicates the desired ammonium ion. [d] A: CH_3CN, B: CH_3CN / $(CH_3)_2CO$ (1:1).

[e] EDT-TTF / mg. No extra supporting electrolytes were added in the solution.

6-3. Preparation of M(dmise)2 Complexes

Synthesis of the Key Intermediate, (dmise)(COPh)2

The synthetic route to the dmise ligand [8 (e), 11] is straightforward but the author somehow could not reproduce it well; particular difficulty was found in separating the desired selone from the unreacted thione compound. A 1.0 M solution of $Et_3O{\cdot}BF_4$ in CH_2Cl_2 [8 (e), 12] did not appear to react smoothly with the starting material at room temperature even for prolonged time. Alternatively $(C_2H_5O)_2CH{\cdot}BF_4$ prepared *in situ* from $(C_2H_5)_2O{\cdot}BF_3$ and $HC(OC_2H_5)_3$ was tried, which is also known to be a powerful and selective ethylating reagent [13 (e), (k), 14], and in fact it was found to react effectively with the thione. Of the available procedures of the S-ethylation, the one described here is probably the most convenient, involving as it does a single-step preparation from inexpensive, commercially available and rather nonhazardous reagents, which are all have storage properties and may readily be handled in the air for short periods of time, whereas triethyloxonium tetrafluoroborate must be stored under ether in a tightly closed screw-cap bottle at 0 - 5 °C, handled in a dry box, and should be used within a few days of the time it is made. Thus the dialkoxycarbonium ion is the reagent of choice in this case.

An alternative method for the second step was also explored: as for the solvent, methyl alcohol was found to be more suitable than ethyl or isopropyl alcohols. In terms of yield, there was far more advantage in direct selenation of the dithiolium salt over the route via the iminium salt which was obtained by treatment of the dithiolium salt with excess morpholine in acetonitrile at room temperature for 3.5 h.

The dithiolium salt is stable and nonhygroscopic and does not require the use of dry box or an inert atmosphere. In this way the route shown in Scheme 6.1 has been found to be most convenient for obtaining the pure (dmise)(COPh)2. An attempt to obtain single crystals of it by leaving a CH_2Cl_2 solution of (dmise)(COPh)2 in the open atmosphere at room temperature was not successful; it only resulted in decomposition to deposit elemental red selenium.

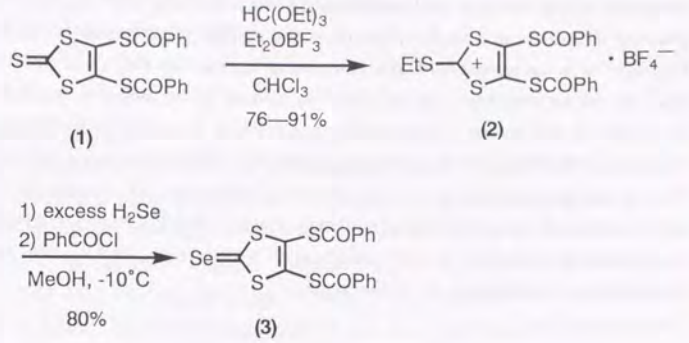

Scheme 6.1.

Synthesis and Chemical Property of [M(dmise)2] Salts

$[(C_4H_9)_2N]_2[M(dmise)_2]$ (M = Ni, Pd, Pt) was synthesized according to the same procedure in ref. [1] without any problem, but recrystallized from acetone alone instead of acetone/isopropyl alcohol, for the desired complex appeared to decompose on exposure to isopropyl alcohol. Methanol was found to dissolve $[(C_4H_9)_2N]_2[M(dmise)_2]$ more than it dissolves the corresponding dmit complex and it did not appear to promote the precipitation when it was added to the solution.

The difference in chemical properties between M(dmise)2 and M(dmit)2 complexes most clearly manifested itself in electrochemical behaviour [8 (e)]. Ni(dmise)2 complexes are less easily oxidized than Ni(dmit)2 complexes and electrocrystallization of the former required more anodic condition, which is consistent with the previous report [8 (e)]. On the contrary, the entire oxidation from $[Pd(dmit)_2]^{2-}$ to $[Pd(dmit)_2]^{x-}$ have been reported to seem to proceed at a single step at a relatively low potential [8 (e)]. In fact Pd-analogues were difficult to handle; they were easily oxidized during recrystallization in the air. The acetone solution of Pt-analogues, whose similar tendency in electrochemical behaviour is reported to be more obvious [8 (h)], easily deposited black insoluble powder which was conceived to be oxidized species on the slightest exposure to the air.

In general, the electrochemical behaviour [8 (e), (h)] indicates that the M(dmise)2 complex has a slightly higher first redox potential {M(II)/M(III); from $[M(dmit)_2]^{2-}$ to $[M(dmit)_2]^{1-}$} than its corresponding dmit-analogue but almost the same second redox potential {M(III)/M(VI); from $[M(dmit)_2]^{1-}$ to $[M(dmit)_2]$} owing to the smaller on-site Coulombic repulsion and the larger polarizability of the ligand molecule. Such

interpretation that the first oxidation becomes more difficult, while the second redox potential less shifts to a higher potential as the number of Se atoms in the molecule increases is in agreement with the observation reported by Olk *et al.* [8 (r)]. This tendency seems somewhat general when the increase of Se atoms in number can be assumed to be the increase in polarizability and decrease in on-site Coulombic repulsion, and when both effects can be assumed to reduce the difference in two redox potentials, for it is also the case with some chalcogen donor molecules [15]. In addition to higher potential required in electrochemical oxidation, a slight instability make the crystallization more difficult than that of dmit-analogues; it would often lead to two extremes, decomposition or seemingly no change at all.

6-4. $[(CH_3)_3HN][Ni(dmise)_2]_2$ and (EDT-TTF)[Ni(dmise)2]

Electrical Properties

The temperature dependence of the resistivity of $[(CH_3)_3HN][Ni(dmise)_2]_2$, which was obtained as black elongated very thin platelets, is shown in Figure 6.1(a). It exhibits weakly metallic behaviour around room temperature with a conductivity (σ_{RT}) of 100 $S \cdot cm^{-1}$; the resistivity gradually increases at low temperatures; the activation energy is 0.005 eV. The metallic region of the salt almost doubles for every 3 kbar increase in pressure. But the insulating phase is not completely suppressed even at 6 kbar. The anisotropy of the resistivity of the single crystal of $[(CH_3)_3HN][Ni(dmise)_2]_2$ by the Montgomery method has not yet been achieved because all the crystals obtained were too thin and fragile.

(EDT-TTF)[Ni(dmise)2] also exhibited metallic conductivity (σ_{RT} = 100 $S \cdot cm^{-1}$) down to *ca.* 100 K and made a smooth transition into an insulator at low temperature {Figure 6.1(b)}.

These species showed totally different electrical properties from the corresponding $Ni(dmit)_2$ salts [4 (v) – (y), 16] and have been found to be the second and third examples of molecular metals based on a $M(dmise)_2$ complex, the first example being β-$[(CH_3)_4N][Ni(dmise)_2]_2$ [8 (c), (e)].

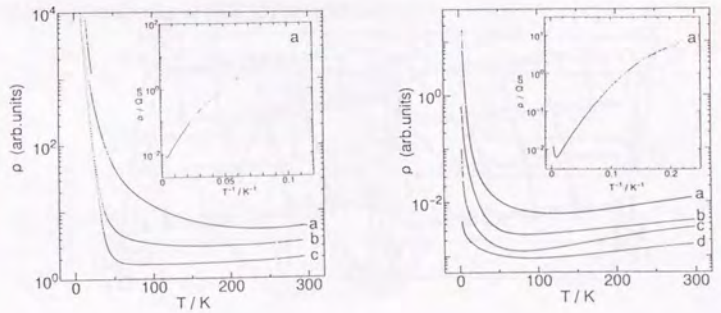

Figure 6.1. (a) Temperature dependence of the resistivity of $[(CH_3)_3HN][Ni(dmise)_2]_2$ under a: 1 bar, b: 3 kbar and c: 6 kbar, and (b) that of (EDT-TTF)[Ni(dmise)2] under a: 1 bar, b: 2 kbar, c: 6.2 kbar and d: 12.2 kbar

Crystal and Electronic Structures

The crystal structure of the $(CH_3)_3HN$ salt is shown in Figure 6.2. The crystal data: triclinic, P $\bar{1}$, a = 7.606(3), b = 17.761(3), c = 6.660(2) Å, α = 100.27(2), β = 114.93(2), γ = 81.84(2) °, V = 800.4(4) Å^3, Z = 1, R = 0.036, R_W = 0.022. The $Ni(dmise)_2$ molecules stack along the *a*-axis almost regularly; the interplanar distances are 3.464 and 3.557 Å. The cations are located near the inversion centre and they take either of the two statistically possible orientations (50 % - 50 % disordered). Such a structural trend is quite different from $[(CH_3)_3HN][Ni(dmit)_2]_2$ [16], but is instead associated with a dmit-based superconductor $[(CH_3)_2(C_2H_5)_2N][Pd(dmit)_2]_2$ [4 (t), (u)]. There are short contacts between two selenium atoms (< 4.0 Å) in addition to many of those between sulfur atoms (< 3.7 Å) within each $Ni(dmise)_2$ column as well as between the columns, which resembles β-$[(CH_3)_4N][Ni(dmise)_2]_2$ [8 (c), (e)]. But the most striking feature is that there are also found short contacts of Se---Se (3.486 and 3.801 Å) *through the cation sheet*, a feature which is also observed in α-$[(CH_3)_4N][Ni(dmise)_2]_2$ (3.277 Å) [8 (c), (e)]. One of the Se---Se distances is even shorter than the shortest S---S contact (3.568 Å) in this salt. Calculated intermolecular overlap integrals between LUMO's of the $Ni(dmise)_2$ molecules are summarized in Figure 6.3. These values well reflect the structural features; stacks of nearly equally spaced acceptor molecules are linked by weak interstack interactions. In addition, a notable unprecedented feature manifests itself between two selone groups; a much larger value { the one with suffix (S) } than most of the other intercolumnar ones.

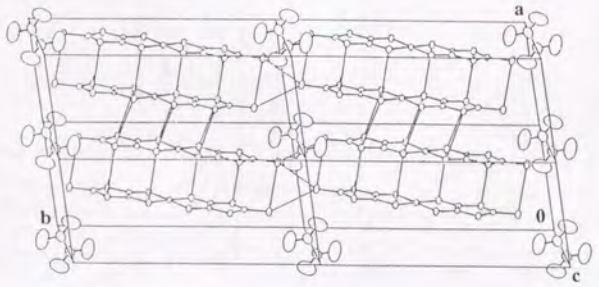

Figure 6.2. Crystal structure of $[(CH_3)_3HN][Ni(dmise)_2]_2$ The $(CH_3)_3HN$ cations are disordered and both of the two possible orientations are depicted. The thin lines indicate the intermolecular short contacts between the chalcogen atoms (S---S < 3.70 Å, Se---Se < 4.00 Å).

In fact the tight-binding band calculation by extended Hückel methods indicated that $[(CH_3)_3HN][Ni(dmise)_2]_2$ has even stronger intermolecular interactions *along the long molecular axis* than in the transverse direction owing to a close selenium-selenium contact. This feature leads to a three-dimentional electronic structure (Figure 6.4), indicating this complex to be a precursor of three-dimensional molecular metal based exclusively on planar π-conjugated molecules. This situation possibly arises from both the small size of the anion $\{[(CH_3)_3HN]^+\}$ and the spatially-extended terminal selenium atoms, which favour the packing motif that allows significant overlap of the selenium orbitals. In short, the $M(dmise)_2$ salt has demonstrated that the goal mentioned in the introduction is achieved; intermolecular interaction was expanded towards the third direction by the substitution of the selone group for the thione group.

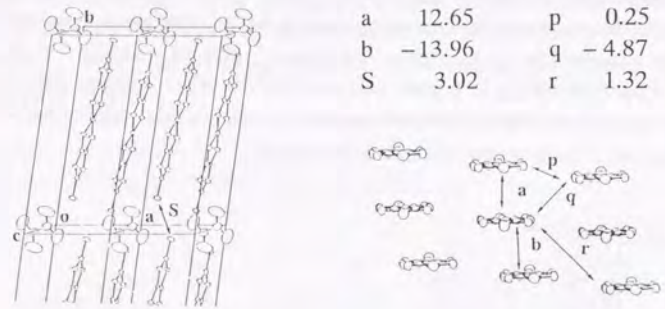

Figure 6.3. Intermolecular overlap integrals (× 10^{-3}) between the LUMO's of the $Ni(dmise)_2$ molecules in $[(CH_3)_3HN][Ni(dmise)_2]_2$

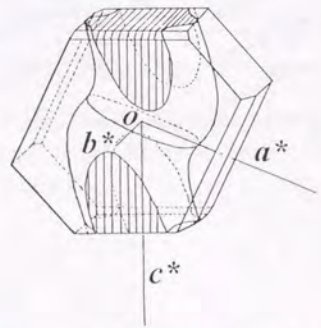

Figure 6.4. Schematic view of the Fermi surface of $[(CH_3)_3HN][Ni(dmise)_2]_2$ calculated by the tight-binding method

On the other hand, the X-ray structural analysis of the black plateletlike crystals of (EDT-TTF)[Ni(dmise)2] has not yet been completed satisfactorily because a crystal of high enough quality has not been available. Therefore a preliminary result is shown here (Figure 6.5). Crystal data: triclinic, P1, a = 23.43, b = 6.47, c = 4.23 Å, α = 86.8, β = 90.2, γ = 95.1 °, V = 637.2 Å^3, Z = 1. The donor (EDT-TTF) and acceptor [Ni(dmise)2] molecules make segregated columns, running in parallel with each other along the (001) direction. They both stack regularly with repeating separations of 3.75 Å for the EDT-TTF and 3.50 Å for the Ni(dmise)2 column. Their molecular planes have tilts from the stacking direction, as is often the case; the dihedral angle between the least-squares planes of the donor and acceptor molecules is 124 °. The general trend mentioned above is quite different from either α–, β–(EDT-TTF)[Ni(dmit)2] [4 (v) – (y)] or (EDT-TTF)2[Pd(dmit)2]2 [17].

The substitution of some selenium atoms for the sulfur atoms in the dmit ligand often results in salts with significantly different packing motifs like [(CH3)4N][Ni(dsit)2]2 [8 (a)] and salts with relatively minor structural differences but with substantially different electronic properties [8 (c), (e), (g)]. Each of the two cases mentioned above is another example of these trends.

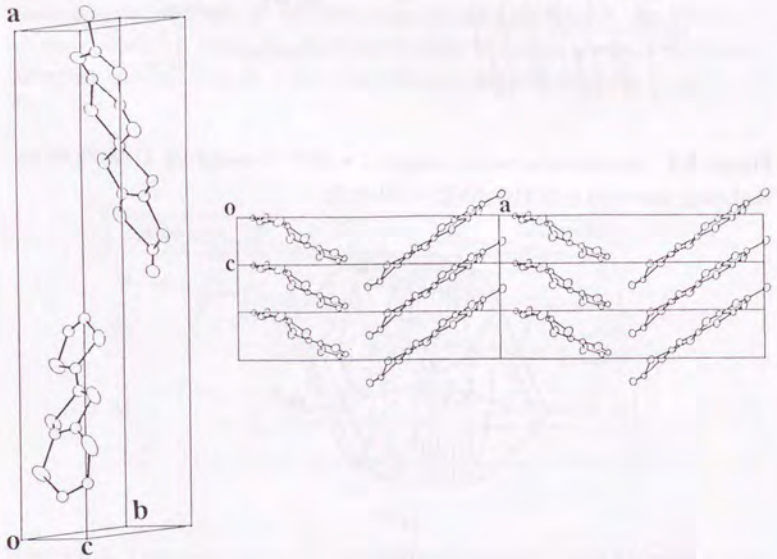

Figure 6.5. Crystal structure of (EDT-TTF)[Ni(dmise)2] A preliminary result (R = 0.165)

6-5. Other M(dmise)2 Complexes

(CH3)x(C2H5)4-xN (x = 0 – 4) Salts of Ni(dmise)2

(CH3)4N Salts of Ni(dmise)2; α– and β–[(CH3)4N][Ni(dmise)2]2

The electrocrystallization yielded needles and plates. The room temperature conductivity and activation energy of the platelike crystal are σ_{RT} = 10 S·cm^{-1}, E_a = 0.04 eV, which are consistent with the reported values [8 (c), (e)]. The semiconductive behaviour hardly changed even at 20 kbar (Figure 6.6), which contrasts with an isostructural, all-sulfur-analogue [(CH3)4N][Ni(dmit)2]2 being superconductive at 7 kbar [4 (d) – (o)]. On the other hand the needle phase crystals were too small and fragile to measure the conductivity. X-ray photographs revealed that the platelike crystals belong to β–phase (monoclinic, C2/c), while the needlelike crystals belong to α–phase (orthorhombic, Pbnb); such correspondence is the inverse of that reported by Cornelissen *et al*. [8 (e)].

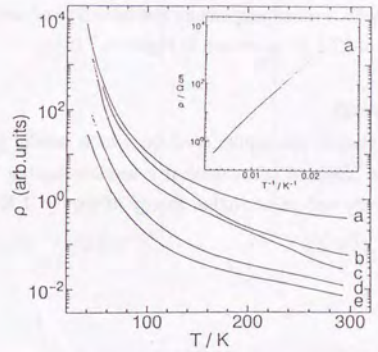

Figure 6.6. (right-hand side) Temperature dependence of the electrical resistivity of β–[(CH3)4N][Ni(dmise)2]2 (the platelike crystal) under a: 1 bar, b: 5.2 kbar, c: 10.4 kbar, d: 15.7 kbar and e: 20.1 kbar

$(CH_3)_3(C_2H_5)N$ Salt of Ni(dmise)2

Irregular shaped plateletlike crystals were obtained and exhibited a semiconducting behaviour with a room temperature conductivity and an activation energy of $\sigma_{RT} = 10^{-1}$ S·cm^{-1}, $E_a = 0.12$ eV as shown in Figure 6.7 (a). In regard to this species as well as the next three but one salts, single crystals of high enough quality for X-ray structural study have not been available.

$(CH_3)_2(C_2H_5)_2N$ Salt of Ni(dmise)2

Very thin long rectangular or square plateletlike crystals of dimension of *ca.* 3.5 × 3.5 mm^2 were obtained and exhibited a semiconducting behaviour with a room temperature conductivity and an activation energy of $\sigma_{RT} = 10^{-1}$ S·cm^{-1}, $E_a = 0.15$ eV as shown in Figure 6.7 (b). The crystals are of high quality but strong diffuse streaks in the X-ray photographs revealed that they may have a complicated crystal structure. The structure was not investigated further.

$(CH_3)(C_2H_5)_3N$ Salt of Ni(dmise)2

Very thin irregular shaped plateletlike crystals were obtained and exhibited a semiconducting behaviour with a room temperature conductivity and an activation energy of $\sigma_{RT} = 10^{-1}$ S·cm^{-1}, $E_a = 0.12$ eV as shown in Figure 6.7 (c).

$(C_2H_5)_4N$ Salt of Ni(dmise)2

Very thin irregular shaped plateletlike crystals, which rapidly grew into a hairy cluster on the anode, were obtained and exhibited a semiconducting behaviour with a room temperature conductivity and an activation energy of $\sigma_{RT} = 1$ S·cm^{-1}, $E_a = 0.12$ eV as shown in Figure 6.7 (d).

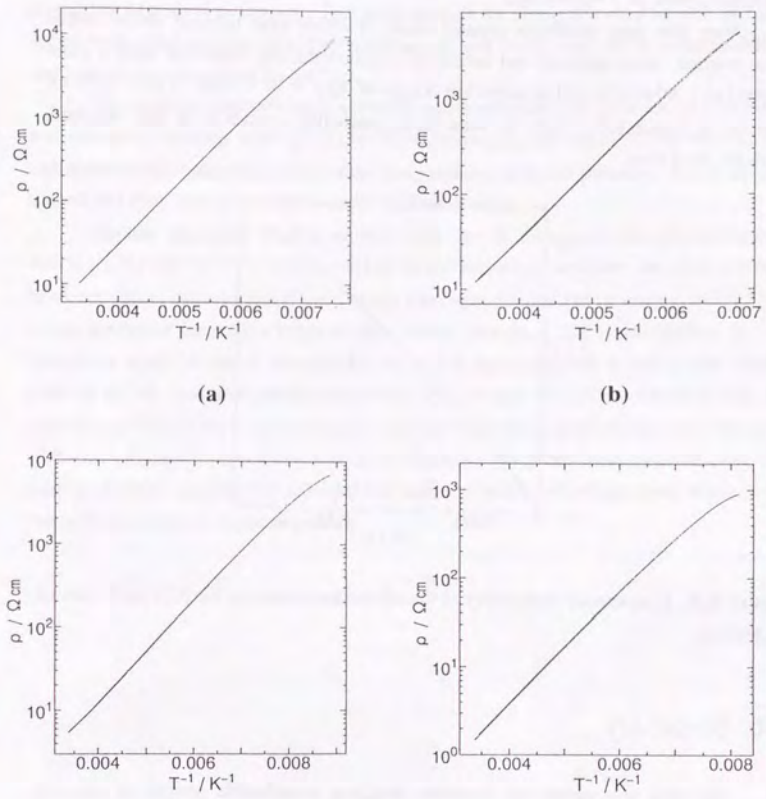

Figure 6.7. Temperature dependence of the $(CH_3)_x(C_2H_5)_{4-x}N$ (x = 0 – 3) salts of Ni(dmise)2; (a) x = 3, (b) x = 2, (c) x = 1 and (d) x = 0

$(CH_3)_4N$ Salts of Pd(dmise)2

Very thin, long needlelike crystals, many of which were twinned and/or forked and/or warped, were obtained and exhibited a semiconducting behaviour with a room temperature conductivity and an activation energy of $\sigma_{RT} = 10^{-1}$ S·cm^{-1}, $E_a = 0.05$ eV as shown in Figure 6.8. From the same batch plateletlike crystals were also obtained, which are insulators.

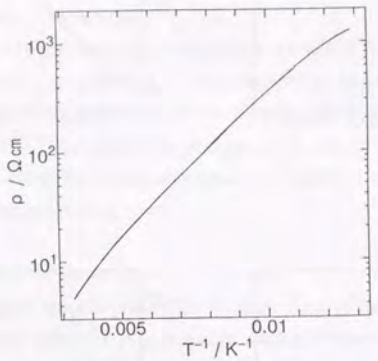

Figure 6.8. Temperature dependence of the needlelike crystals of the $(CH_3)_4N$ salts of Pd(dmise)2

6-6. Summary

The dmit compounds are currently attracting considerable interest as versatile building blocks of molecular-based conducting materials. Yet the dmit complex molecules are apt to stack to make one-dimensional columns with little intercolumnar interaction. This often results in a metal instability at low temperatures and in fact most of the charge-transfer salts of the complexes are semiconductors even at room temperature. The substitution of selenium atoms for some of the peripheral sulfur atoms in the ligand has not much improved the situation maybe because the small intercolumnar interaction does not originate in the insufficiency of the chalcogen-chalcogen contacts but rather originates in the cancellation of the overlaps due to the asymmetry of the molecular orbitals. In the meantime, the selone group in the dmise ligand is highly promising for extending the intermolecular interaction towards its protruding direction. The use of smaller counter cations or chalcogen donors adds to the promise. However there are few studies on the solid state property of such M(dmise)2 salts partly because there are few reported way of synthesis without difficulty or roundabout route.

In this work, a new synthetic route of dmise ligand has been developed by modifying a reported procedure. This route inherits the straightforward as well as easy access with a high overall yield of the previous one and is still superior in reproducibility and ease of the isolation of the product.

The standard electrochemical synthesis produced a series of new M(dmise)2 salts and complex. Among them $[(CH_3)_3HN][Ni(dmise)_2]_2$ and (EDT-TTF)[Ni(dmise)2] exhibited metallic behaviour around room temperature at ambient pressure, which are the second and third examples of the metallic M(dmise)2 salts.

Another important finding of this work lies in the quasi-three-dimensionality which $[(CH_3)_3HN][Ni(dmise)_2]_2$ realized in the electronic structure; the tight-binding band calculation indicates that it has a nearly three-dimensional Fermi surface owing to a strong *intersheet* interaction between their selone groups. The Fermi surface is not completely closed in the c^* direction but the fact to be emphasized is that it has closed sections in all three independent directions; a^*, b^* and c^*. This situation can be described as "nearly three-dimensional". This has long been a goal among chemists who deal with a design of organic conductors and the news that planar π-conjugated molecule such as a dmise complex has achieved this situation would encourage many scientist to research the related or new compounds.

References

[1] G. Steimecke, H. J. Sieler, R. Kirmse and E. Hoyer, *Phosphorus Sulfur*, **7**, 49(1979).

[2] (a) W. Knop and G. Schnedermann, *J. Prakt. Chem.*, **37**, 461(1846);
(b) J. A. McCleverty, *Prog. Inorg. Chem.*, **10**, 49(1968);
(c) G. N. Schrauzer, *Transition Met. Chem.*, **4**, 299(1968);
(d) G. N. Schrauzer, *Acc. Chem. Res.*, **2**, 72(1969);
(e) K. Krogmann, *Angew. Chem. Int. Ed. Engl.*, **8**, 35(1969);
(f) E. Hoyer, W. Dietzsch and W. Schroth, *Z. Chem.*, **11**, 41(1971);
(g) H. R. Zeller, *Festkoerperprobleme*, **13**, 31(1973);
(h) W. E. Geiger, Jr., C. S. Allen, T. E. Mines and F. C. Senftleber, *Inorg. Chem.*, **16**, 2003(1977);
(i) R. Kirmse, J. Stach and W. Dietzsch, *Inorg. Chim. Acta*, **29**, L181(1978);
(j) K. W. Browal and L. V. Interrante, *J. Coord. Chem.*, **3**, 27(1973);
(k) G. Steimecke, R. Kirmse and E. Hoyer, *Z. Chem.*, **15**, 28(1975);
(l) R. Kirmse, J. Stach, W. Dietzsch, G. Steimecke and E. Hoyer, *Inorg. Chem.*, **19**, 2679(1980), and references cited therein;

[3] (a) M. Mizuno, A. F. Garito and M. P. Cava, *J. Chem. Commun.*, **1978**, 18.
(b) K. S. Varma, A. Bury, N. J. Harris and A. E. Underhill, Synthesis, **1987**, 837;
(c) E. M. Engler, V. Y. Lee, R. R. Shcumaker, S. S. P. Parkin, R. L. Green and J. C. Scott, *Mol. Cryst. Liq. Cryst.*, **107**, 19(1984);
(d) J. M. Williams and coworkers, *Inorg. Synth.*, **26**, 386(1989);
for general review, see
(e) A. Krief, *Tetrahedron*, **42**, 1209(1986).

[4] (a) M. Bousseau, L. Valade, M. -F. Bruniquel, P. Cassoux, M. Garbauskas, L. V. Interrante and J. Kasper, *Nouv. J. Chim.*, **8**, 3(1985);
(b) M. Bousseau, L. Valade, J. -P. Legros, P. Cassoux, M. Garbauskas, and L. V. Interrante, *J. Am. Chem. Soc.*, **108**, 1908(1986);
(c) L. Brossard, M. Ribault, M. Bousseau, L. Valade and P. Cassoux, *C. R. Acad. Sci. Paris. Sér. 2*, **302**(5), 205(1986);
(d) H. Kim, A. Kobayashi, Y. Sasaki, R. Kato and H. Kobayashi, *Chem. Lett.*, **1987**, 1799;
(e) A. Kobayashi, H. Kim, Y. Sasaki, R. Kato, H. Kobayashi, S. Moriyama, Y. Nishio, K. Kajita and W. Sasaki, *Chem. Lett.*, **1987**, 1819;
(f) A. Kobayashi, H. Kim, Y. Sasaki, S. Moriyama, Y. Nishio, K. Kajita, W. Sasaki, R. Kato and H. Kobayashi, *Synth. Met.*, **27**, B339(1988);
(g) K. Kajita, Y. Nishio, S. Moriyama, R. Kato, H. Kobayashi and W. Sasaki, *Solid State Commun.*, **65**, 361(1988);
(h) H. Kobayashi, R. Kato, A. Kobayashi, T. Mori, H. Inokuchi, Y. Nishio, K. Kajita and W. Sasaki, *Synth. Met.*, **27**, A289(1988);
(i) H. Tajima, M. Tamura, T. Naito, A. Kobayashi, H. Kuroda, R. Kato, H. Kobayashi, R. A. Clark and A. E. Underhill, *Mol. Cryst. Liq. Cryst.*, **181**, 233(1990);
(j) H. Tajima, T. Naito, M. Tamura, A. Takahashi, S. Toyoda, A. Kobayashi, H. Kuroda, R. Kato, H. Kobayashi, R. A. Clark and A. E. Underhill, *Synth. Met.*, **41-43**, 2417(1991);
(k) M. Tamura, R. Masuda, T. Naito, H. Tajima, H. Kuroda, A. Kobayashi, K. Yakushi, R. Kato, H. Kobayashi, M. Tokumoto, N. Kinoshita and H. Anzai, *Synth. Met.*, **41-43**, 2499(1991);
(l) L. R. Groeneveld, B. Schuller, G. J. Kramer, J. G. Haasnoot and J. Reedijk, *Rec. Trav. Chim. Pays-Bas*, **105**, 507(1986);
(m) L. R. Groeneveld, G. J. Kramer, T. B. L. W. von Marinelli, H. B. Brom, J. G. Haasnoot and J. Reedijk, *Organic and Inorganic Low-Dimensional Crystalline Materials*, P. Delhaes and M. Drillon, Eds., Plenum Press, New York, 1987, p.349;
(n) E. Canadell, E. I. Rachidi, S. Ravy, J. -P. Pouget, L. Brossard and J. P. Legros, *J. Phys. (Paris)*, **50**, 2967(1989);
(o) E. Canadell, S. Ravy, J. -P. Pouget and L. Brossard, *Solid State Commun.*, **75**, 633(1990);
(p) L. Brossard, M. Ribault, L. Valade and P. Cassoux, *J. Phys. (Paris)*, **50**, 1521(1989);
(q) L. Brossard, H. Hurdequint, M. Ribault, L. Valade, J. -P. Legros and P. Cassoux, *Synth. Met.*, **27**, B157(1988);
(r) A. Kobayashi, H. Kim, Y. Sasaki, K. Murata, R. Kato and H. Kobayashi, *J. Chem. Soc., Faraday Trans.*, **86**, 361(1990);
(s) A. Kobayashi, H. Kobayashi, A. Miyamoto, R. Kato, R. A. Clark and A. E. Underhill, *Chem. Lett.*, **1991**, 2163;
(t) A. Kobayashi, R. Kato, R. A. Clark, A. E. Underhill, A. Miyamoto, K. Bun, T. Naito and H. Kobayashi, *Synth. Met.*, **55-57**, 2927(1993);
(u) H. Kobayashi, K. Bun, T. Naito, R. Kato and A. Kobayashi, *Chem. Lett.*, **1992**, 1909;
(v) R. Kato, H. Kobayashi, A. Kobayashi, T. Naito, M. Tamura, H. Tajima and H. Kuroda, *Chem. Lett.*, **1989**, 1839;
(w) H. Tajima, S. Ikeda, A. Kobayashi, H. Kuroda, R. Kato and H. Kobayashi, *Solid State Commun.*, **86**, 7(1993);

(x) H. Tajima, M. Inokuchi, A. Kobayashi, T. Ohta, R. Kato, H. Kobayashi and H. Kuroda, *Chem. Lett.*, **1993**, 1235;

(y) H. Tajima, M. Inokuchi, S. Ikeda, M. Arifuku, T. Naito, M. Tamura, T. Ohta, A. Kobayashi, R. Kato, H. Kobayashi and H. Kuroda, *Synth. Met.*, in press.

[5] (a) H. Kobayashi, R. Kato and A. Kobayashi, *Isr. J. Chem.*, **27**, 301(1986);

(b) A. Kobayashi, H. Kim, Y. Sasaki, R. Kato and H. Kobayashi, *Solid State Commun.*, **62**(2), 57(1987);

(c) R. Kato, H. Kobayashi, H. Kim, A. Kobayashi, Y. Sasaki, T. Mori and H. Inokuchi, *Synth. Met.*, **27**(3-4), B359(1988);

(d) R. Kato, H. Kobayashi, H. Kim, A. Kobayashi, Y. Sasaki, T. Mori and H. Inokuchi, *Chem. Lett.*, **1988**, 865;

(e) S. Alvarez, R. Vicente and R. Hoffmann, *J. Am. Chem. Soc.*, **107**, 6253(1987).

[6] for general reviews on dmit compounds, see

(a) P. Cassoux, L. Valade, H. Kobayashi, A. Kobayashi, R. A. Clark and A. E. Underhill, *Coord. Chem. Rev.*, **110**, 115(1991);

(b) R. -M. Olk, B. Olk, W. Dietzsch, R. Kirmse, E. Hoyer, *Coord. Chem. Rev.*, **117**, 99(1992).

[7] H. Kobayashi, R. Kato and A. Kobayashi, *Synth. Met.*, **41-43**, 2495(1991).

[8] (a) M. A. Beno, A. M. Kini, U. Geiser, H. H. Wang, D. K. Carlson, J. M. Williams, *The Physics and Chemistry of Organic Superconductors*, G. Saito, S. Kagoshima, Eds., Springer Verlag, Berlin, 1990, p.369;

(b) M. A. Beno, A. M. Kini, S. Buds, H. H. Wang, J. M. Williams, *Materials Research Society Symp. Proc.*, **173**, 177(1990);

(c) J. P. Cornelissen, D. Reefman, J. G. Haasnoot, A. L. Spek, J. Reedijk, *Recl. Trav. Chim. Pay-Bas*, **110**, 345(1991);

(d) J. P. Cornelissen, J. G. Haasnoot, J. Reedijk, C. Faulmann, J. -P. Legros, P. Cassoux, P. J. Nigrey, *Inorg. Chim. Acta*, **202**, 131(1992);

(e) J. P. Conelissen, B. Pomarède, A. L. Spek, D. Reefman, J. G. Haasnoot, J. Reedijk, *Inorg. Chem.*, **32**, 3720(1993);

(f) C. Faulmann, J. -P. Legros, P. Cassoux, J. P. Cornelissen, J. G. Haasnoot, J. Reedijk, *Synth. Met.*, **55-57**, 2063(1993);

(g) C. Faulmann, J. -P. Legros, P. Cassoux, J. P. Cornelissen, L. Brossard, M. Inokuchi, H. Tajima, M. Tokumoto, *J. Chem. Soc., Dalton Trans.*, **1994**, 249;

(h) R. -M. Olk, R. Kirmse, E. Hoyer, C. Faulmann and P. Cassoux, *Z. anorg. allg. Chem.*, **620**, 90(1994);

(i) T. Naito, A. Sato, K. Kawano, A. Tateno, H. Kobayashi and A. Kobayashi, *J. Chem. Soc., Chem. Commun.*, **1995**, 351;

(j) R. -M. Olk, W. Dietzsch, J. Mattusch, J. Stach, C. Nicke, E. Hoyer, W. Meiler and W. Robien, *Z. anorg. allg. Chem.*, **544**, 199(1987);

(k) R.-M. Olk, W. Dietzsch, K. Köhler, R. Kirmse, J. Reinhold, E. Hoyer, L. Golič and B. Olk, *Z. anorg. allg. Chem.*, **567**, 131(1988);

(l) P. J. Nigrey, *Synth. Met.*, **27**, B365(1988);

(m) R.-M. Olk, B. Olk, W. Dietzsch and E. Hoyer, *Z. Chem.*, **29**, 250(1989);

(n) R.-M. Olk, A. Röhr, J. Sieler, K. Köhler, R. Kirmse, W. Dietzsch, E. Hoyer and B. Olk, *Z. anorg. allg. Chem.*, **577**, 206(1989);

(o) R.-M. Olk, C. Semmelmann, R. Kirmse, K. Köhler, E. Hoyer, B. Olk, *Z. anorg. allg. Chem.*, **581**, 59(1990);

(p) R.-M. Olk, B. Olk, J. Rohloff and E. Hoyer, *Z. Chem.*, **30**, 445(1990);

(q) B. Olk, R. -M. Olk, J. Sieler and E. Hoyer, *Synth. Met.*, **41-43**, 2585(1991);

(r) R.-M. Olk, B. Olk, J. Rohloff, J. Reinhold, J. Sieler, K. Trübenbach, R. Kirmse and E. Hoyer, *Z. anorg. allg. Chem.*, **609**, 103(1992) and references cited therein.

[9] R. Kato, T. Mori, A. Kobayashi, Y. Sasaki and H. Kobayashi, *Chem. Lett.*, **1984**, 1.

[10] (a) D. D. Perrin and W. L. F. Armarego, *Purification of Laboratory Chemicals* (Pergamon Press, New York, 3rd edn., 1988.);

(b) L. Carlsen, H. Egsgaard and J. R. Andersen, *Anal. Chem.*, **51**(9), 1593(1979).

[11] (a) D. L. Klayman and T. Scott-Griffin, *J. Am. Chem. Soc.*, **95**, 177(1973);

(b) A. Moradpour, V. Peyrussan, I. Johansen and K. Bechgaard, *J. Org. Chem.*, **48**, 388(1983).

[12] V. Y. Khodorkovskii, J. Kreicberga, K. A. Balodis, O. Y. Neiland, *Isv. Akad. Nauk, Latv. SSR, Ser. Khim.*, **1988**, 120.

[13] (a) H. Meerwein, G. Hinz, P. Hofmann, E. Kroning and E. Pfeil, *J. Prakt. Chem.*, **147**(2), 257(1937);

(b) H. Meerwein, E. Bettenberg, H. Gold, E. Pfeil and G. Willfang, *J. Prakt. Chem.*, **154**(2), 83(1940);

(c) H. Meerwein, P. Borner, O. Fuchs, H. J. Sasse, H. Schrodt and J. Spille, *Chem. Ber.*, **89**(9), 2060(1956);

(d) H. Meerwein, in *Methoden der Organischen Chemie* (Houben-Weyl), **Vol. 6/3**, Georg Thieme Verlag, Stuttgart, 1965, p.325;

(e) S. Kabuss, *Angew. Chem.*, **78**, 714(1966) [*Angew. Chem. Int. Ed. Engl.*, **5**, 675(1966)];

(f) R. B. Silverman and R. A. Olofson, *Chem. Commun.*, **1968**, 1313;
(g) T. J. Curphey, *Org. Syntheses*, **51**, 142(1971);
(h) H. Meerwein, *Org. Synth.*, **Coll. Vol. 5**, 1080(1973);
(i) H. Meerwein, *Org. Synth.*, **Coll. Vol. 5**, 1096(1973);
(j) D. J. Raber, P. Gariano, Jr., A. O. Brod, A. L. Gariano and W. C. Guida, *Org. Synth.*, **Coll. Vol. 6**, 576(1988);
(k) T. J. Curphey, *Org. Synth.*, **Coll. Vol. 6**, 1019(1988) and references cited therein.
[14] U. Pindur and C. Flo, *Synth. Commun.*, **19**(13&14), 2307(1989).
[15] (a) R. Kato, H. Kobayashi, A. Kobayashi and Y. Sasaki, *Chem. Lett.*, **1985**, 1231;
(b) N. Okada, H. Yamochi, F. Shinozaki, K. Oshima and G. Saito, *Chem. Lett.*, **1986**, 1861;
(c) V. Y. Lee, *Synth. Met.*, **20**, 161(1987);
(d) S. -Y. Hsu and L. Y. Chiang, *J. Org. Chem.*, **52**, 3444(1987);
(e) K. Nakasuji, M. Sasaki, T. Kotani, I. Murata, T. Enoki, K. Imaeda, H. Inokuchi, A. Kawamoto and J. Tanaka, *J. Am. Chem. Soc.*, **109**, 6970(1987);
(f) W. Chen, M. P. Cava, M. A. Takassi and R. M. Metzger, *J. Am. Chem. Soc.*, **110**, 7903(1988);
(g) C. Rovira, N. Santaló and J. Veciana, *Tetrahedron Lett.*, **30**(51), 7249(1989);
(h) M. Sallé, A. Gorgues, J. -M. Fabre, K. Bechgaard, M. Jubault and F. Texier, *J. Chem. Soc., Chem. Commun.*, **1989**, 1520;
(i) T. Suzuki, H. Yamochi, G. Srdanov, K. Hinkelmann and F. Wudl, *J. Am. Chem. Soc.*, **111**, 3108(1989);
(j) K. Nakasuji, J. Toyoda, K. Imaeda, H. Inokuchi, I. Murata, A. Oda, A. Kawamoto and J. Tanaka, *Synth. Met.*, **41-43**, 2529(1991);
(k) H. Tani, K. Masumoto, N. Azuma and A. Ono, *Chem. Lett.*, **1994**, 779.
[16] (a) J. -P. Legros, L. Valade, B. Garreau, B. Pomarède, P. Cassoux, L. Brossard, S. Dubois, A. Audouard and J. -P. Ulmet, *Synth. Met.*, **55-57**, 2146(1993);
(b) B. Pomarède, B. Garreau, I. Malfant, L. Valade, P. Cassoux, J. -P. Legros, A. Audouard, L. Brossard, J. -P. Ulmet, M. -L. Doublet and E. Canadell, *Inorg. Chem.*, **33**, 3401(1994) and references cited therein.
[17] B. Garreau, B. Pomarède, C. Faulmann, J. -M. Fabre, P. Cassoux and J. -P. Legros, *C. R. Acad Sci. (Paris). Sèrie II*, **313**, 509(1991).

Chapter 7.

Optical Study on Electronic Structures of Molecular Superconductors Based on M(dmit)2 and Their Related Salts

7-1. Introduction

As reviewed in the introduction in the preceding Chapter, the metal-dmit complexes M(dmit)$_2$ (M = Ni, Pd, Pt, Au, ⋯) are one of the most important building blocks, which is now only a score old but a rapidly expanding group of compounds. The M(dmit)$_2$ complex molecules have two prominent features compared with other building blocks of molecular conductors. One is the thione located at the end of the π−conjugation, which could enable a potential three dimensionality in the intermolecular interactions in the solid states by the thione-thione short contacts. The related matter has already been examined in the preceding Chapter. The second feature is the small energy separation between the HOMO and LUMO† in the isolated neutral M(dmit)$_2$. In fact some cases have been found where the two energy levels are partly inverted in the strongly dimerized M(dmit)$_2$ solids. This fact has been recently confirmed in certain Pd(dmit)$_2$ and Pt(dmit)$_2$ salts from experiments [1 (f), (g), 2 (c), (d)] and calculation [1 (k)]. From the author's point of view, the M(dmit)$_2$ solids are particularly interesting because they may have unique electronic structures due to these characteristics. An optical study is known to be one of the most powerful tool to elucidate such a problem of electronic structures.

In terms of the purpose, the author chose the following six compounds for the optical study. They are the three molecular superconductors with closed-shell cations reported to date and three more compounds of closely related structures to them; $(CH_3)_4N[Ni(dmit)_2]_2$ (abbreviated as "the Ni salt" below) [1], β−$(CH_3)_4N[Pd(dmit)_2]_2$ (abbreviated as "the β−Pd salt" below) [1 (c), 3, 4], $(CH_3)_2(C_2H_5)_2N[Pd(dmit)_2]_2$ (abbreviated as "the Me_2Et_2N salt" below) [4 (b), 5], β−$(CH_3)_4As[Pd(dmit)_2]_2$ (abbreviated as "the As salt" below) [3], $Cs[Pd(dmit)_2]_2$ (abbreviated as "the Cs salt" below) [2] and $(CH_3)_4N[Pt(dmit)_2]_2$ (abbreviated as "the Pt salt" below) [6]. The reason can be summarized as follows;

† In this chapter, the author calls the lowest unoccupied molecular orbital of the isolated $[M(dmit)_2]$ molecule as LUMO and the highest occupied molecular orbital of it as HOMO. Thus the name of every molecular orbital can be uniquely decided irrespective of the oxidation state of $[M(dmit)_2]^{n-}$.

—all but the Me_2Et_2N salt are isostructural and the Me_2Et_2N salt can be treated in the same way in the optical study thanks to the similar crystal structure, thus the comparison would help the understanding of the results,

—such materials are significant because they exhibit electrical and magnetic properties based exclusively on the electronic structures consist of the $M(dmit)_2$ molecules, while the donor-acceptor complexes often exhibit complicated properties which can originate from both donor and acceptor molecules [1 (f), 7],

—although they are merely a small part of a wide spectrum of the reported $M(dmit)_2$ species, they can be regarded as good models, for they cover various properties from insulators to superconductors.

Since the details of the electronic structure of the $M(dmit)_2$ solids are hardly known, the obtained experimental information can be expected to be seminal and to contribute to the understanding and development of the $M(dmit)_2$-based molecular (super)conductors. This chapter describes a series of optical study on these dmit-complexes.

7-2. Theoretical for Analysis

The general theoretical background of the optical study is discussed in detail [8]. The analyses was carried out by the curve-fitting (or dispersion analysis) method [9 (b)] and modified Kramers-Kronig analysis [10]. In the former case, the complex dielectric function was expressed as the Drude-Lorentz model;

$$\varepsilon(\omega) = \varepsilon_c - \frac{\omega_p^2}{\omega(\omega + \frac{i}{\tau})} + \sum_j \frac{S_j\,\omega_j^2}{(\omega_j^2 - \omega^2) - i\,\gamma_j\,\omega_j\,\omega} \qquad (7.1)$$

where ε_c, ω_p and τ are the background dielectric constant, the plasma frequency of intraband transition and relaxation rate of free carriers, respectively, while S_j , ω_j and γ_j are the parameters of the Lorentz oscillator for the excitation j . The reflectance $R(\omega)$ and the complex dielectric function $\varepsilon(\omega)$ is related by the following equation.

$$R(\omega) = \frac{|\varepsilon(\omega)| + 1 - \sqrt{2\{|\varepsilon(\omega)| + \mathrm{Re}[\varepsilon(\omega)]\}}}{|\varepsilon(\omega)| + 1 + \sqrt{2\{|\varepsilon(\omega)| + \mathrm{Re}[\varepsilon(\omega)]\}}} \qquad (7.2)$$

As we will see later, from the curve-fitting analysis of the optical spectra, the Drude parameters such as the anisotropical optical mass $(m^*)_i$ along the polarization vector (i) are obtainable. The $(m^*)_i$ is defined by Equation (7.3) using the Fermi-Dirac occupation number f(E).

$$\frac{1}{(m^*)_i} = \frac{\int f(E)\frac{\partial E^2}{\partial k_i^2}\,d\vec{k}}{h^2\int f(E)\,d\vec{k}} \qquad (7.3)$$

$(m^*)_i$ is actually derived from $(\omega_p)_i^2$ by use of Equation (7.4),

$$(m^*)_i = \frac{4\pi e^2 N}{(\omega_p)_i^2} \qquad (7.4)$$

while m and m^* are related by

$$m^* = \frac{m}{\sum_j f_j} \qquad (7.5)$$

The dielectric function was also calculated through the Kramers-Kronig transformation of the reflectance spectra [10]. The extrapolation of the reflectance spectra was performed according to the Hagen-Rubens relation [8],

$$R(\omega) \approx 1 - \sqrt{\frac{2\omega}{\pi\,\sigma_0}} \qquad \text{(cgs)} \qquad (7.6)$$

where σ_0 is the dc conductivity.

The oscillator strength of an absorption band was obtained as follows [9 (b)]. In the case of dispersion analysis, the author used one dispersion term for each absorption band.

$$\varepsilon^j(\omega) = \frac{S_j\,\omega_j^2}{(\omega_j^2 - \omega^2) - i\,\gamma_j\,\omega_j\,\omega} \qquad (7.7.1)$$

for an interband transition, and

$$\varepsilon^j(\omega) = \frac{\omega_p^2}{\omega(\omega + \frac{i}{\tau})} \qquad (7.7.2)$$

for the intraband transition. Then the oscillator strength of the band (j) was calculated by the following equation [9 (b)],

$$f_j = \frac{m}{2\pi^2 e^2 N} \int_0^\infty \mathrm{Im}[\varepsilon^j(\omega)]\, \omega\, d\omega \qquad (7.8)$$

where N is the number density of electrons concerned with the transition j, m is the electron mass and e is the electron charge.

In the Kramers-Kronig analysis, the oscillator strength was calculated as follows [9 (b)],

$$f_j = \frac{m}{2\pi^2 e^2 N} \int_{\omega_a}^{\omega_b} \mathrm{Im}[\varepsilon(\omega)]\, \omega\, d\omega \quad (7.9)$$

where ω_a and ω_b are the lower and upper limit of wavenumbers of the band in question. The case where an interband transition superposes on the intraband transition is discussed in ref. [8 (c)].

The oscillator strength f_j of the transition j and the plasma frequency $(\omega_p)_j$ are related by

$$f_j = \frac{(\omega_p)_j^2\, m}{4\pi e^2 N} \qquad (7.10)$$

Within the framework of single-particle exitation, the complex conductivity for the polarization (i) at 0 K was calculated by use of the following formula.

$$\sigma_i(\omega) = \frac{2}{i\ \Omega h^3} \sum_n \frac{\omega}{\omega_{n0}} \frac{[\hat{H},\hat{P}_i]_{0n}[\hat{H},\hat{P}_i]_{n0}}{\omega^2 - \omega_{n0}^2 + i\gamma\ \omega} \qquad (7.11)$$

where $\hat{P}_i$ is the projection of the dipole operator $\hat{P}$ along the i direction, Ω is the crystal volume, γ is the electronic relaxation rate, which was tentatively assumed to be 0.1 eV, and 0 and n stand for the ground and excited states, respectively. The Hamiltonian and dipole operators are expressed as follows [9 (c), (h)],

$$\begin{aligned} \hat{H} &= \sum_{pl,qm} t_{pl,qm} a_{pl}^\dagger a_{qm} \\ &= \sum_k \sum_{l,m} [t_{0l,qm} \exp\{i\vec{k}\cdot(\vec{r}_0 - \vec{r}_q)\}] a_{kl}^\dagger a_{km} \end{aligned} \qquad (7.12)$$

$$\hat{\vec{P}} = e \sum_{p,l} \vec{r}_{p,l} a_{pl}^\dagger a_{pl} \qquad (7.13)$$

where $a_{pl}^\dagger$ and a_{pl} are the creation and annihilation operators of electron at the site (l) in the unit cell (p), $t_{pl,qm}$ is the transfer integral and $\vec{r}_{p,l}$ is the position vector.

On the same basis, the square of the plasma frequency ω_p^2 was calculated as follows

$$\omega_p^2 = \frac{4\pi^2 e^2 d^2 t}{V} \qquad (7.14)$$

where V and d respectively denote the volume and the spacing of the dimer. Here the excitation energy is assumed to equal to the double of the transfer energy.

7-3. Experimental

Materials

The single crystals were prepared by the reported procedures [1 – 6]. All but the Cs salt, which was a streamlined elliptical plate, the crystals were basically rectangular (or a fraction of it; see the scheme below) thin (~ 0.005 mm thick) black plates with typical dimensions of 1 × 2 mm^2, but some crystals were irregular shaped plates of more or less smaller sizes. The plateletlike crystals used in this work usually had edges or diagonal lines parallel to the *a*- and/or *b*-axes. The X-ray photographs revealed that their developed crystal faces coincide with the conducting planes. They all belong to the monoclinic system with space group C2/c except for the Me_2Et_2N salt, which belongs to P $\bar{1}$ [1 – 6].

Crystal Structure and Electrical Properties

Figure 7.1 shows the electrical behavior of all the species in discussion [1 – 6]. At ambient pressure, their resistivities all increase at low temperatures. The Cs salt exhibits metallic conductivity down to 56.5 K, where a metal-insulator (MI) transition occurs [2]. The Pt salt shows a nearly constant resistivity which may be considered to be barely metallic or rather high conductive down to 220 – 230 K, where a rapid increase in the resistivity sets in at low temperature [6]. The Me_2Et_2N salt is weakly metallic around room temperature and make a smooth transition into a semiconductor at low temperature with somewhat sample dependent behavior [4 (b), 5]. The Ni [1 (a) – (c)], β–Pd [4] and

Me_2Et_2N salts exhibit superconductivity under moderate pressure, whereas the As [3], Cs and Pt salts are non-superconducting under up to 10 kbar or higher pressure.

Figure 7.2 depicts the common structure of the five compounds, the Ni, As, Cs, Pt and the β−Pd salts (monoclinic, C2/c) [1 – 6]. The dmit-complex molecules stack (along the [110] or [11 $\bar{0}$] direction) forming a conduction sheet in the *ab*-plane. The sheet alternates with the insulating sheet of the cations along the *c*-axis. All columns are parallel in a sheet but those two in the neighboring sheets are torsional, which situation was called solid-crossing columns [4 (b), 5]. The only substantial difference in the crystal structure of the Me_2Et_2N salt (triclinic, P $\bar{1}$) from the others is that the acceptor columns are oriented in the same direction [101] in every sheet in the Me_2Et_2N salt (Figure 7.3) [4 (b), 5].

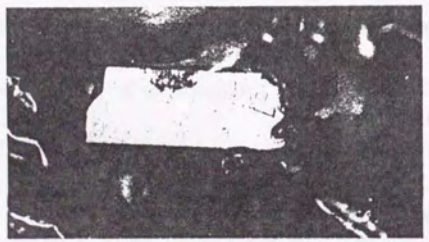

Scheme 7.1. Photograph of the single crystal of β−$(CH_3)_4As[Pd(dmit)_2]_2$

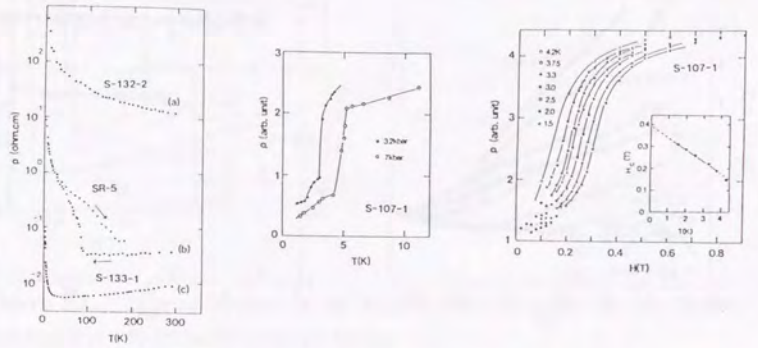

(a)

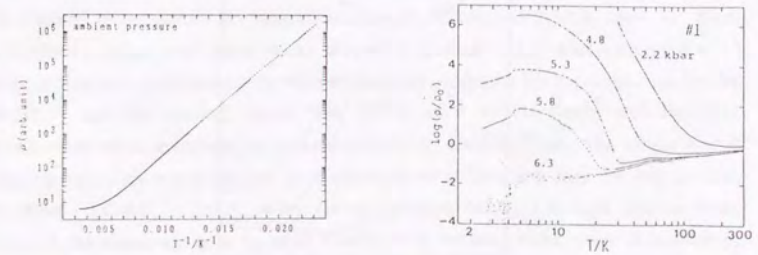

(b)

Figure 7.1. Electrical behavior of the M(dmit)2 salts discussed in this Chapter [1 – 6]; (a) the Ni, and (b) the β−Pd salts

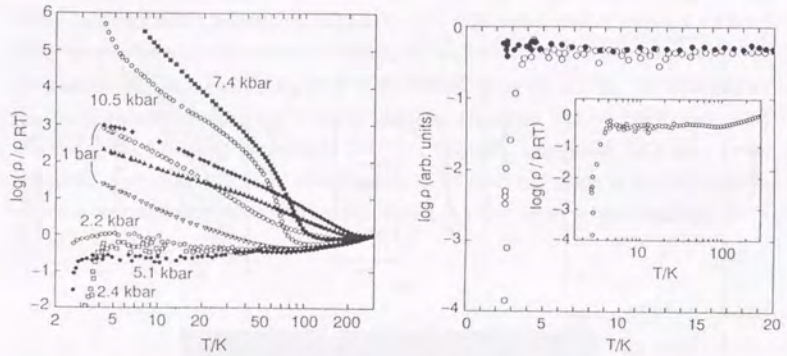

(c)

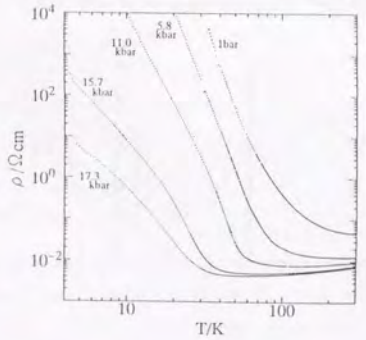

(d)

Figure 7.1. Electrical behavior of the M(dmit)2 salts discussed in this Chapter (continued) [1 – 6]; (c) the Me_2Et_2N and (d) the As salts

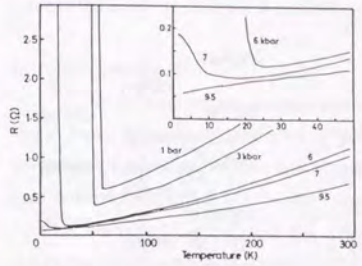

(e)

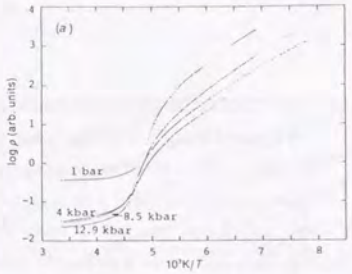

(f)

Figure 7.1. Electrical behavior of the M(dmit)2 salts discussed in this Chapter (continued) [1 – 6]; (e) the Cs and (f) the Pt salts

Optical Measurements

General

The polarized reflectance spectra of the first five salts (the Ni, As, Cs, Pt and the β−Pd salts) were measured on the (001) face by making the beam of normal incidence focus on the clean, smooth surfaces from 25000 cm^{-1} to 400 cm^{-1}. The light polarizations were determined by rotating the polarizer so as to observe the maximal and the minimal reflectance at the longest wavelength descernible (3330 cm^{-1}). Such determined principal axes turned out to be parallel to the *a*- and *b*- axes within the ± 5 ° error, which was confirmed by the Weissenberg and oscillation photographs. As for the Me_2Et_2N salt, the spectral region was 25000 cm^{-1} to 800 cm^{-1} and the light polarizations were determined as mentioned above on the (010) face. The output signal from the detectors was amplified by a preamplifier at first and then by the Lock-in Amplifier (EG&G, 5205). When filters, gratings, detectors or light sources were changed, the measurement at the same wavenumber, or over some range if necessary, was repeated to check for any artifact. The absorption spectra from ultraviolet to near-infrared region of the freshly prepared CH_3CN solutions of $[(C_4H_9)_4N]_n[M(dmit)_2]$ (M = Ni, Pd; n = 1, 2) were recorded on a Hitachi 340 spectrometer. In order to avoid oxidation by air ($[(C_4H_9)_4N]_2[M(dmit)_2] \rightarrow [(C_4H_9)_4N][M(dmit)_2]$), the solutions of $[(C_4H_9)_4N]_2[M(dmit)_2]$ (M = Ni, Pd) were added with a few drops of the CH_3ONa / CH_3OH solution and triethylamine at the actual measurements [11]. The calculation of the conductivity spectra based on the tight-binding model was made by the method

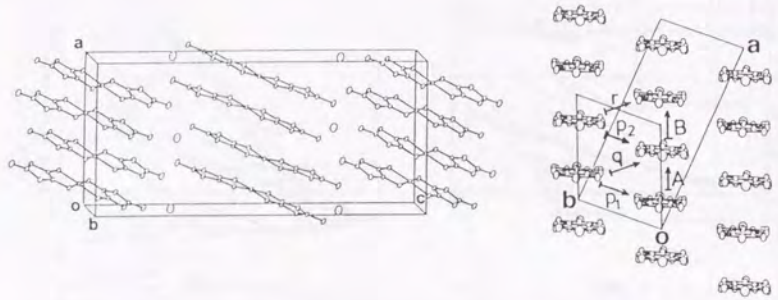

Figure 7.2. Crystal structure common to the Ni, β–Pd, As, Cs and Pt salts [2 (d)]

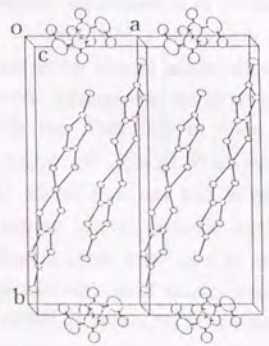

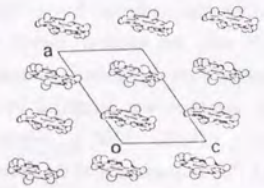

Figure 7.3. Crystal structure of the Me_2Et_2N salt [5]

described in refs. [9 (c), (e), (g), (h)]. All the calculations were carried out by use of a HITACHI M-680H computer at The Computer Centre of The University of Tokyo. Further detail of the analysis is available in ref. [8].

Infrared Spectra

The infrared region measurements were carried out using a JASCO MIR-300 single beam infrared microspectro-reflectometer along with the Ge bolometer (at low temperatures and some of the room temperature measurements; 5000 – 400 or 800 cm^{-1}; Laboratories Inc., HD-3) or the two-color infrared detector { at room temperature; InSb (4200 – 1800 cm^{-1}) / HgCdTe (1800 – 720 cm^{-1}): Infrared Associates, Inc. } automated with personal computer (NEC PC-8801) through GPIB. The light sources are a tungsten lamp (≥ 3350 cm^{-1}) and a Nichrome wire (≤ 3350 cm^{-1}). The reflectance at every 50 cm^{-1} was measured on both sample and standard reflector (silver mirror) alternately. On low temperature measurements, a continuous-flow cryostat (Oxford Instruments CF104) was used to cool the sample. The temperature was monitored by Au (Fe)/Chromel thermocouple attached to the goniometer on which the sample and the standard were mounted.

Visible and Near Infrared Spectra

The visible/near-infrared region (25000 – 4200 cm^{-1}) measurements were carried by use of an Olympus MMSP-RK microspectrophotometer controled by personal computer (NEC PC-9801E) through GPIB. The light source is a 350 W tungsten halogen lamp with a reflection mirror (Sylvania). The detectors are a photomultiplier tube (25000 – 10800 cm^{-1}) and a PbS photoconductive cell cooled with Dry Ice-methanol mixture (11600 – 4200 cm^{-1}). The reflectance at every 200 cm^{-1} was measured on both sample and standard reflector (a silicon single crystal) alternately. At low temperature measurements, a closed cycle cryogenic refrigerator (Model 21 Compressor combined with CTi SPECTRIM^{tm}; Cryogenic Technology Inc.) was used to cool the sample. The temperature was monitored by Au (Fe)/Chromel thermocouple attached onto the sample holder head on which the sample and the standard were mounted. Further details of the microspectrophotometric technique, the temperature control and other details of the apparatus used in this experiment are described elsewhere [9].

7-4. Optical Properties

Itemized Discussion of the Common Features of the M(dmit)2 Salts

An Omnibus View of Information from Optical Study

The reflectance measurement with the polarization mentioned above informs us of the electronic states along and perpendicular to the most conductive direction of each salt. The most conductive direction in the isostructural five salts is therefore found to be along the *a*-axis, while it is along the stacking direction [101] in the Me_2Et_2N salt. Such spectra may be referred to as *//a* and *//b* in the C2/c salts, while // and ⊥ in the Me_2Et_2N salt, below.

Figures 7.4 and 7.5 show the reflectance and conductivity spectra of all the six M(dmit)2 salts, respectively. First the discussion centers on the Cs and As salts, chiefly because they possess the general trend shared among the six salts. The discussion here is meant for understanding what kind of information and discussion are available from such spectra, and the quantitative details will not be repeated for all of the species. In the next section, it will become apparent to be of much help to compare all the spectra with each other to understand their properties further.

The Dispersion in Infrared Region

At room temperature the reflectance nearly saturates in the infrared region and this dispersion appears as if it cannot be assigned unambiguously to Drude-like nor Lorentz-type. Such situation is often observed when the Drude-like spectrum is modulated by a broad electronic transition across an optical gap [8 (c)]. Yet as for the metallic salts, *i.e.* the Ni, Cs and Pt salts the Lorentz model failed to reproduce it, while as for the semiconducting salts the Drude model was unsuited. What is more, the often observed [1 (a) – (e)] sample dependence in the electrical behavior of the Ni salt was not observed at all in the reflectance spectra [1 (f)], instead the spectra have been demonstrated that this material remains inherently metallic down to 25 K.

With the temperature lowering most of the dispersions in the infrared region make clear Lorentzians or Drude-type ones. As for the salts with MI transitions, the transitions are well described in the change of the shape of the infrared dispersions. These situations correspond to the results of dc conductivity measurements of all the salts, which revealed resistivities with bare temperature dependence around room temperature and clear semiconductive or metallic behavior at lower temperatures. This spectral change indicates a rapid increase of relaxation rate at low temperature (see Table 7.5). As for the Cs salt, the calculated optical conductivities σ_{opt} at varied temperatures,

$$\sigma_{opt} = \frac{\omega_p^2 \tau}{4\pi} \qquad (7.15)$$

which is, in other words, the extrapolated conductivity to zero wavenumber $\sigma_{\omega \to 0}$, and the observed dc conductivity σ_{dc} agree well with each other as well as their ratio, viz. the anisotropy (see Table 7.1). But we should note that σ_{opt} here includes the contribution from the interband transition observed in the infrared region. The superlattice of the Cs salt can be responsible for this small gap [2].

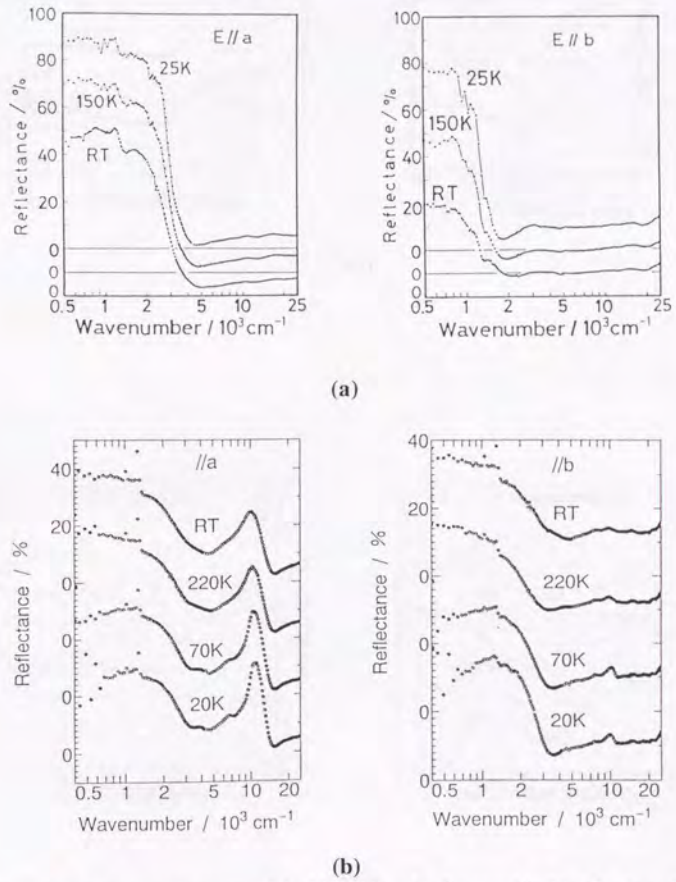

Figure 7.4. Reflectance spectra of the M(dmit)2 salts discussed in this Chapter ; (a) the Ni, and (b) the β–Pd salts

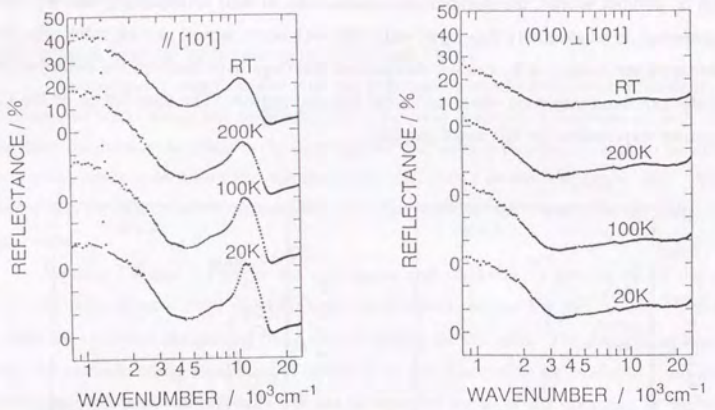

(c)

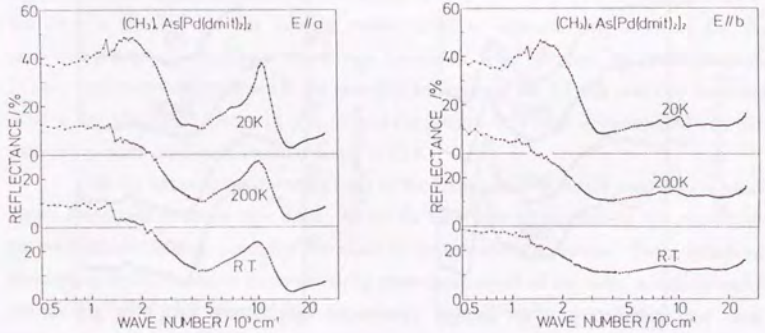

(d)

Figure 7.4. Reflectance spectra of the M(dmit)2 salts discussed in this Chapter (continued) ; (c) the Me_2Et_2N and (d) the As salts

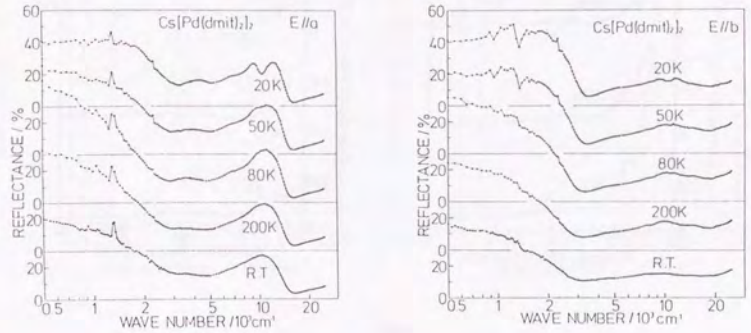

(e)

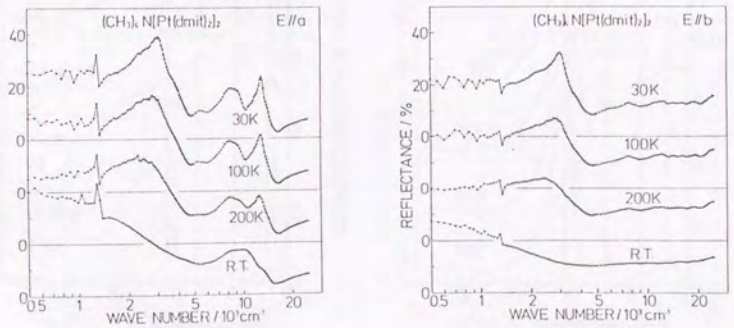

(f)

Figure 7.4. Reflectance spectra of the M(dmit)2 salts discussed in this Chapter (continued) ; (e) the Cs and (f) the Pt salts

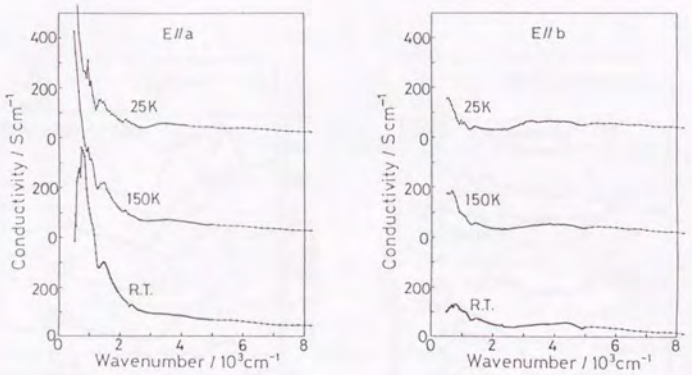

(a)

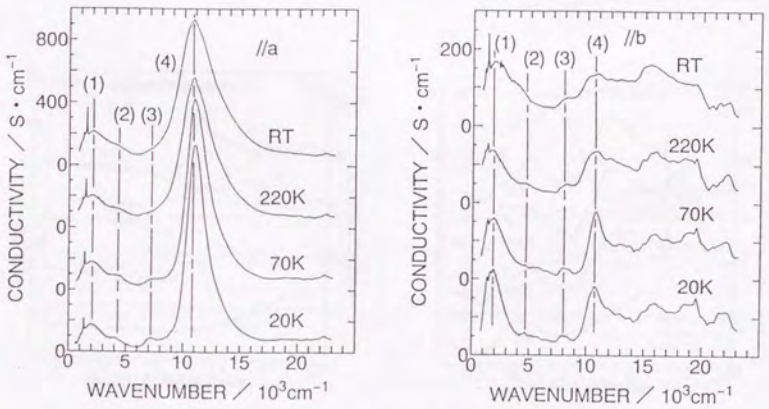

(b)

Figure 7.5. Conductivity spectra of the M(dmit)2 salts discussed in this Chapter ; (a) the Ni, and (b) the β−Pd salts

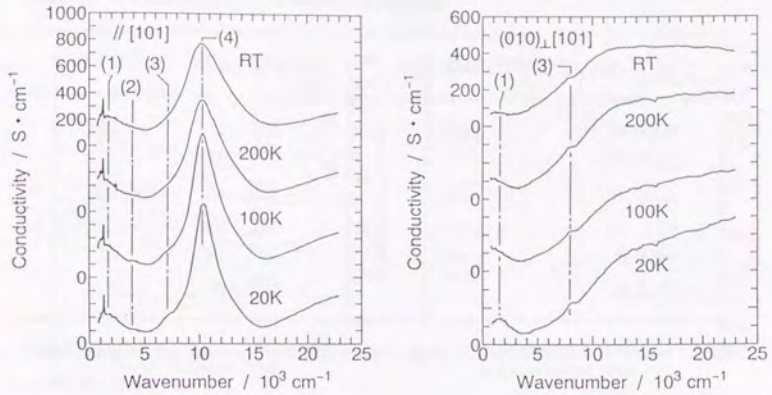

(c)

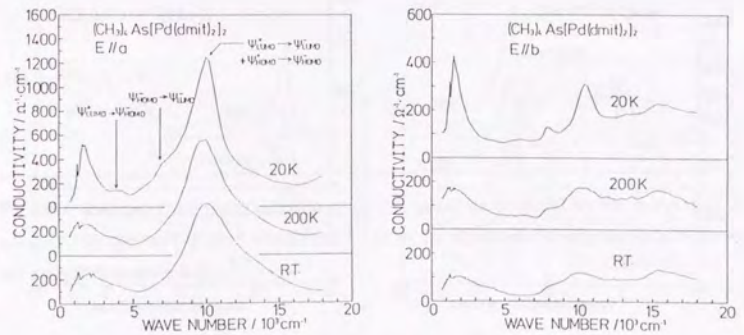

(d)

Figure 7.5. Conductivity spectra of the M(dmit)2 salts discussed in this Chapter (continued); (c) the Me_2Et_2N and (d) the As salts

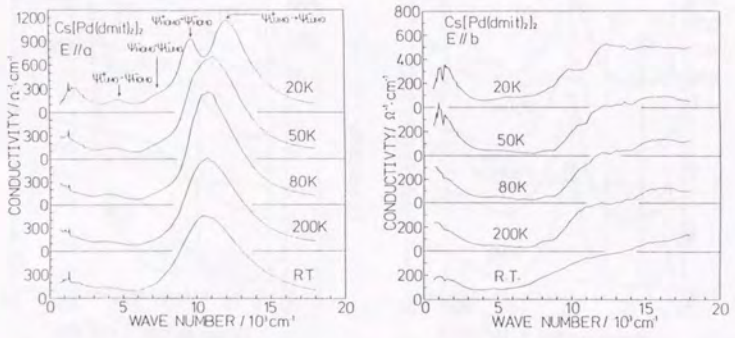

(e)

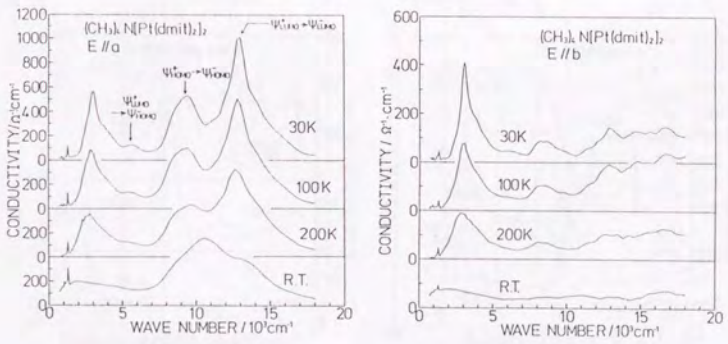

(f)

Figure 7.5. Conductivity spectra of the M(dmit)2 salts discussed in this Chapter (continued); (e) the Cs and (f) the Pt salts

Table 7.1. The calculated optical conductivity σ_{opt}, dc conductivity σ_{dc} and the optical mass m^* of Cs[Pd(dmit)2]2 at varied temperatures

T / K	σ_{opt} / S·cm^{-1}	σ_{dc} / S·cm^{-1} [a]	m^*/m_e
293	//*a* 220	200	//*a* 2.23
	//*b* 170		//*b* 3.12
200	//*a* 310	260	//*a* 3.17
	//*b* 240		//*b* 3.94
80	//*a* 410	400	//*a* 3.55
	//*b* 370		//*b* 3.39

[a] Measured by the four-probe method nearly along most conductive direction (//[100]) in the *ab*- plane

Table 7.2. Plasma frequency ω_p [10^3 cm^{-1}] of Cs[Pd(dmit)2]2 at varied temperatures

		RT	200 K	80 K	50 K	20 K
//*a*	RF[a]	7.60	6.38	6.03	6.55	7.96
	KK[b]	6.11	6.21	6.36	6.27	6.17
//*b*	RF	6.44	5.73	6.17	5.88	6.03
	KK	5.35	5.01	5.56	5.62	5.60
$(\omega_p)a^2/(\omega_p)b^2$ [c]						
	RF	1.4	1.3	1.0	1.2	1.7
	KK	1.3	1.5	1.3	1.2	1.2

[a] Values obtained from the dispersion analysis [b] Values obtained by the integral of the conductivity spectra (0 cm^{-1} – 6600 cm^{-1}) from the Kramers-Kronig analysis [c] Errors are estimated to be ± 0.2.

Table 7.3. Plasma frequency ω_p [10^3 cm^{-1}] of β-$(CH_3)_4As[Pd(dmit)_2]_2$ at varied temperatures[a]

	RT	200 K	20 K
//*a*	6.46	6.13	6.51
//*b*	3.79	4.72	5.15
$(\omega_p)_a^2/(\omega_p)_b^2$ [b]	2.9	1.7	1.6

[a] Values obtained by the integral of the conductivity spectra (0 cm^{-1} – 7000 cm^{-1}) from the Kramers-Kronig analysis. Note that small optical gaps are neglected. [b] Errors are estimated to be ± 0.2.

If one assume that the principal optical axes in each conduction sheet are parallel and perpendicular, respectively, to the stacking axes, and that the conduction electrons are confined in each conduction sheet, one can derive the following relation between the plasma frequencies along and perpendicular to the stacking axes ($\omega_{p//}$, $\omega_{p\perp}$) and the observed ones (ω_{pa}, ω_{pb}).

$$\left\{ \begin{array}{l} (\omega_{p//}\cos\theta)^2 + (\omega_{p\perp}\sin\theta)^2 = \omega_{pa}^2 \\ (\omega_{p//}\sin\theta)^2 + (\omega_{p\perp}\cos\theta)^2 = \omega_{pb}^2 \end{array} \right\} \quad (7.16)$$

where θ is the angle between the *a* and the stacking axes. By solving the simultanious equations (7.16), the values of $\omega_{p//}$ and $\omega_{p\perp}$ were determined as shown in Table 7.4. The As salt has higher anisotropy within the *ab*-plane at room temperature than the rest (see also Table 7.9), though it rapidly approaches two-dimensional with decreasing the temperature. In these species, the table tells that an acceptor sheet by itself has a larger anisotropy than the crystal does due to the small interaction between the columns and that they owe the observed isotropic property to the crystal structure where the stacking directions of the $M(dmit)_2$ slabs are alternating from sheet to sheet { [110] and [1 $\bar{1}$0] }. This is a demonstration of "multi Fermi surfaces" [1 (a) – (e), 7 (f)] in terms of optical study.

Table 7.4. Square of plasma frequency ω_p^2 [eV^2] of $Cs[Pd(dmit)_2]_2$ and β-$(CH_3)_4As[Pd(dmit)_2]_2$ at varied temperatures[a]

	RT	200 K	80 K	50 K	20 K
β-$(CH_3)_4As[Pd(dmit)_2]_2$					
//	0.77	0.63			0.71
⊥	0.11	0.29			0.35
$(\omega_p)_{//}^2/(\omega_p)_\perp^2$ [b]					
	7.0	2.2			2.0
$Cs[Pd(dmit)_2]_2$					
//	0.61	0.64	0.66	0.63	0.61
⊥	0.41	0.34	0.44	0.46	0.46
$(\omega_p)_{//}^2/(\omega_p)_\perp^2$ [b]					
	1.5	1.9	1.5	1.4	1.3

[a] By use of $(\omega_p)_{//a}$, $(\omega_p)_{//b}$ in Tables 7.2 and 7.3 (KK) and the simultaneous equations (7.16)
[b] Errors are estimated to be ± 0.2.

In regard to the metallic salts, thanks to the situation that the Drude part overwhelms the total contribution of other overlapping dispersions at low temperatures, the dispersion analysis produced Drude parameters (Table 7.5).

Table 7.5. Drude parameters of $Cs[Pd(dmit)_2]_2$ at varied temperatures[a]

	RT		200 K		80 K	
	//*a*	//*b*	//*a*	//*b*	//*a*	//*b*
ε_c	3.54	2.09	3.65	1.90	3.84	2.09
ω_p / 10^3 cm^{-1}	7.61	6.44	6.38	5.73	6.03	6.17
τ / 10^{-3} cm	0.23	0.24	0.45	0.44	0.67	0.58

[a] Values obtained from the dispersion analysis

The Strong Dispersion around 10000 cm^{-1}

On the other hand the strong dispersion appear at *ca.* 10×10^3 cm^{-1} in every *//a* (or //) spectrum of the $Pd(dmit)_2$ and $Pt(dmit)_2$ salts. This peak demonstrates that their conduction bands mainly consist of the HOMO of the acceptor molecules [1 (f), (g), 2 (c), (d), 12] by the following reasons.

First of all this peak does not have any corresponding absorption band in the solution spectra (cf. Figure 7.8), whose dipole moment is polarized toward the molecular long axis due to the symmetry of the molecular orbitals. The dipole moment of this transition is polarized toward the dimerization direction. On the other hand, the transition energy is too high to attribute it to a usual charge transfer transition in a 2:1 salt. The intensity expressed by the square of the plasma frequency ω_p^2, it amounts to *ca.* 2×10^8 cm^{-2} in every $Pd(dmit)_2$ and $Pt(dmit)_2$ salts in question (cf. Table 7.6).

The calculated overlap integrals (t_0) between the neighboring molecules (for the Cs salt, see Table 7.7) by use of the extended Hückel method clearly manifest the strong dimerization; the values corresponding to A (HOMO-HOMO) and B (LUMO-LUMO) in Figure 7.2 are significantly larger than the others. Therefore this system can be described by the following dimer model. In such a strongly dimerized $M(dmit)_2$ salt, one should take the possibility into consideration that the anti-bonding HOMO level exceeds the bonding LUMO level of the $M(dmit)_2$ dimer. Thus the possible cases are two, which are shown in Figure 7.6.

To begin with let us consider only the three parameters, t_1, t_2 and ΔE (Figure 7.6), where t_1 and t_2 are respectively the transfer integrals between the HOMOs and the LUMOs, and ΔE is the energy separation between the HOMO and the LUMO. Since we neglect transfer integrals other than t_1 and t_2, only the two optical transitions are allowed, *i.e.* from the bonding HOMO (Ψ^+_{HOMO}) to the anti-bonding HOMO (Ψ^-_{HOMO}) and from the bonding LUMO (Ψ^+_{LUMO}) to the anti-bonding LUMO (Ψ^-_{LUMO}). Using only such a simple dimer model and Equation (7.14), the electronic structure in the $Pd(dmit)_2$ and $Pt(dmit)_2$ salts are proved to be the one illustrated in the case (2) in Figure 7.6. Let us take the case of the Cs salt as an example.

If we assign the dispersion at 10500 cm^{-1} in the spectra of $Cs[Pd(dmit)_2]_2$ to be the transition depicted in the case (1), the value of the excitation energy ($2t_2$) should be 10500 cm^{-1} (1.3 eV). Then by use of Equation (7.14) and the values V = 694 $Å^3$, d = 2.73 Å and $2t_2$ = 10500 cm^{-1} (1.3 eV), the expected value of the square of the plasma frequency along the *a*-axis is estimated to be 82×10^6 cm^{-2}. Here the volume of the dimer V is assumed to be the quotient of the unit cell volume devided by the number of the dimer in the unit cell (Z), and d is assumed to be the *a*-axis component of the spacing of the dimer. This value is considerably smaller than the observed ones (Table 7.6).

On the other hand if we assign the transition to that depicted in the case (2), the total value of the square of the plasma frequency is estimated to be (82×10^6) $\times$ 3 = 246

$\times 10^6$ cm^{-2}. Here both $2t_1$ and $2t_2$ are expected to be 10500 cm^{-1} (1.3 eV). The assumption $2t_1 = 2t_2$ is consistent with the calculated overlap integrals shown in Table 7.7. As for the As salt, the same value is estimated to be 201×10^6 cm^{-2}, using the parameters V = 823 $Å^3$, d = 2.80 Å and t = 0.6 eV. These values are consistent with the observed ones in Table 7.6.

The absence of the strong absorption band in the *//b* spectra is explained as follows; since the transition is inherently the charge-transfer excitation within the dimers, the transition dipole points nearly to the [110] and [1 $\bar{1}$0] direction, which are combined to be a resultant vector pointing to the [100] (*//a*) direction, *i.e.* normal to the *//b* direction.

In the *//a* reflectance spectra, this peak splits into two independent peaks at the MI transition temperature (56.5 K) as shown in Figure 7.7. In the *//a* conductivity spectra { Figure 7.5 (e) }, after steady sharpening of the peak with decrease in the temperature, a certain broadening occurred at 50 K, which is a sign of splitting, and then the peak turned into two discrete ones at 20 K. The splitting involves that the coincident two energy separation, that between Ψ^-_{HOMO} and Ψ^+_{HOMO} ($2t_1$) and that between Ψ^-_{LUMO} and Ψ^+_{LUMO} ($2t_2$) of the $Pd(dmit)_2$ dimer, respectively shift to higher and lower energies at the transition. Such splitting strongly supports the interpretation of the spectra and thus the proposed model of the band structure because it also well explains the consequent due shifts of all other peaks quantitatively.

It was pointed out that the tight-binding band calculation considering the LUMOs of the $Pd(dmit)_2$ was less suitable than in the case of the isostructural $Ni(dmit)_2$ salt to explain the their observed properties at ambient pressure [3]. The difference in the actual conduction bands can be one of the possible reasons.

As is referred to in Chapter 6, the most striking difference in the electrical properties of the dmit compounds lies in the metal instability despite its molecular structural similarity to BEDT-TTF. Such difference originates from the difference in the symmetry of the frontier orbitals, namely, the LUMOs of $M(dmit)_2$ [13], which dominates the intermolecular interaction concerning the conduction band. Consequently the dmit salts often suffer from low-dimensionality and narrow bands, both of which are apt to lead to a ground state with a band gap. On the contrary if the conduction band mainly consists of the HOMO of the $M(dmit)_2$, which has the same symmetry as that of BEDT-TTF, the resultant electronic structure can be expected far more isotropic. This is illustrated by the band structures determined from this optical study, which are shown later (Figures 7.10 and 7.12).

Table 7.6. The peak position (ω_j), square of plasma frequency ($\omega_p{}^2$) and the oscillator strength (f_j) of the strong absorption band around 10000 cm^{-1} in the *//a* spectra [2 (c)][a]

	ω_j / 10^3 cm^{-1}	$\omega_p{}^2$ / 10^6 cm^{-2}	f_j
Cs[Pd(dmit)2]2			
RT	10.6	213	0.83
200 K	10.8	221	0.86
80 K	10.8	239	0.93
50 K	11.0	238	0.92
20 K	9.6 / 12.0[b]	227	0.88
β-$(CH_3)_4$As[Pd(dmit)2]2			
RT	10.0	163	0.75
200 K	10.0	177	0.82
20 K	10.0	187	0.86

[a] Values obtained by the integral of the conductivity spectra (6000 cm^{-1} – 16000 cm^{-1}) from the Kramers-Kronig analysis [b] Splitted as shown in Figure 7.7

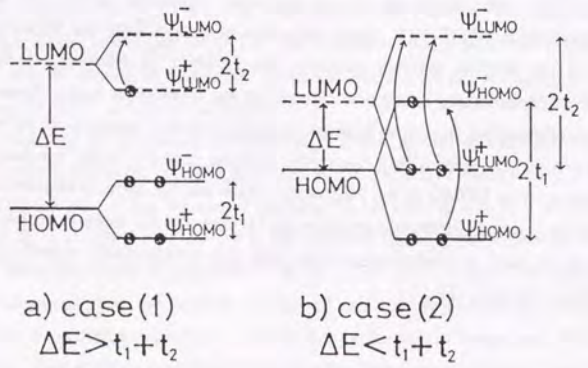

Figure 7.6. Schematic energy diagrams for the strongly dimerized M(dmit)2 salts

The Conductivity Spectra from Kramers-Kronig Analysis

Kramers-Kronig analysis provided conductivity spectra, which manifest some features that are obscure in the reflectance spectra. For example, there reveal themselves the Lorentzian peaks in each spectrum below 3500 cm^{-1} characteristic to the semiconductors, except for the Ni and Cs salts in metallic region.

By extending a primitive dimer model to the tight-binding band model, the band structure was calculated considering all the transfer integrals for the overlapping mode depicted in Figure 7.2 as well as the interactions between HOMO and LUMO. The author tried to reproduce the observed spectra (Figure 7.5) by simulating the transfer integrals as parameters [2 (c)].

The initial values (t_0) were those estimated from the overlap integrals given in Table 7.7. The ΔE (= the energy gap between HOMO and LUMO) was assumed to be 0.8 eV, which value is consistent with the one estimated from the solution spectra (0.9 eV; see Figure 7.8) [2 (c)]. The calculated conductivity spectra (Figure 7.9) from the optimized set of the transfer integrals reproduced quantitatively and exclusively the observed ones, showing the same structural detail (Figure 7.9). The *//b* spectra is also well reproduced. The resultant transfer integrals (t) are also tabulated in Table 7.7. Comparison of the two sets of integrals tells that the general trend of the transfer integrals is not altered. Interestingly, the shape and line-width of the strong absorption at *ca.* 10 × 10^3 cm^{-1} are very susceptible to the values of the transfer integrals p1, p2, q and r; the shape and line-width approach those of the As salt when the values of p1, p2, q and r reduce, and on the contrary when the values increase they appraoch those of the Cs salt. In fact the peak is slightly broader in the Cs salt than in the As salt (see Figures 7.4 and 7.5). This means that the electronic structure of the As salt is more one-dimensional than that of the Cs salt, which is consistent with Table 7.4.

It should be referred to that thus obtained parameters gave a closed Fermi surface for the Cs salt as shown in Figure 7.10. But this is incompatible with the open Fermi surface calculated by Canadell [2 (b), (d)] and cast a question on the mechanism of the MI transition in the Cs salt. The X-ray diffuse study suggested that a partial nesting of the Fermi surface, namely a formation of CDW can be responsible for the transition [2 (d)]. If this is the case, the author reconcile the optical results with calculated band structure, since small modifications to the band dispersion might result in closing of the Fermi surface and, in any case, a partial nesting is possible in both of the proposed Fermi surfaces [2 (d)].

The corresponding calculation was not attempted on the As salt because the tractable band model is not applicable to this semiconducting species. However the many similarities mentioned above suggest that the same band picture as the Cs salt may be as effective in the case of the As salt if we add a small gap at the Fermi level { see Figure 7.12 (later) and text }. It is not thought that the following discussion need modification

as for this salt as well as in the case of the other $M(dmit)_2$ salts that exhibit semiconducting behavior from room temperature.

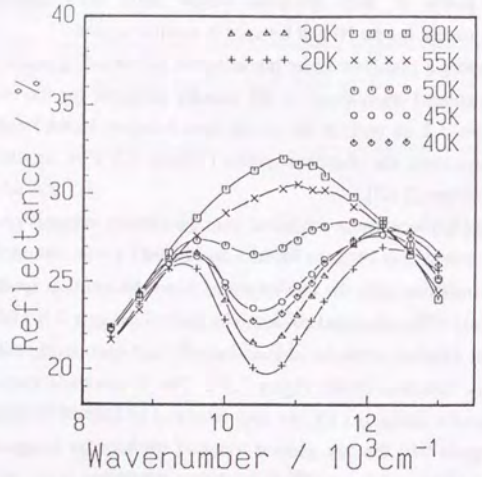

Figure 7.7. Splitting of the strong dispersion around 10000 cm^{-1} in the reflectance spectrum (*//a*) of the Cs salt

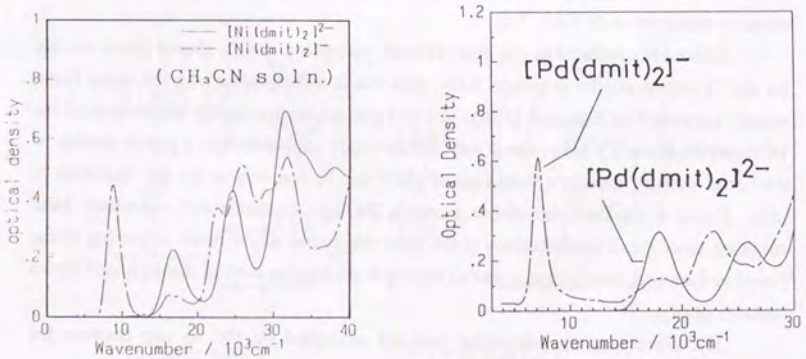

Figure 7.8. Absorption spectra of $[(C_4H_9)_4N]_n[M(dmit)_2]$ (M = Ni, Pd; n = 1, 2) in acetonitrile solution

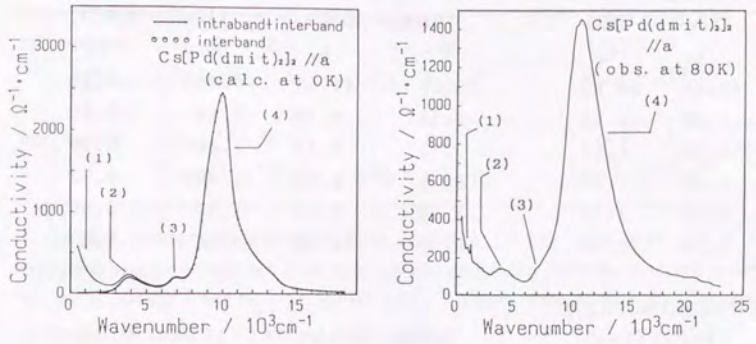

(a)

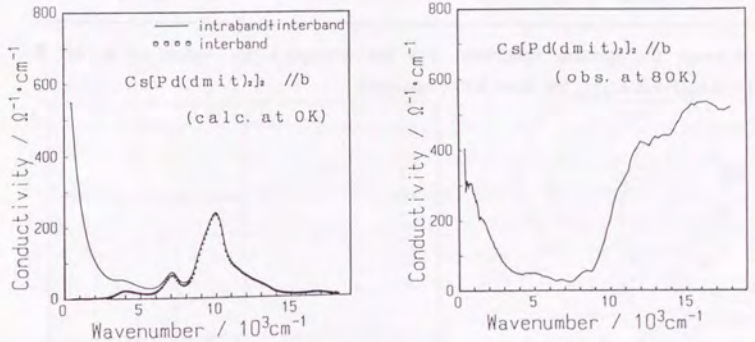

(b)

Figure 7.9. Conductivity spectra of the Cs salt (left) calculated at 0 K, and (right) observed at 80 K, (a) *//a*, (b) *//b*, respectively; Note that the observed *//b* spectrum includes the contribution from the intramolecular excitations ($\geq 15 \times 10^3$ cm^{-1}), which are ignored in the calculation.

Table 7.7. Transfer integrals (t, t_0 / 10^{-2} eV) used in the calculation of the conductivity spectra of Cs[Pd(dmit)2]2[a]

Cs[Pd(dmit)2]2

	LUMO – LUMO		HOMO – HOMO		LUMO – HOMO	
	t	t_0	t	t_0	t	t_0
A	60.00	44.83	65.00	44.60	-0.40	-0.28
B	-3.00	-3.00	9.50	9.34	-5.40	-3.40
p1	1.20	1.17	3.70	2.93	1.40	0.89
p2	1.20	1.17	3.70	2.93	1.40	0.72
q	1.20	1.19	3.00	3.03	1.40	0.80
r	2.10	2.08	6.30	6.29	-3.00	-1.87

β-(CH3)4As[Pd(dmit)2]2

	LUMO – LUMO	HOMO – HOMO	LUMO – HOMO
	t_0	t_0	t_0
A	41.99	40.63	0.08
B	- 4.00	9.60	-4.01
p1	0.99	2.09	0.41
p2	0.99	2.09	0.61
q	0.97	3.73	1.16
r	2.28	5.79	-1.63

[a] Although the spectral simulation was not attempted, the values of t_0 for β-(CH3)4As[Pd(dmit)2]2 are listed for comparison.

Table 7.8. Comparison of the main peaks in the calculated (at 0 K) and observed (at 80 K) conductivity spectra of Cs[Pd(dmit)2]2[a]

	peak (1)	peak (2)	peak (4)
calc. spectra	$(\omega_{p,a})^2 = 38.6$	$\nu = 3.88$	$\nu = 9.93$
	$(\omega_{p,b})^2 = 36.5$	$(\omega_p)^2 = 11.3$[c]	$(\omega_p)^2 = 233.5$[d]
obs. spectra	$(\omega_{p,a})^2 = 36.4$[b]	$\nu = 3.85$	$\nu = 11.2$
	$(\omega_{p,b})^2 = 38.1$[b]	$(\omega_p)^2 = 11.4$[c]	$(\omega_p)^2 = 233.2$[d]

[a] The peak numbers correspond to those in Figure 7.9 (a). The peak (3) is not compared because it could not be decomposed unambiguously from the observed spectra: ν's are in 10^3 cm^{-1} and ω_p's are in 10^6 cm^{-2}. [b] Values obtained from the dispersion analysis [c] Obtained by the integral of the spectrum from 2800 cm^{-1} to 5200 cm^{-1} [d] Obtained by the integral of the spectrum from 5000 cm^{-1} to 15000 cm^{-1}

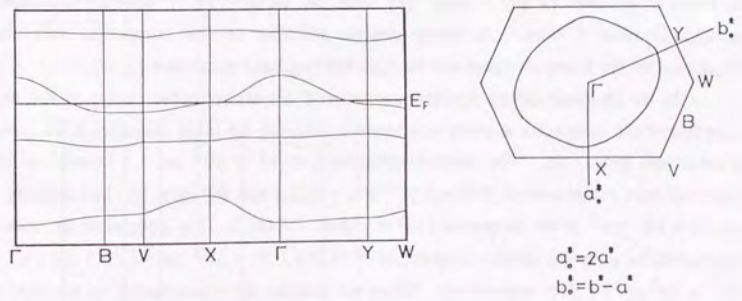

Figure 7.10. Band electronic structure and Fermi surface of the Cs salt obtained from the transfer integrals (t) in Table 7.7

Reflectance Spectra of β–(CH3)4N[Pd(dmit)2]2

In the *//a* spectra two dispersions occurring in the infrared and mid-infrared regions catch our eye. The former dispersion well reflects the characteristics of the conduction electrons, as is the case with the other salts mentioned above.

In the mid-infrared region the strong dispersion appeared at *ca.* 10×10^3 cm^{-1} demonstrates that the conduction band mainly consists of the HOMO of the acceptor molecules [1 (f), (g), 2 (c), (d), 13].

On the other hand *//b* spectra show an only imposing dispersion in the infrared region, which is attributable to the conduction electrons. The spectral features and the absolute reflectance values in the infrared dispersion almost correspond to those in the *//a* spectra, which implies a small anisotropy in the *ab*-plane in this compound. Other dispersions are some intramolecular transitions in the visible region (Figure 7.8) [2 (c)].

Conducitvity Spectra of β–(CH3)4N[Pd(dmit)2]2

The Kramers-Kronig transformation produced the conductivity spectra. They clearly manifest the peak positions in the infrared region and developing two peaks with the temperature lowering { (2) and (3) in Figure 7.5 (b)}, both of which are ambiguous in the reflectance spectra. The spectra indicate an exsistence of an energy gap of 1.1×10^3 cm^{-1}, which is consistent with the result of dc conductivity measurements ($E_g = 2 \times E_a = 0.14$ eV $= 1.1 \times 10^3$ cm^{-1}) [3, 4]. The small but sharp peak at 1.2×10^3 cm^{-1} is attributed to an electron-molecular vibration (emv) coupling, which is generally observed in dimeric systems [9 (c) – (m), 14] such as BEDT-TTF { bis(ethylenedithio)-tetrathiafulvalene } salts. A strong dimeric structure of this compound was also supported by the X-ray analyses and the tight-binding band calculation [3, 4].

In the *//b* conductivity spectra, the infrared dispersion rather comes to the fore than that of the *//a* spectra at every temperature, whereas the other dispersions are much weaker and indiscrete. The latter dispersions ($\geq 15 \times 10^3$ cm^{-1}) consist of the intramolecular transitions of $[Pd(dmit)_2]^{n-}$ (n = 0, 1) and the same one that appears at *ca.* 10×10^3 cm^{-1} in the *//a* spectra { (4) in Figure 7.5 (b) }. The integral of the optical conductivities gives the plasma frequencies of $(3.8 \pm 0.1) \times 10^3$ cm^{-1} (*//a*) and $(4.1 \pm 0.1) \times 10^3$ cm^{-1} (*//b*), respectively. When we consider the ratio between the two optical masses, $(m^*)_a / (m^*)_b$ as an index of the anisotropy in the *ab*-plane, it was estimated to be 0.9 ± 0.1 at 20 K.

Concerning this salt the calculated conductivity spectra also well agree with the observed ones (compare the two Figures 7.5 (b) and 7.11).

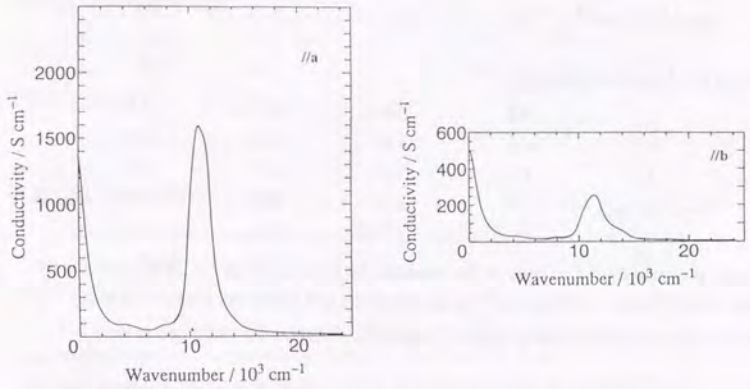

Figure 7.11. Calculated conductivity spectra of the β–Pd salt

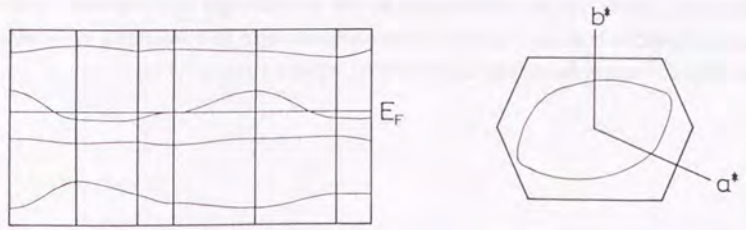

Figure 7.12. Electronic band structure and Fermi surface of the β–Pd salt obtained from the transfer integrals corresponding to the spectra in Figure 7.11

Table 7.9. Plasma frequency ω_p [10^3 cm^{-1}] of $Pd(dmit)_2$ salts at varied temperatures[a]

β-$(CH_3)_4N[Pd(dmit)_2]_2$

	RT	220 K	70 K	20 K
//a	4.5	4.4	3.9	3.8
//b	4.0	3.6	3.7	4.1
$(\omega_p)_a^2/(\omega_p)_b^2$ [b]	1.2	1.5	1.2	0.8

$(CH_3)_2(C_2H_5)_2N[Pd(dmit)_2]_2$

	RT	200 K	100 K	20 K
//	4.6	4.8	4.9	4.5
⊥	2.9	3.2	3.3	3.5
$(\omega_p)_{//}^2/(\omega_p)_\perp^2$ [b]	2.5	2.2	2.1	1.7

[a] Values obtained by the integral of the conductivity spectra (0 cm^{-1} – 3500 cm^{-1} for the β-Pd salt and 0 cm^{-1} – 3200 cm^{-1} for the Me_2Et_2N salt) from the Kramers-Kronig analysis Note that small optical gaps are neglected. [b] Errors are estimated to be ± 0.1.

$(CH_3)_2(C_2H_5)_2N[Pd(dmit)_2]_2$

It is intriguing that all the spectral features stated above are also the case with the Me_2Et_2N salt, which has an apparently one-dimensional structure (Figure 7.3). This is because the conduction band of the Me_2Et_2N salt also mainly consists of the HOMOs of $Pd(dmit)_2$ molecules and these orbitals enable fairly isotropic intermolecular interactions as in the cases of BEDT-TTF salts [1 (h), 9 (c) – (m), 14 (a) – (l), 15]. The ratio between the two optical masses, $(m^*)_{//} / (m^*)_\perp$ was estimated to be 1.3 ± 0.1 at 20 K. In the spectra at room temperature – 100 K of this material, the infrared dispersion keenly resembles a Drude-type one, which means that this material might be a semimetal. Such marginal position between a metal and a semiconductor might have something to do with the observed sample dependence in the electrical behavior { Figure 7.1 (c) }.

Table 7.10. Square of Plasma frequency ω_p^2 [eV^2] of $Pd(dmit)_2$ salts at varied temperatures[a]

	RT	220 K	200 K	100 K	70 K	20 K
β-$(CH_3)_4N[Pd(dmit)_2]_2$						
//	0.32	0.32	—	—	0.24	0.21
⊥	0.24	0.17	—	—	0.20	0.30
$(\omega_p)_{//}^2/(\omega_p)_\perp^2$ [b]	1.3	1.9	—	—	1.2	0.8
$(CH_3)_2(C_2H_5)_2N[Pd(dmit)_2]_2$						
//	0.32	—	0.36	0.36	—	0.31
⊥	0.13	—	0.16	0.17	—	0.19
$(\omega_p)_{//}^2/(\omega_p)_\perp^2$ [b]	2.5	—	2.2	2.1	—	1.7

[a] By use of $(\omega_p)_{//a}$, $(\omega_p)_{//b}$ in Table 7.9 and the simultaneous equations (7.16)
[b] Errors are estimated to be ± 0.1.

Table 7.11. The peak position (ω_j), square of the plasma frequency (ω_p^2) and the oscillator strength (f_j) of the strong absorption band around 10000 cm^{-1} in the *//a* spectra

	ω_j / 10^3 cm^{-1}	ω_p^2 / 10^6 cm^{-2} [a]	f_j
β-$(CH_3)_4N[Pd(dmit)_2]_2$			
RT	10.4	159	0.71
220 K	10.6	151	0.68
70 K	10.6	140	0.63
20 K	10.8	140	0.63
$(CH_3)_2(C_2H_5)_2N[Pd(dmit)_2]_2$			
RT	10.4	161	0.76
200 K	10.4	160	0.76
100 K	10.4	171	0.81
20 K	10.4	156	0.74

[a] Values obtained by the integral of the conductivity spectra (6000 cm^{-1} – 16000 cm^{-1}) from the Kramers-Kronig analysis Errors are estimated to be ± 4.

Table 7.12. Transfer integrals (t, t_0 / 10^{-2} eV) used in the calculation of the conductivity spectra of β-$(CH_3)_4N[Pd(dmit)_2]_2$[a]

	LUMO – LUMO		HOMO – HOMO		LUMO – HOMO	
	t	t_0	t	t_0	t	t_0
A	67.8	40.7	-64.7	-37.6	-8.8	-8.8
B	-5.6	-2.9	-7.1	-7.1	-3.8	-2.8
p1	0.8	0.8	2.6	2.6	0.5	0.0
p2	0.8	0.8	2.6	2.6	0.5	0.0
q	1.3	1.3	-1.9	-1.9	-1.4	-1.4
r	0.7	0.7	-12.9	-5.9	-2.3	-2.3

[a] The energy separation between HOMO and LUMO (ΔE) was assumed to be 0.90 eV.

$(CH_3)_4N[Pt(dmit)_2]_2$

At room temperature the Pt salt exhibited a typical Drude-type dispersion in the infrared spectra, which was replaced by a Lorentz-type interband transition centered at *ca.* 3×10^3 cm^{-1} below 200 K. The change in the infrared specra coincides with the sudden split in the mid-infrared peak in two. Since the shoulders around 8.5×10^3 cm^{-1} and 13×10^3 cm^{-1}, which are already present at room temperature, remain until low temperatures, the two peaks are different from the developed shoulders. The conductivity spectra (*//b*) exhibited the corresponding change; at room temperature the intense mid-infrared absorption was not observable at all, but below 200 K it turned up with a conspicuous broad peak centered around 3×10^3 cm^{-1}. Such change in the spectra involves the change in the transition moment of the mid-infrared peak, which is roughly in the direction of the $Pt(dmit)_2$ columns and that, in turn, a structural phase transition has occurred. This interpretation is consistent with other data [6];

— the resistivity measurement showed that the salt made a clear transition at 220 - 230 K with a gradually developing energy gap of $E_g = 2 \times E_a \sim 0.4$ eV = 3.2×10^3 cm^{-1} (see Figure 7.1 (f)),

— the X-ray diffuse scattering experiment revealed a structural transition below the same temperature.

The Pt salt requires additional comment on its electronic band structure. There are two peculiar shoulders on both sides of the strong absorption band in the mid-infrared region in its reflectance spectra (*//a*) as noted above. The resultant broad complex dispersion was not reproduced by any combination of Lorentz functions. Similarly, due to these shoulders, the calculation based on the same model of the band structure as the $Pd(dmit)_2$ salts failed to reproduce the mid-infrared peak in the conductivity spectra. Therefore detailed identification of the spectral structures and corresponding electronic structures should probably be considered tentative until more information is available. Nevertheless the proposed model of the band structure may be valid also for this salt as a basis for the following discussion.

7-5. Elctronic Structures of the Six Compounds

The Ni, As, β–Pd and Me_2Et_2N Salts

The optical results above insist that the electronic structures of the Ni, As, β–Pd and Me_2Et_2N salts exhibit no transition at all the temperatures (RT – ~ 20 K) at ambient pressure. This study support that the Ni salt may have the proposed electronic structure derived from the tight-binding band calculation considering LUMO-LUMO interactions alone [1]. On the other hand as for the three $Pd(dmit)_2$ salts, taking all the discussion

above into consideration, the schematic band model can be like what is shown in Figure 7.13. In the same figure the assignment of main peaks are also indicated.

The Cs and Pt Salts

The Cs and Pt salts exhibit MI transitions at low temperature at 1 bar. Their reflectance and conductivity spectra revealed not only that the transition involves opening of the gap (or developing the negligible gap into an observable one) at the Fermi level, but also that the transition alters the energy separation between the two HOMOs (Ψ^-_{HOMO} and Ψ^+_{HOMO}) as well as the separation between the two LUMOs (Ψ^-_{LUMO} and Ψ^+_{LUMO}). This situation is most clearly manifested in the change in the spectra of these salts, as is mentioned above.

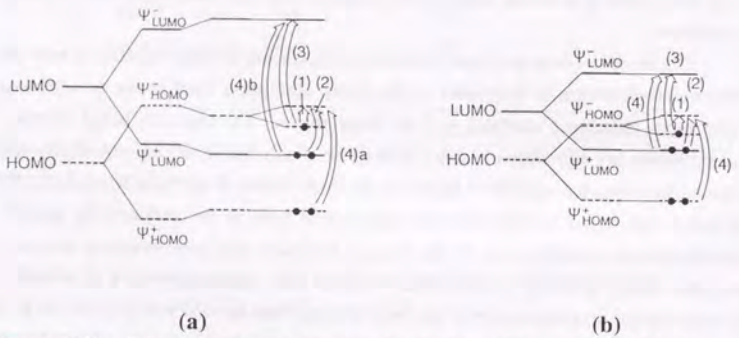

Figure 7.13. Schematic energy diagram and optical transitions of the Pd(dmit)2 and Pt(dmit)2 salts; (a) that of the Cs and Pt salts, and (b) that of the As, β–Pd, Me_2Et_2N salts: The numbers correspond to those in Figures 7.5 (b) and 7.9 (a). Note that small energy gaps are neglected. The transitions (4)a and (4)b denote the splitted ones after the MI transition, which used to be the single peak indicated by (4).

Differences and Similarities in Electronic Structures of the Six M(dmit)2 Salts —the Remaining Questions

Among these six compounds the Pd(dmit)2 and Pt(dmit)2 salts have enough a strong dimeric structure so that the energy level inversion occurs and its conduction band consists mainly of the HOMO of M(dmit)2 [1 (f), (g), 2 (c), (d), 12]. This results in the keen feature in the *//a* (//) spectra; the appearance of the outstanding peak around 10×10^3 cm^{-1}. As for the Ni salt the conduction band has been found to consist chiefly of the LUMO, as is usual with an acceptor compound. Therefore when one discuss the properties of these salts based on the calculated band structures, all that one have to consider is the interaction between LUMO–LUMO in the Ni(dmit)2 salt, whereas the HOMO, which would be a closed shell without the energy level inversion, also should be taken into consideration in the Pd(dmit)2 and Pt(dmit)2 salts. Still remains the fact that Ni(dmit)2 and Pd(dmit)2 salts exhibit superconductivity in common. On the other hand, M(dmit)2 salts whose conduction band consists of HOMO are divided into the superconducting and non-superconducting salts. To be elucidated is the relation between the difference in the electronic structures revealed by this study and the difference in the electrical properties.

7-6. Summary

In order to derive an experimental information about the difference in electronic structures, the polarized reflectance spectra of a series of the M(dmit)2 complexes, $(CH_3)_4N$[Ni(dmit)2]2, β–$(CH_3)_4As$[Pd(dmit)2]2, Cs[Pd(dmit)2]2, $(CH_3)_4N$[Pt(dmit)2]2, β–$(CH_3)_4N$[Pd(dmit)2]2 and $(CH_3)_2(C_2H_5)_2N$[Pd(dmit)2]2 were measured from 25000 cm^{-1} through to 400 cm^{-1} or 800 cm^{-1} at varied temperatures. The obtained reflectance and conductivity spectra well describe the details of the electronic structures such as the band gap, emv coupling, anisotropy, temperature dependence of the conductivity and other features. They revealed the unprecedented electronic structure of the Pd(dmit)2 and Pt(dmit)2 compounds, where the strong dimerization make the anti-bonding HOMO level exceed the bonding LUMO level of the M(dmit)2 dimer, and consequently the Fermi level lies in the anti-bonding HOMO band.

It has been confirmed that among the M(dmit)2 salts which are semiconducting at low temperature, some exhibit MI transitions, while the others are semiconductive from room temperature. This study showed that the transition does not simply open a small energy gap at the Fermi level, but involves shifts of the four bands, those of LUMO and HOMO from M(dmit)2 dimers.

References

[1] (a) H. Kim, A. Kobayashi, Y. Sasaki, R. Kato and H. Kobayashi, *Chem. Lett.*, **1987**, 1799;

(b) A. Kobayashi, H. Kim, Y. Sasaki, R. Kato, H. Kobayashi, S. Moriyama, Y. Nishio, K. Kajita and W. Sasaki, *Chem. Lett.*, **1987**, 1819;

(c) A. Kobayashi, H. Kim, Y. Sasaki, S. Moriyama, Y. Nishio, K. Kajita, W. Sasaki, R. Kato and H. Kobayashi, *Synth. Met.*, **27**, B339(1988);

(d) K. Kajita, Y. Nishio, S. Moriyama, R. Kato, H. Kobayashi and W. Sasaki, *Solid State Commun.*, **65**, 361(1988);

(e) H. Kobayashi, R. Kato, A. Kobayashi, T. Mori, H. Inokuchi, Y. Nishio, K. Kajita and W. Sasaki, *Synth. Met.*, **27**, A289(1988);

(f) H. Tajima, M. Tamura, T. Naito, A. Kobayashi, H. Kuroda, R. Kato, H. Kobayashi, R. A. Clark and A. E. Underhill, *Mol. Cryst. Liq. Cryst.*, **181**, 233(1990);

(g) H. Tajima, T. Naito, M. Tamura, A. Takahashi, S. Toyoda, A. Kobayashi, H. Kuroda, R. Kato, H. Kobayashi, R. A. Clark and A. E. Underhill, *Synth. Met.*, **41-43**, 2417(1991);

(h) M. Tamura, R. Masuda, T. Naito, H. Tajima, H. Kuroda, A. Kobayashi, K. Yakushi, R. Kato, H. Kobayashi, M. Tokumoto, N. Kinoshita and H. Anzai, *Synth. Met.*, **41-43**, 2499(1991);

(i) L. R. Groeneveld, B. Schuller, G. J. Kramer, J. G. Haasnoot and J. Reedijk, *Rec. Trav. Chim. Pays-Bas*, **105**, 507(1986);

(j) L. R. Groeneveld, G. J. Kramer, T. B. L. W. von Marinelli, H. B. Brom, J. G. Haasnoot and J. Reedijk, *Organic and Inorganic Low-Dimensional Crystalline Materials*, P. Delhaes and M. Drillon, Eds., Plenum Press, New York, 1987, p.349;

(k) E. Canadell, E. I. Rachidi, S. Ravy, J. -P. Pouget, L. Brossard and J. P. Legros, *J. Phys. (Paris)*, **50**, 2967(1989);

(l) E. Canadell, S. Ravy, J. -P. Pouget and L. Brossard, *Solid State Commun.*, **75**, 633(1990).

[2] (a) R. A. Clark and A. E. Underhill, *Synth. Met.*, **27**, B515(1988);

(b) S. Ravy, E. Canadell and J. -P. Pouget, in G. Saito and S. Kagoshima, Eds., *The Physics and Organic Superconductors*, Vol. 51, Springer Verlag, Berlin, 1990, p.252;

(c) H. Tajima, T. Naito, M. Tamura, A. Kobayashi, H. Kuroda, R. Kato, H. Kobayashi, R. A. Clark and A. E. Underhill, *Solid State Commun.*, **79**(4), 337(1991);

(d) A. E. Underhill, R. A. Clark, I. Marsden, M. Allen, R. H. Friend, H. Tajima, T. Naito, M. Tamura, H. Kuroda, A. Kobayashi, H. Kobayashi, E. Canadell, S. Ravy and J. -P. Pouget, *J. Phys. Condensed Mater.*, **3**, 933(1991).

[3] A. Kobayashi, H. Kim, Y. Sasaki, K. Murata, R. Kato and H. Kobayashi, *J. Chem. Soc., Faraday Trans.*, **86**(2), 361(1990).

[4] (a) A. Kobayashi, H. Kobayashi, A. Miyamoto, R. Kato, R. A. Clark and A. E. Underhill, *Chem. Lett.*, **1991**, 2163;

(b) A. Kobayashi, R. Kato, R. A. Clark, A. E. Underhill, A. Miyamoto, K. Bun, T. Naito and H. Kobayashi, *Synth. Met.*, **55-57**, 2927(1993).

[5] H. Kobayashi, K. Bun, T. Naito, R. Kato and A. Kobayashi, *Chem. Lett.*, **1992**, 1909.

[6] A. Kobayashi, A. Miyamoto, H. Kobayashi, R. A. Clark and A. E. Underhill, *J. Mater. Chem.*, **1**(5), 827(1991).

[7] (a) M. Bousseau, L. Valade, M. -F. Bruniquel, P. Cassoux, M. Garbauskas, L. V. Interrante and J. Kasper, *Nouv. J. Chim.*, **8**, 3(1985);

(b) M. Bousseau, L. Valade, J. -P. Legros, P. Cassoux, M. Garbauskas, and L. V. Interrante, *J. Am. Chem. Soc.*, **108**, 1908(1986);

(c) L. Brossard, M. Ribault, M. Bousseau, L. Valade and P. Cassoux, *C. R. Acad. Sci. Paris. Sér. 2*, **302**(5), 205(1986);

(d) L. Brossard, H. Hurdequint, M. Ribault, L. Valade, J. -P. Legros and P. Cassoux, *Synth. Met.*, **27**, B157(1988);

(e) L. Brossard, M. Ribault, L. Valade and P. Cassoux, *J. Phys. (Paris)*, **50**, 1521(1989);

(f) A. Kobayashi, H. Kim, Y. Sasaki, R. Kato and H. Kobayashi, *Solid State Commun.*, **62**(2), 57(1987);

(g) R. Kato, H. Kobayashi, A. Kobayashi, T. Naito, M. Tamura, H. Tajima and H. Kuroda, *Chem. Lett.*, **1989**, 1839;

(h) H. Tajima, S. Ikeda, A. Kobayashi, H. Kuroda, R. Kato and H. Kobayashi, *Solid State Commun.*, **86**, 7(1993);

(i) H. Tajima, M. Inokuchi, A. Kobayashi, T. Ohta, R. Kato, H. Kobayashi and H. Kuroda, *Chem. Lett.*, **1993**, 1235;

(j) H. Tajima, M. Inokuchi, S. Ikeda, M. Arifuku, T. Naito, M. Tamura, T. Ohta, A. Kobayashi, R. Kato, H. Kobayashi and H. Kuroda, *Synth. Met.*, in press.

[8] See, for example,

(a) F. Wooten, *Optical Properties of Solids*, Academic, New York (1972);

(b) D. Pines and P. Nozières, *The Theory of Quantum Liquids*, **Vol. 1**, Benjamin, New York, 1966;

(c) C. Jacobsen, *Semiconductor and Semimetals*, E. Cornwell, Ed., Academic

Press, 1988, Vol. 27, p.293.

[9] (a) K. Yakushi, M. Iguchi and H. Kuroda, *Bull. Chem. Soc. Jpn.*, **52**, 3180(1979);
(b) Y. Iyechika, K. Yaushi and H. Kuroda, *Bull. Chem. Soc. Jpn.*, **53**, 603(1980);
(c) H. Kuroda, K. Yakushi, H. Tajima, A. Ugawa, M. Tamura, Y. Okawa, A. Kobayashi, R. Kato, H. Kobayashi and G. Saito, *Synth. Met.*, **27**, A491(1988);
(d) H. Tajima, K. Yakushi, H. Kuroda, G. Saito and H. Inokuchi, *Solid State Commun.*, **49**, 769(1984);
(e) H. Kuroda, K. Yakushi, H. Tajima and G. Saito, *Mol. Cryst. Liq. Cryst.*, **125**, 135(1985);
(f) H. Tajima, K. Yakushi, H. Kuroda and G. Saito, *Solid State Commun.*, **56** 251(1985);
(g) H. Tajima, K. Yakushi, H. Kuroda and G. Saito, *Solid State Commun.*, **56** 159(1985);
(h) H. Tajima, Ph.D. Thesis, The University of Tokyo, 1985;
(i) H. Tajima, H. Kanbara, K. Yakushi, H. Kuroda and G. Saito, *Solid State Commun.*, **57**(12), 911(1986);
(j) K. Yakushi, H. Kanbara, H. Tajima, H. Kuroda, G. Saito and T. Mori, *Bull. Chem. Soc. Jpn.*, **60**, 4251(1987);
(k) M. Tamura, K. Yakushi, H. Kuroda, A. Kobayashi, R. Kato and H. Kobayashi, *J. Phys. Soc. Jpn.*, **57**(9), 3239(1988);
(l) A. Ugawa, Ph.D. Thesis, The University of Tokyo, 1989;
(m) M. Tamura, Ph.D. Thesis, The University of Tokyo, 1995, and the references cited therein.

[10] (a) R. K. Ahrenkiel, *J. Opt. Soc. Am.*, **61**, 1651(1971);
(b) F. Stern, *Solid State Phys.*, **15**, 299(1963);
(c) G. Leveque, *J. Phys., C, Solid State Phys.*, **10**, 4877(1977);
(d) F. W. King, *J. Chem. Phys.*, **71**, 4726(1979);
(e) J. S. Plaskett and P. N. Schatz, *J. Chem. Phys.*, **38**, 612(1963).

[11] (a) G. Steimecke, H. -J. Sieler, R. Kirmse, E. Hoyer, *Phosphorus Sulfur*, **7**, 49(1979);
(b) A. Davison, N. Edelstein, R. H. Holm, A. H. Maki, *Inorg. Chem.*, **3**(6), 814(1964).

[12] C. Faulmann, J. -P. Legros, P. Cassoux, J. Cornelissen, L. Brossard, M. Inokuchi, H. Tajima and M. Tokumoto, *J. Chem. Soc., Dalton Trans.*, **1994**, 249.

[13] (a) H. Kobayashi, R. Kato and A. Kobayashi, *Isr. J. Chem.*, **27**, 301(1986);
(b) A. Kobayashi, H. Kim, Y. Sasaki, R. Kato and H. Kobayashi, *Solid State Commun.*, **62**(2), 57(1987);
(c) R. Kato, H. Kobayashi, H. Kim, A. Kobayashi, Y. Sasaki, T. Mori and H. Inokuchi, *Synth. Met.*, **27**(3-4), B359(1988);
(d) R. Kato, H. Kobayashi, H. Kim, A. Kobayashi, Y. Sasaki, T. Mori and H. Inokuchi, *Chem. Lett.*, **1988**, 865;
(e) S. Alvarez, R. Vicente and R. Hoffmann, *J. Am. Chem. Soc.*, **107**, 6253(1987).

[14] (a) C. S. Jacobsen, J. M. Williams and H. H. Wang, *Solid State Commun.*, **54**(11), 937(1985);
(b) M. G. Kaplunov, E. B. Yagubskii, L. P. Rosenberg and Yu. G. Borodko, *phys. stat. sol. (a)*, **89**, 509(1985);
(c) K. Yakushi, H. Tajima, H. Kanbara, M. Tamura, H. Kuroda, G. Saito, H. Kobayashi, R. Kato and A. Kobayashi, *Physica*, **143B**, 463(1986);
(d) C. S. Jacobsen, D. B. Tanner, J. M. Williams, U. Geiser and H. H. Wang, *Phys. Rev. B*, **35**(18), 9605(1987);
(e) J. R. Ferraro, H. H. Wang, U. Geiser, A. M. Kini, M. A. Beno, J. M. Williams, S. Hill, M. -H. Whangbo and M. Evain, *Solid State Commun.*, **68**(10), 917(1988);
(f) K. Yakushi, H. Tajima, T. Ida, M. Tamura, H. Hayashi, H. Kuroda, A. Kobayashi, H. Kobayashi and R. Kato, *Synth. Met.*, **24**, 301(1988);
(g) A. Ugawa, G. Ojima, K. Yakushi and H. Kuroda, *Phys. Rev. B*, **38**(7), 5122(1988);
(h) K. Kornelsen, J. E. Eldridge, C. C. Homes, H. H. Wang and J. M. Williams, *Solid State Commun.*, **72**(5), 475(1989);
(i) A. Ugawa, K. Yakushi and H. Kuroda, *Mol. Cryst. Liq. Cryst.*, **181**, 269(1990);
(j) T. Sugano and M. Kinoshita, *The Physics and Chemistry of Organic Supercondcutors*, G. Saito and S. Kagoshima, Eds., Springer Proceedings in Physics, Vol. 51, Springer-Verlag, Berlin, Heidelberg, 1990, p.315;
(k) H. Tajima, M. Tamura, H. Kuroda, T. Mori and H. Inokuchi, *Bull. Chem. Soc. Jpn.*, **63**(2), 538(1990);
(l) R. Masuda, H. Tajima, H. Kuroda, H. Mori, S. Tanaka, T. Mori and H. Inokuchi, *Synth. Met.*, **55-57**, 2489(1993);
for early references concerning emv-coupling, see
(m) M. J. Rice, *Solid State Commun.*, **31**, 93(1979);
(n) M. J. Rice, V. M. Yartsev and C. S. Jacobsen, *Phys. Rev. B*, **21**(8), 3437(1980).

[15] (a) G. Saito, T. Enoki, K. Toriumi and H. Inokuchi, *Solid State Commun.*, **42**, 557(1982);
(b) H. Kobayashi, T. Mori, R. Kato, A. Kobayashi, Y. Sasaki and G. Saito, *Chem. Lett.*, **1983**, 581;
(c) H. Kobayashi, R. Kato, T. Mori, A. Kobayashi, Y. Sasaki, G. Saito and H. Inokuchi, *Chem. Lett.*, **1983**, 759;
(d) H. Kobayashi, A. Kobayashi, Y. Sasaki, G. Saito, T. Enoki and H. Inokuchi, *J. Am. Chem. Soc.*, **105**, 297(1983);
(e) H. Kobayashi, R. Kato, T. Mori, A. Kobayashi, Y. Sasaki, G. Saito, T. Enoki and H. Inokuchi, *Mol. Cryst. Liq. Cryst.*, **107**, 33(1984);
For recent reviews, see
(f) J. M. Williams, J. R. Ferraro, R. J. Thorn, K. D.Carlson, U. Geiser, H. H. Wang, A. M. Kini and M-H. Whangbo, *Organic Superconductors (Including Fullerenes)*, Prentice Hall, New Jersey, 1992;
(g) T. Ishiguro and K. Yamaji, *Organic Superconductors*, Springer-Verlag, Berlin, 1989.

Chapter 8.

Concluding Remarks

As time passes from the 20th to the 21st century, the research of the molecular-based materials also appears to be proceeding to the next stage. As referred to in Chapter 1 the physists and chemists have solved problems and overcome difficulties one by one whenever they encountered them in the course of the study, and now the rich chemistry and new interesting physics characteristic of the molecular-based materials have been brought to light. Among a wide spectrum of the organic materials found so far a prior importance of the chalcogen-containing planar π−conjugated molecules is beyond doubt when one considers the role that they have played for the last decade. For example a sulfur-based donor ET has produced a number of organic superconductors with remarkably higher T_c's that few might had expected at the beginning of the research. But what is most remarkable and should be emphasized about ET is the rapid development and successive discoveries of the new ET-based metals and superconductors. The rapidity of the succession and the number of the new findings surpass all the previous organic materials, which impetuously accerelated the activity and advancement from step to stride. However it is also apparent that even the ET salts could not sustain the animation now in this field for another decade without the appearance of the next new materials. It may be also the case even with the high-T_c copper oxides or anything else. Many other important materials that have left the marks on the history of the field illustrates how keenly a novel material based is required in order to develop the research field further.

In this study the author tried to synthesize a new series of planar π−conjugated molecules and their charge-transfer salts to find a novel conducting material with new electrical property. The target molecules cover from donor to acceptor and from organic to inorganic molecules, and all contain selenium atoms because the selenium-containing molecules have been rather less utilized as building blocks for conducting materials compared to sulfur-containing ones except for some important series like the TMTSF salts. As a result four kinds of new donor molecules each with several charge-transfer salts and other new ones that are based on the known molecules have been obtained. At first sight of their chemical formulae, they might appear simple extension of what have been synthesized by previous workers. Yet the author's incentive to them arises from quite a different purpose and interest. A new material does not necessarily mean what no one has ever seen, but means what no one has ever found or pointed out that there is a

unique importance there. Some of the experimental results shown in this study clearly demonstrate that they are new materials in the above-mentioned sense, though there remains much to be further clarified or established in the properties of them. A novel material hopefully might appear at any day, but it cannot be known when to come. However one thing is certain: as often concluded in reviews of the organic molecular-based conducting materials, the future for the advent of "high-T_c organic superconductors / ferromagnets" and other novel materials appears bright towards the coming century, yet it may largely depend upon how the researchers patiently pursue a really new material.

Based on Planar π-Conjugated Molecules

Toshio Naito